

NOAA Technical Memorandum ERL PMEL-53

TOPOGRAPHIC EFFECTS OF THE ALASKAN STREAM ON SHELF CURRENTS

Gary S. E. Lagerloef  
Glenn A. Cannon

Pacific Marine Environmental Laboratory  
Seattle, Washington  
April 1984



**UNITED STATES  
DEPARTMENT OF COMMERCE**

**Malcolm Baldrige,  
Secretary**

**NATIONAL OCEANIC AND  
ATMOSPHERIC ADMINISTRATION**

**John V. Byrne,  
Administrator**

**Environmental Research  
Laboratories**

**Vernon E. Derr  
Director**

#### NOTICE

Mention of a commercial company or product does not constitute an endorsement by NOAA Environmental Research Laboratories. Use for publicity or advertising purposes of information from this publication concerning proprietary products or the tests of such products is not authorized.

---

Contribution No. 676 from NOAA/Pacific Marine Environmental Laboratory

## Table of Contents

	Page
List of Figures . . . . .	vi
List of Plates . . . . .	vii
List of Tables . . . . .	vii
Abstract . . . . .	viii
Introduction . . . . .	1
Chapter 1: Regional Geographic, Climatologic and Oceanographic Setting . . . . .	10
A. Geography . . . . .	10
B. Climatology . . . . .	10
C. Northeastern Gulf Shelf and Ocean Currents . . . . .	11
D. Northwestern Gulf, Kodiak Outer Shelf and Alaskan Stream Flow . . . . .	12
E. Coastal Currents, Runoff and Sea-level. . . . .	17
F. Kodiak Shelf Oceanographic Summary . . . . .	19
Chapter 2: Data Description; Central Kodiak Shelf . . . . .	21
A. Mean Currents . . . . .	21
B. Satellite Infra-Red Images . . . . .	23
C. Local Wind Measurements . . . . .	27
D. Time Series . . . . .	28
E. CTD Data . . . . .	28
Chapter 3: Theoretical Discussion . . . . .	32
A. The Taylor-Proudman Column . . . . .	32
B. The Vorticity Equation . . . . .	35
C. The Potential Vorticity and Ekman Pumping Approximations . . . . .	41
Chapter 4: Topographic Effects on the Kodiak Shelf Flow . . . . .	45

A.	The Numerical Potential Vorticity Model . . . . .	45
B.	Model Results and the Along-Isobath Flow Limit . . . . .	49
C.	Comparison with the Ekman Pumping Equation . . . . .	58
D.	Comparison with the Hudson Shelf Valley . . . . .	61
E.	Summary . . . . .	62
Chapter 5:	The Alaskan Stream Driven Mean Shelf Flow . . . . .	64
A.	Statement of the Problem . . . . .	64
B.	The Large Scale Along-Shelf Averaged Vorticity Balance . . . . .	66
C.	The Arrested Topographic Wave and Along-Shelf Pressure Gradient . . . . .	70
D.	The Alaskan Stream as a Boundary Condition . . . . .	75
E.	An Additional Solution with Arbitrary Depth . . . . .	77
F.	The Alaskan Stream and Shelf Break Currents . . . . .	83
G.	Solutions which Include Coastal Winds . . . . .	87
H.	Residual Flow from Tidal Current Rectification . . . . .	93
I.	Chapter Summary . . . . .	96
Chapter 6:	Flow Variability . . . . .	98
A.	Seasonal variability . . . . .	98
B.	Statistical analysis: Empirical Orthogonal Functions (EOF) . . . . .	100
C.	Response to Synoptic Atmospheric Storms . . . . .	108
Chapter 7:	Discussion of Other Shelf Domains . . . . .	114
A.	Purpose . . . . .	114
B.	East Florida Shelf and South Atlantic Bight . . . . .	114
C.	The Middle Atlantic Bight . . . . .	119
D.	Washington/Oregon Shelf . . . . .	123

<b>Chapter 8: Summary . . . . .</b>	<b>127</b>
<b>A. Results . . . . .</b>	<b>127</b>
<b>B. Implications . . . . .</b>	<b>130</b>
<b>Acknowledgments . . . . .</b>	<b>131</b>
<b>Bibliography . . . . .</b>	<b>132</b>
<b>Appendix . . . . .</b>	<b>138</b>

## List of Figures

Number	Page
1. Kodiak Island Shelf and Vicinity . . . . .	2
2. Alaskan Stream . . . . .	13
3. Stratification of Shelf Waters . . . . .	18
4. Mean Currents; Central Kodiak Shelf . . . . .	22
5. Current, Wind and Pressure Time Series . . . . .	29
6. Sigma-t Profiles from Kiliuda Trough . . . . .	30
7. Schematic Shelf Profile and Coordinates . . . . .	36
8. Schematic of the Numerical Model . . . . .	46
9. Schematic Topography Grid . . . . .	47
10. Model Results Varying $\varepsilon$ . . . . .	50
11. Model Results Varying $\zeta_0$ . . . . .	53
12. Barotropic Flow from Galt (1980) . . . . .	59
13. Solution with Shelf Break Current Forcing . . . . .	78
14. Solution with Along-shelf Pressure Forcing . . . . .	79
15. Streamline Pattern for Shelf Break Forcing . . . . .	80
16. Isotacs of the Alaskan Stream off Kodiak . . . . .	85
17. Streamlines for Wind Forcing and No Shelf Break Flow . . . . .	90
18. Streamlines for Opposing Shelf Break Flow and Wind . . . . .	91
19. Streamlines for Similar Shelf Break Flow and Wind . . . . .	92
20. Current meter EOFs . . . . .	103
21. Bottom Pressure EOFs . . . . .	106
22. EOF time series . . . . .	109
23. Synoptic weather maps . . . . .	110

List of Plates

Plates I	Satellite Infra-red Images . . . . .	24
II	Satellite Infra-red Images . . . . .	25
III	Satellite Infra-red Images . . . . .	26

List of Tables

Number		Page
1.	WGC Mean Currents . . . . .	16
2.	Scales and Parameters . . . . .	34
3.	Topographic Gradients and Mean Currents . . . . .	56
4.	Current Meter EOF Eigenvectors . . . . .	105

## ABSTRACT

Current meter observations from a deep trough on the Kodiak Island shelf show that the flow is largely barotropic and follows depth contours around the trough to form a cyclonic vortex. This year-round feature is interpreted as a Taylor-Proudman column and is reproduced with a numerical potential vorticity model. When the velocity scale is appropriately small ( $\sim 5 \text{ cm s}^{-1}$ ), the lowest order balance approaches  $\vec{U} \cdot \vec{\nabla} H = 0$ , and the flow is constrained to follow isobaths in good agreement with the data. As a consequence, stronger currents accompany steeper topography as streamlines which follow isobaths converge.

This flow pattern is sustained by the predominantly southwestward regional mean shelf flow, which is shown here to be driven by the Alaskan Stream, an adjacent oceanic boundary current over the continental slope. A linear parabolic vorticity equation is solved with boundary conditions for the geostrophic shelf break current and no wind forcing. These create a vorticity across the shelf which is balanced by vortex stretching of cross-isobath flow, resulting in an along-shelf current increasing seaward from zero at the coast and a pressure gradient sloping downward along-shelf in the flow direction. The addition of wind forcing through a coastal boundary condition modifies these results by adding a near shore current to account for the observed seasonal and shorter period variability on the Kodiak shelf. The largest responses occurred when storms brought along-shelf winds to a considerable length of the northern Gulf of Alaska coastline, regardless of the locally measured winds near Kodiak.

The relevance of these various results is made clear by comparing the Kodiak shelf with other well studied shelf domains. Major features of the theory presented here for boundary current forcing modified by wind stress are consistent with the South Atlantic Bight and the Gulf Stream and may be applicable to the Mid Atlantic Bight as well.

## INTRODUCTION

Circulation in a continental shelf region occurs as a response to one or more forcing mechanisms such as wind stress or the neighboring oceanic pressure field. This response is dependent on the prevailing oceanographic (i.e. density field) conditions and the shelf geomorphology. The strong influence of topography on these flows has become well recognized, especially the dominant depth variation from the coast seaward to the ocean basin. The inclusion of this variation in the vorticity balance led to the description of topographic Rossby (shelf) waves (see, e.g. Buchwald and Adams, 1968). The topographic vorticity term is likewise critical to modeling the wind forcing on the shelf (e.g. forced wave response, Gill and Schumman, 1974) as well as accounting for the predominant along-shelf orientation of subtidal and subinertial currents. Csanady (1978) studied the importance of the cross-shelf topography to the mean shelf flow with the "Arrested Topographic Wave" model. The topography is a major term in the vorticity balance and influences the pattern of steady currents in response to various forcing mechanisms.

In idealized cases the along-shelf topographic variations are small and can be ignored. In many applications, however, they are significant and the Kodiak Shelf represents an extreme case, with deep canyons or troughs transecting the shelf, separated by shallow banks (Figure 1). The along shelf length scale of these features is small (20-100 km), with a vertical relief scale of 100-200 m.

The Kodiak shelf is further distinguished by having at its seaward edge a strong, year-round, southwestward flowing oceanic

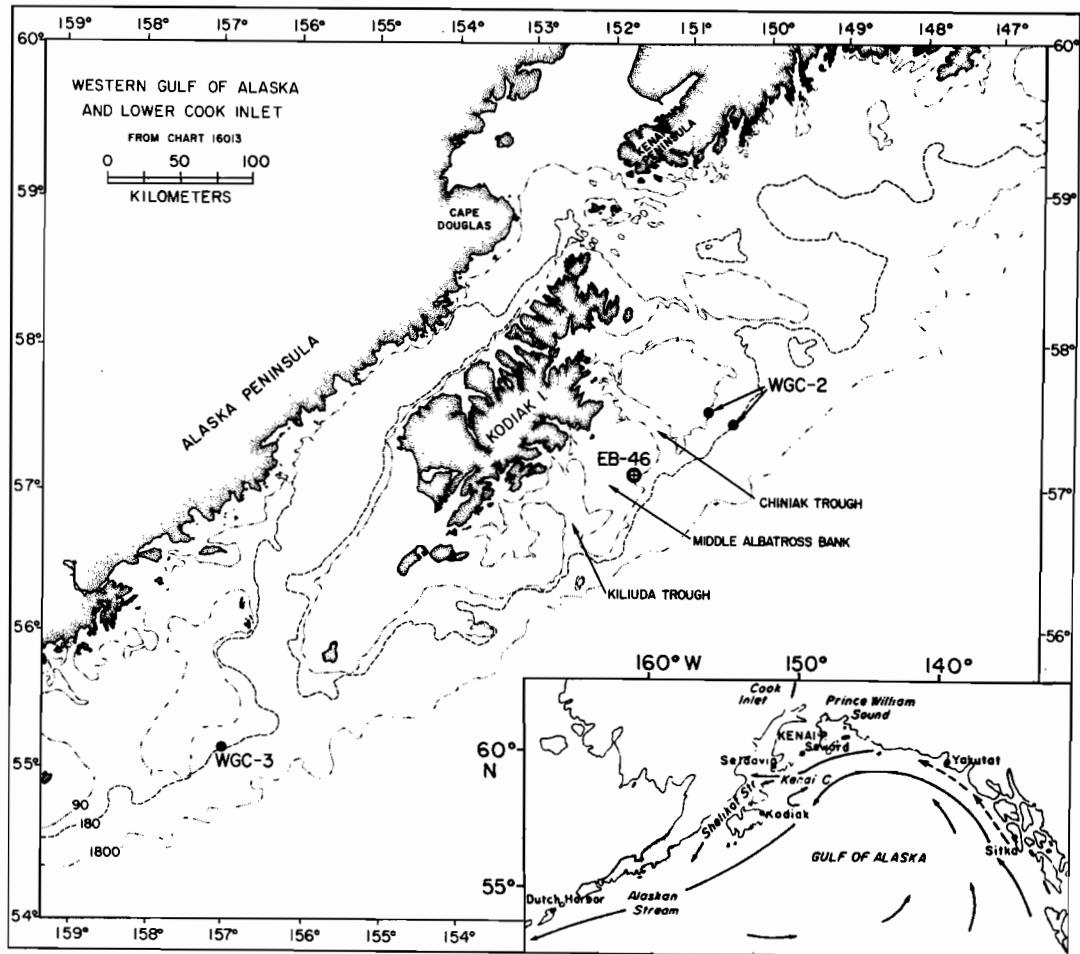


Figure 1. The Kodiak Island shelf showing Kiliuda and Chiniak Troughs separated by Middle Albatross Bank, and the locations of the WGC current meter moorings and data buoy EB-46. Depth is contoured in meters.

Inset: The northern Gulf of Alaska showing schematically the regional oceanographic circulation.

boundary current, the Alaskan Stream. It will be shown how this current has a major influence on the predominantly southwestward shelf flow. The purpose of this paper is to describe the circulation regime of the Kodiak shelf using current meter data in conjunction with numerical and analytical models. Emphasis is on the mean flow with respect to two topics: 1) the steering effect of the large complex variations in topography and 2) the importance of the Alaskan Stream as a driving mechanism. The two parts of the study are distinguished by the length scales over which they are important. The smaller scale pertains to the local steering effect of the topography. The driving mechanisms for the mean flow are studied over large along shelf scales ( $\sim 1000$  km) on which the shelf responds to the oceanic pressure field and atmospheric forcing. Background for these topics is reviewed below with additional material presented in each of the pertinent chapters.

Topographic effects on coastal circulation in several other regions have been illuminated by the long-term current measurements which have become available in the past decade. Cannon and Lagerloef (1983) give a review of these recent studies. Flow in canyons in general appears to interact with changing flow conditions on the surrounding shelf. In turn, they are often affected by variations in wind stress or other larger scale effects.

Regions of upwelling can be confined to canyon heads, as noted by Shaffer (1976) for upwelling studies off the African coast. Similar observations were made by Nelson *et al.* (1978) in the upper Hudson Shelf Valley, U.S. east coast, where upchannel flow was correlated

with westerly (upwelling favorable) winds. In these cases, the flow tends to be driven hydraulically by an along-axis pressure gradient balanced by friction. A model by Freeland and Denman (1983) shows that pressure gradients along the axis of the northern spur of the Juan de Fuca Canyon, U.S. west coast, can raise water from depths of 450 meters on to the shelf.

These cases tend to be descriptions of narrow canyons and of near-bottom canyon currents. If spatial scales are larger, the flow may be more geostrophic, modified topographically by following depth contours. Hsueh (1980) used a quasi-geostrophic equation, balancing vorticity induced by flow over topography with bottom Ekman pumping, to describe the wind-driven flow in the lower Hudson Shelf Valley. More recently, Meyer *et al.* (1982) have shown that both the vorticity balance used by Hsueh and the along axis pressure driven flow are important to the dynamics of the Hudson Shelf Valley.

In the Juan de Fuca Canyon, U.S. west coast, flow was primarily up-down and axis correlated with up-down welling favorable coastal winds except in one instance where along axis density distribution was important (Cannon, 1972). Observations of nearby shelf currents indicate that cyclonic vorticity exists over this canyon in either the up or down welling regime but is limited to the near-bottom layer due to the vertical decoupling effect of stratification (Cannon *et al.*, 1972; Cannon and Lagerloef, 1983). Numerical modeling studies by Hurlburt (1974), Peffly and O'Brien (1976), and Preller and O'Brien (1980) showed that the distribution of upwelling is controlled by

topography and favors the equatorward side of canyons, primarily due to bottom currents being deflected upward.

Banks or shoals will also affect a coastal flow regime. Eide (1979) described an anti-cyclonic flow around the Halten Bank off the west coast of Norway. In this case, the mean circulation is not locally wind forced but is associated with the Norwegian current and modified by a topographic feature. Eide showed that the observations qualitatively agree with a stratified Taylor-Proudman column model of Hogg (1973). A similar anticyclonic flow is associated with the Georges Bank off New England (Butman et al., 1982). The Taylor-Proudman column concept would seem appropriate to the Georges Bank based on Eide's results, but has not yet been applied. Loder (1980) has suggested that a significant component of the mean flow around Georges Bank may be caused by topographic rectification of tidal currents, a mechanism which produces a mean along isobath current with shallow water to the right of the flow direction. Nevertheless, both the Halten and Georges Bank flows can be interpreted in terms of potential vorticity conservation since they are both characterized by an anti-cyclonic flow feature around a shoal or bank.

The Kodiak Shelf possesses both shallow banks and deep canyons or troughs. The current meter data, presented below in Chapter 2, show a mean along isobath counter-clockwise current around the Kiliuda Trough. This indicates that the width scale of the canyon ( $\sim 20$ - $30$  km) is large enough for the flow to be primarily geostrophic rather than constrained along-axis as in some cases noted above. This concept is justified in the scaling arguments given in Chapter 3 where

a potential vorticity equation is introduced for application to the Kodiak Shelf. The presence of a cyclonic vortex over the canyon implies potential vorticity conservation analogous to the aforementioned anticyclonic vortex over the Halten Bank off Norway.

The potential vorticity equation is then adapted to a numerical model of the Kodiak Shelf in Chapter 4. It demonstrates the steering effect of the topography and duplicates a flow pattern which agrees with the measured mean currents. Quantitative estimates also show that the local topographic steepness influences mean current speed by converging streamlines which are constrained to follow isobaths.

The model makes use of boundary conditions that assume a larger scale southwestward flow for the shelf and the forcing for this flow is the focus of the second major topic of this paper. Three major types of coastal (subtidal) currents can be identified, categorized by their major forcing (Winant 1980). These are: 1) direct wind forced, 2) forced by large-scale oceanic circulation for which the coastal area is a boundary, and 3) density driven by fresh water runoff at the coast. Added to these should be forcing by an along-shelf pressure field established by forcing on another part of the shelf (Csanady, 1978) and the tidal rectification process (Loder, 1980; Robinson, 1981).

Wind forcing is the most prevalent and frequently studied mechanism for driving coastal currents and reports of observational and theoretical studies of many coastal areas are common in the literature. In his review, Winant (1980) contended that, while differences in climate and geomorphology are important, the along-shore

pressure gradients must be taken into account to assess the variety of responses of different systems to local winds.

An along-shore pressure field may be caused by local or non-local coastal winds (Csanady 1978). Hickey and Pola (1983) have accounted for the seasonal fluctuations in the along-shelf pressure field on the U.S. west coast by showing the response to both local and non-local winds with Csanady's model.

An along-shelf pressure gradient may also be indigenous to the larger scale oceanic circulation, or caused by steric differences due to the regional density field (e.g., Csanady, 1979). Csanady (1978) also showed how such an externally imposed pressure field drives an along-shelf current through momentum and vorticity balances. He suggested this mechanism for the mean southwestward flow of the Mid-Atlantic Bight. Beardsley and Winant (1979) supported this concept with evidence that a regional circulation model by Semtner and Mintz (1977) produced the necessary pressure gradient. One result of this forcing is that the along-shelf velocity increases seaward, owing to the momentum balance requirements and increasing depth. This contrasts with locally wind driven currents which are strongest near the coast.

On shelves bordered by rather benign eastern ocean boundary current systems, such as the U.S. west coast, local wind forcing usually prevails for both synoptic and seasonal time scales. The shelf of the northern Gulf of Alaska is different in that a strong oceanic gyre is present with a western boundary current bordering the Kodiak Shelf. The effect of this circulation on the coastal currents

and the importance of the along-shelf pressure gradient are treated analytically in Chapter 5. It is shown how the predominantly south-westward flow of the Kodiak Shelf is linked to this oceanic boundary current and how this is modified by superimposing a coastal wind stress. To do this, new solutions to the "Arrested Topographic Wave" equation of Csanady (1978) are derived. When a boundary condition is applied which represents the presence of a shelf break current, a parallel flow is generated on the shelf which, in the absence of wind stress, decreases to zero at the coast. An along-shelf pressure gradient is also generated which, were it the driving force, would create a similar shelf flow pattern. The shelf break current, which forms the boundary condition for this solution, is dynamically linked to the Alaskan Stream (20 to 40 km seaward) by horizontally integrating a baroclinic planetary vorticity equation across the stream.

Features of the measured flow variability are discussed conceptually in Chapter 6. Both the seasonal modulation of near-shore currents and their response to intense atmospheric storms can be accounted for with application of the results from Chapters 4 and 5. It is concluded that the most successful approach is to treat the Kodiak Shelf as a component of a larger shelf system. When the larger scale response is put into perspective, the local response can be understood in terms of how the large scale circulation affects the boundary conditions of the small scale problem. In this way it is possible to resolve an otherwise confusing set of observations.

In Chapter 7, the major circulation features of three well-studied shelves are reviewed and compared with the results given here

for the Northwest Gulf of Alaska. Attention is focused on the major forcing mechanisms of the mean flow, in particular, the importance of the along-shelf pressure gradient and ocean boundary currents. The three shelves are the South Atlantic Bight, the Mid Atlantic Bight and the Washington-Oregon Shelf. The implications for oceanic boundary current forcing given here are consistent with the effects of the Gulf Stream on the circulation and along-shelf pressure field of the South Atlantic Bight. The Mid Atlantic Bight is thought to be driven by the along-shelf pressure gradient associated with the regional ocean circulation, however, it is here suggested that the importance of a shelf break current should also be considered. On the Washington-Oregon shelf, seasonal wind forcing dominates, but the along-shelf pressure gradient is very important to the dynamics. All the shelves are governed by essentially the same momentum and vorticity balances. The differences are in the proper boundary conditions for the vorticity equation and the relative importance of the various momentum terms.

## Chapter 1: Regional Geographic, Climatologic and Oceanographic Setting

### A. Geography

Kodiak Island is located in the northwestern Gulf of Alaska (Figure 1), separated from the mainland by a narrow, deep channel, Shelikof Strait. The major bathymetric trend is NE/SW and a shelf of about 100 km width borders the southeastern coast of the island. The shelf topography is very rugged, characterized by deep cross-shelf troughs (150-200 m depths) separated by banks (30-100 m depths). The shelf break is typically along the 200 m isobath except where this isobath turns shoreward at the axes of the shelf valleys and troughs. Seaward of the shelf break, the bottom drops off sharply to depths in excess of 5000 meters in the axis of the Aleutian Trench. The island itself is about 250 km in length. The adjoining shelf, however, is a component of a shelf-slope-trench system that extends northeast/southwest for more than 1000 km.

### B. Climatology

The regional meteorology is dominated by the Aleutian Low in the winter when frequent cyclonic storms transit the northern gulf from west to east. During the summer, the North Pacific High occupies the region and brings light and variable winds. Royer (1975) presented monthly mean wind driven Ekman transport estimates for the northern gulf computed from ten years of climatic data which showed strong

wintertime onshore downwelling favorable transports and much weaker offshore transports in summer.

### C. Northeastern Gulf Shelf and Ocean Currents

The deep ocean circulation is clearly dominated by the Pacific Sub Arctic Gyre, a cyclonic circulation which inhabits the entire gulf. The northward flowing Alaska Current, a broad diffuse eastern boundary current, comprises the eastern limb of the gyre. This flow also entrains a considerable amount of recirculated water in the gyre (Reed, 1980). Direct current measurements from the shelf break in the northeast gulf showed a mean along-shelf flow of about  $16 \text{ cm s}^{-1}$ , varying from about  $20 \text{ cm s}^{-1}$  in winter to  $12 \text{ cm s}^{-1}$  during the summer (Lagerloef et al., 1981). Inner and outer shelf processes are decoupled in that area because very low frequency ( $<.1 \text{ cpd}$ ) eddy-like fluctuations in the Alaska Current do not propagate onto the shelf (Hayes, 1979; Royer, et al., 1979, Lagerloef et al., 1981). Within  $\sim 25 \text{ km}$  of the coast, a baroclinic coastal current flows northwest, driven seasonally by fresh water runoff peaking in October (Royer, 1981). A mid shelf doldrums-like region with eddies apparently isolates the coastal current from the Alaska current (Royer, 1982).

Near the northern apex of the Gulf of Alaska some portion of the Alaska Current may transit the shelf via a deep trough and flow north of Kodiak, (Muench et al., 1978). However, this westward flow is dominated by the low salinity coastal current, here called the Kenai Current (Schumacher and Reed, 1980). Nearshore currents in this region have distinct seasonal signal. Royer (1975) indicated that

winter onshore Ekman transport caused downwelling and flushing of the shelf waters and that the accompanying vigorous wind mixing reduced vertical stratification. The summer conditions brought a relaxing of the downwelling and perhaps weak upwelling of denser, more saline bottom water onto the shelf to augment the increased stratification caused by insolation and runoff. Schumacher and Reed (1980) showed that the near shore flow was predominantly westward year round, continuing southwestward through Shelikof Strait. The flow had a strong peak in November owing to the seasonal peak in runoff from surrounding watersheds. A secondary flow maximum, driven by the regional wind stress occurred in late winter.

D. Northwestern Gulf, Kodiak Outer Shelf and Alaskan Stream Flow

In the northwestern gulf, including the area adjacent to Kodiak Island, most of the oceanic water follows the bathymetric trend of the shelf and flows southwestward, where it intensifies into a narrow (50 km wide) western boundary current, the Alaskan Stream (Favorite and Ingraham, 1977). This flow (Figure 2) is distinguished from the Alaska Current discussed above and dominates the waters of the continental slope. Dynamically computed surface currents are 50 to 150  $\text{cm s}^{-1}$  and the mean transport is  $\sim 12$  Sv relative to 1500 db (Favorite and Ingraham, 1977; Reed et al., 1980). Reed et al. (1980) compared transport measurements (relative to 1500 db) over a four year period with transport estimated from integrated wind stress curl over the gulf. Deviations from the mean measured transport were 4 Sv or less and were not statistically related to the order of magnitude

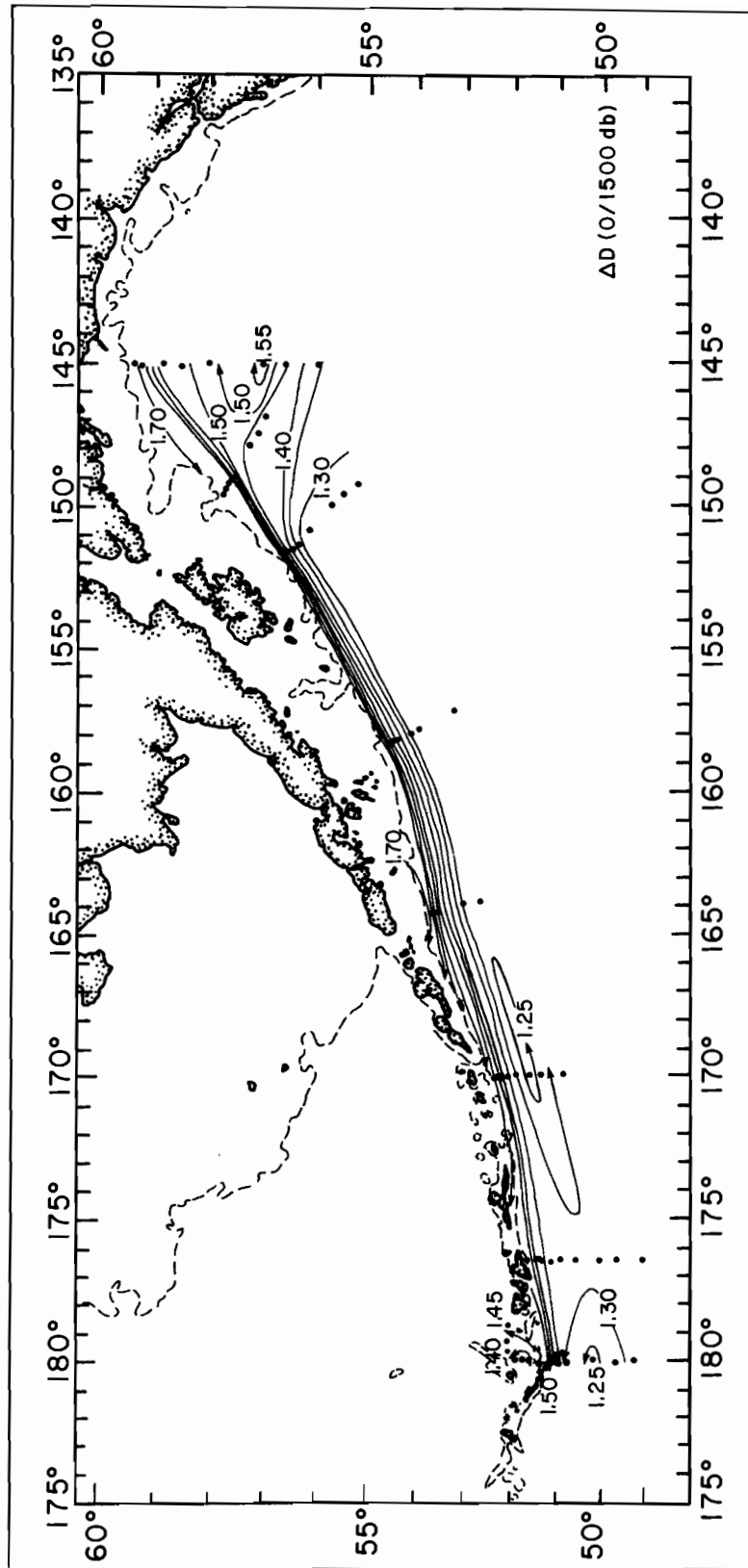


Figure 2. Contours of geopotential anomaly relative to 1500 db showing the extent of the Alaskan Stream in the Northwest Gulf of Alaska. (From Wright, 1981.)

variations in wind stress curl. There was no evidence of significant seasonal (i.e., winter-summer) variability in the measured transport. This implies that either the gyre does not spin up in response to the seasonally varying atmospheric conditions or that transport variations of the Alaskan Stream are dominated by other causes.

Direct measurements of the Alaskan Stream were made by Reed *et al.* (1981) from February to August, 1980, at a depth of 980 m over a bottom depth of 1600 m. Seven-day averaged currents southwestward at speeds of 10 to 20  $\text{cm s}^{-1}$ , except during a reversal of some 50 days duration. There was no correlated sea level fluctuation on Kodiak Island associated with this event, but it was accompanied by an *in situ* temperature increase of about 0.5°C. The authors attributed the reversal to advection of a baroclinic eddy-like feature. Such features are evident in the geopotential fields from some hydrographic surveys of the stream (Reed *et al.*, 1980; Wright, 1981). Reed (1983, personal communication) has recently examined current meter data from the Alaskan Stream from the winter and spring of 1982 and found extremely consistent southwestward flow with very little variance for an interval in excess of 8-months. Speeds at 300 meters below the surface averaged  $\sim 50 \text{ cm s}^{-1}$ .

From the data presented by Favorite and Ingraham (1977) Reed *et al.* (1980) and Wright (1981), the core of the stream adjacent to Kodiak Island is interpreted here to be located laterally between the 1000 and 2000 m isobaths. Reed *et al.* (1980) estimated the inshore edge to be near the 300 m isobath where the geopotential field indicated a flow reversal or zone of weak flow. The baroclinic

(vertical) shear is small in the upper 100-200 m of the stream; thus the seaward boundary for the Kodiak shelf water appears as a nearly barotropic current (above the horizon of the shelf break) which increases seaward. This point is of major importance for later discussions of boundary conditions.

It is evident that currents along the outer shelf in the northwestern gulf are largely influenced by the oceanic circulation and do not vary seasonally. Niebauer *et al.* (1981) came to this conclusion in their analysis of a year-long time series of currents measured over the 300 m isobath slightly east of Kodiak Island. Mooring deployments were 3 to 4 months duration and typical mean currents in the upper 100 m were  $30\text{-}50\text{ cm s}^{-1}$  along-shelf to the southwest. Another series of outer shelf currents was measured near Kodiak at stations WGC-2 and WGC-3 (Figure 1) and at WGC-1 (location, not shown, was farther west near Dutch Harbor) and tabulated by Muench and Schumacher (1980). The 20 m depth currents averaged over the mooring periods are excerpted from their paper in Table 1. At WGC-1, these averages varied between 11 and  $27\text{ cm s}^{-1}$  along-shelf to the southwest but there is no seasonal pattern to the variability. At WGC-3, the mean southwest flow was even more consistent. Mooring WGC-2 was relocated between two deployments to a point 15 km inshore of the original. Subsequent measurements from the new location were considerably weaker, and once this is taken into account, there was no evident seasonal variability at this mooring either.

Shay and Hickey (1983) compared data segments from the WGC moorings with predictions from a wind-driven model of Hickey and Hamilton

Table 1

Shelf break currents at ~20m, averaged over the mooring duration, from station WGC-1, WGC-2 and WGC-3. (From Muench and Schumacher 1980.)

WGC-1	54.04°N 163.05°W	Speed cm s <sup>-1</sup>	Direction °T
	05 Sep 75 - 01 Nov 75	27.2	264
	02 Nov 75 - 12 Mar 76	12.2	243
	13 Mar 76 - 11 Jun 76	25.1	253
	12 Jun 76 - 30 Sep 76	11.2	253
	01 Oct 76 - 28 Apr 77	23.6	258
	30 Apr 77 - 08 Sep 77	16.2	262
WGC-2	57.45°N 150.49°W	Speed cm s <sup>-1</sup>	Direction °T
	22 Sep 75 - 17 Nov 75	33.5	227
	Data missing	----	---
	10 Mar 76 - 08 Jun 76	21.8	227
	New location 57.56°N 150.82°W		
	11 Jun 76 - 16 Oct 76	3.2	245
	21 Oct 76 - 29 Mar 77	2.3	241
	26 Mar 77 - 06 Sep 77	4.7	220
WGC-3	55.19°N 156.96°W	Speed cm s <sup>-1</sup>	Direction °T
	13 Jun 76 - 14 Oct 76	21.4	256
	20 Oct 76 - 02 Mar 77	26.1	240
	Data missing	----	---
	01 May 77 - 05 Aug 77	24.1	255

(1980) and found that the subtidal fluctuations were not clearly related to wind forcing. Mysak (1982) has proposed a barotropic instability model for the Alaskan Stream as a source for eddy-like fluctuations which could account for sub-tidal variability in the outer shelf currents.

#### E. Coastal currents, Runoff and Sea Level

Peak stratification in the coastal waters of the Gulf of Alaska occurs around October, due largely to accumulated runoff from watersheds along the northern gulf coastal perimeter (Royer, 1981). Most of this water remains confined to a coastal flow, the Kenai Current, and passes through Shelikof Strait (Schumacher and Reed, 1980). Little of this flow appears along the Kodiak Shelf and local drainage from the island does not appear to be significant. For example, Figure 3 (from Schumacher *et al.*, 1979) shows that during the peak runoff period the upper 50 m of the water column are much less stratified over the Kodiak shelf than over the shelf to the north. The baroclinic geopotential field in the shelf waters, relative to 50 or 100 db, appears to be weak and variable and may, at times, indicate eddies and northeastward transport (Reed *et al.*, 1980; Schumacher *et al.*, 1979; Favorite and Ingraham, 1977). This contrasts the predominantly southwestward flow indicated by the current measurements discussed above. Vertical shear from these direct measurements was such that near bottom (+10 meters) speeds were usually greater than one-half the near surface values, which indicates that the flow is predominantly barotropic over the Kodiak shelf.

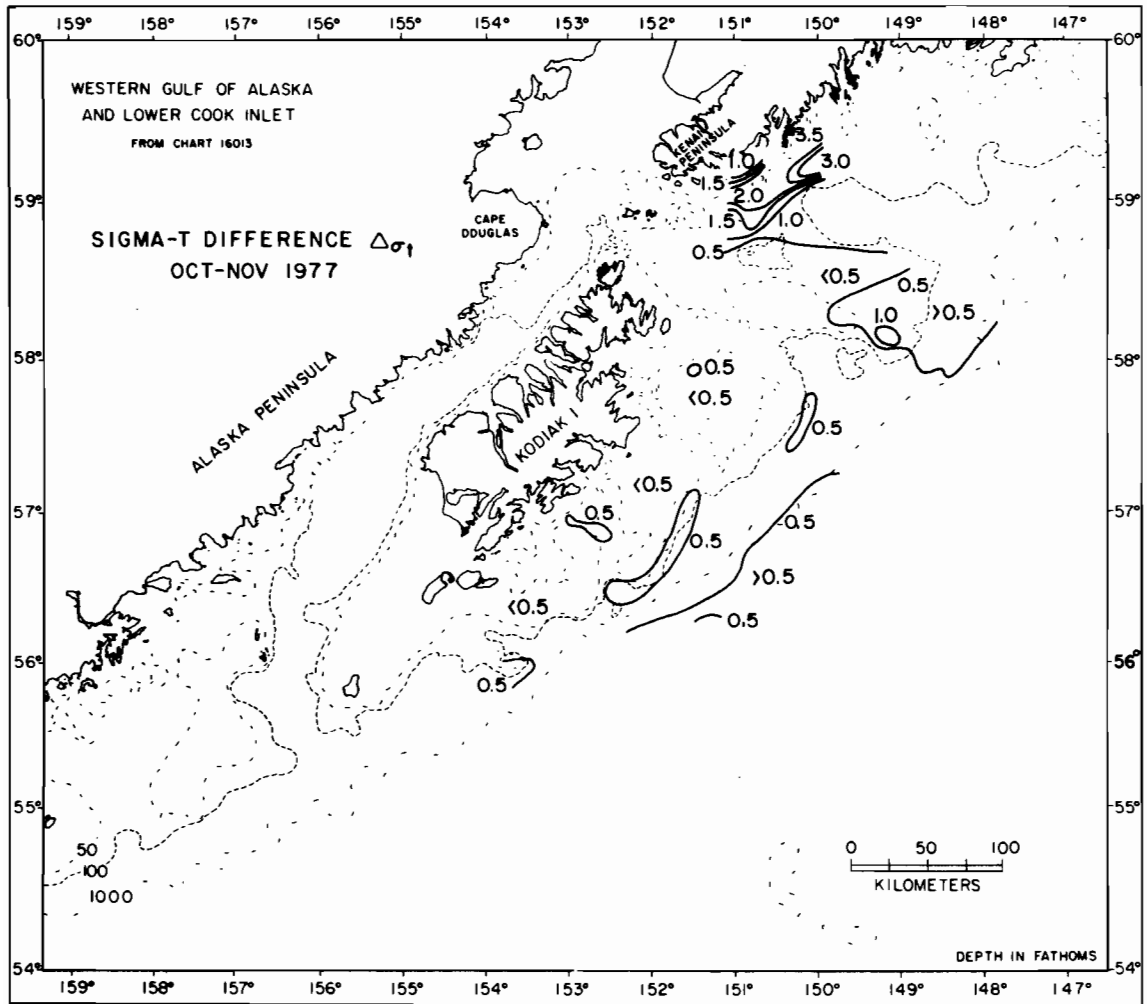


Figure 3. Sigma-t difference  $\Delta\sigma_t$  between 50 m and the surface for October and November 1977. Contour interval is 0.5 units. (From Schumacher *et al.*, 1977.)

Reed and Schumacher (1981) analysed mean monthly adjusted sea level variations around the Gulf of Alaska and interpreted their findings in terms of geostrophic response to the flow regime. The six tide station locations are shown in the inset of Figure 1. Seasonal ranges were significantly less at Kodiak and Dutch Harbor than at the stations to the east. The timing of the maxima at Seaward and Seldovia indicated that the signal was affected by the runoff peak and the Kenai Current. Further east and south, Yakutat and Sitka were affected by a barotropic coastal flow.

The seasonal range at Kodiak was small, in part, because the Kenai Current follows the mainland coast through Shelikof Strait. Recently, Schumacher *et al.* (1982) have suggested that a baroclinic flow through Unimak Pass into the Bering Sea may, in fact, originate as the Kenai current and that this is a continuous coastal flow along the southern side of the Alaska Peninsula. The Dutch Harbor tide station is west of Unimak Pass and therefore would not respond to this baroclinic current. The small annual ranges of adjusted sea-level at Kodiak and Dutch Harbor indicate that they are not influenced by the coastal currents but instead, reflect the seasonal variations in the oceanic circulation, which appear to be much smaller by comparison.

#### **F. Kodiak Shelf Oceanographic Summary**

The Kodiak shelf is a bathymetrically complex region with deep troughs orthogonal to the general NE/SW alignment of the shelf break which is about 100 km offshore. The flow along the shelf is strongly affected by these large topographic variations. The oceanographic

setting differs from the other coastal waters in the northern Gulf of Alaska in that coastal runoff is not as important a factor and the flow appears to be largely barotropic. The outer shelf currents, along with the bordering Alaskan Stream, flow along shelf to the southwest year-round and do not appear to have significant seasonal variability in spite of a substantial seasonal change in regional wind stress. Low frequency (sub-tidal) variability in the shelf break currents is also not well accounted for by local wind forcing and a strong coupling between the outer shelf currents and the Alaskan Stream is well supported by the available data.

## Chapter 2: Central Kodiak Shelf Data

### A. Mean Currents

The data for this analysis were collected as part of a multi-year study to provide environmental background for the development and transportation of oil through the northern Gulf of Alaska coastal region. Most of the oceanographic knowledge outlined in the previous section results from this overall survey. The current meter observations from the central Kodiak shelf have been briefly described by Muench and Schumacher (1980). Herein, they are used to address the scientific questions that comprise this paper.

Six current meter moorings (K5-K10) were deployed in the Kiliuda Trough region (Figure 4). These arrays consisted of Aanderra RCM-4 current meters in a taut-wire configuration with subsurface flotation at about 20 m. All data were processed with a 35 hour low-pass filter to remove tidal and inertial signals. Moorings K6-K10 were occupied for a four-month period during the winter of 1977-1978 and again for four months during the summer 1978. Mooring K5 was occupied for the same winter period a year earlier (1976-1977) and is included as a supportive observation.

The record length mean currents at stations K5-K8 were larger than one standard deviation of variability and followed the trend of the bathymetry. The vertical shear, whether due to viscosity or stratification, does not indicate a significant deflection from along-isobath flow. Since the winter and summer flow patterns were similar, the vectors from moorings K6-K8 indicate that they were on the

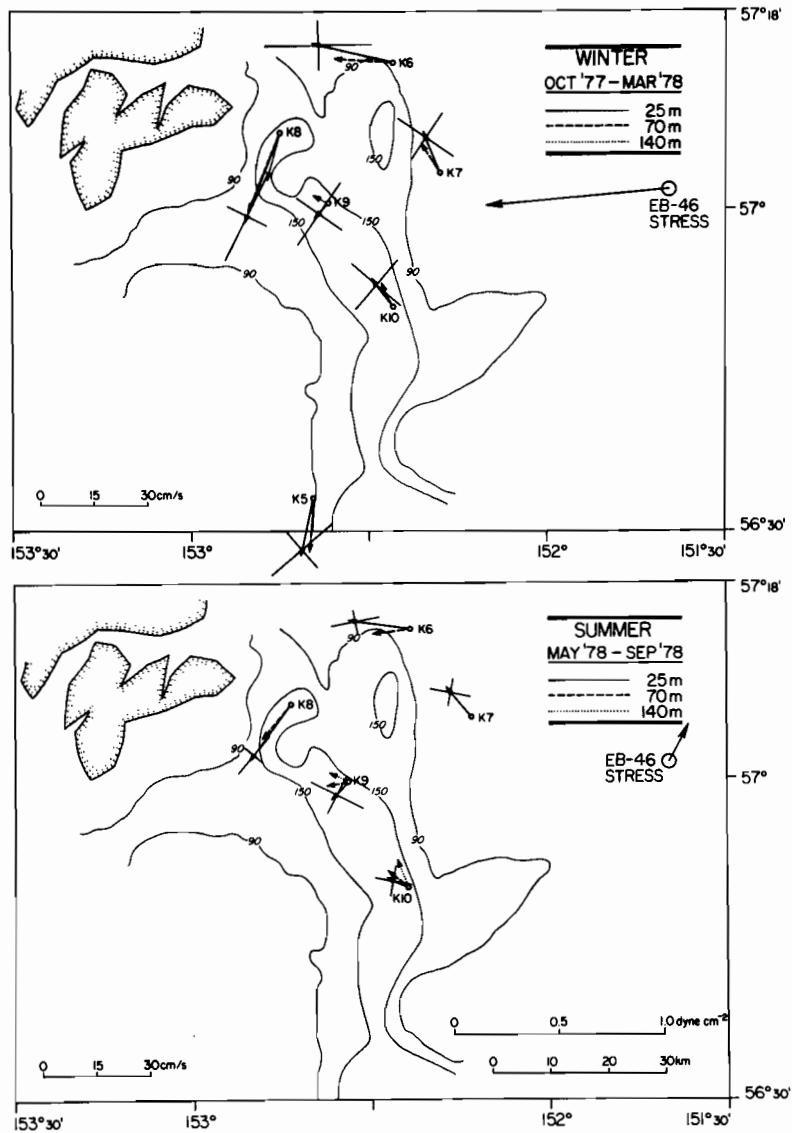


Figure 4. Mean ( $\sim 4$  month) currents near Kiliuda Trough and wind-stress at EB-46 during winter (top) and summer (bottom). Error crosses represent one standard deviation (35 hour low-pass) in the major and minor axes of variance for currents at 25 m depth. Mooring K5 was in place during the same winter period one year earlier and is not concurrent with the others. Depth is contoured in meters.

perimeter of a steady cyclonic vortex or loop current associated with Kiliuda Trough. It appears that moorings K9 and K10 were near the middle of the feature, with mean currents that were insignificant at less than one standard deviation. Vertical shear in mean-flow direction was apparent mid-trough, but may have been significant only during the summer.

#### B. Satellite Infra-Red Images

Additional evidence for the quasi-steady, cyclonic circulation pattern trapped over the Kiliuda Trough can be found in a series of three mid-winter infra-red satellite images, taken on February 22, 23, and 27, 1979 (Plates I, II, III). On February 22, a tongue of warm water extended shoreward over the eastern edge of the trough (Plate I). The subsequent images show that this water mass moved around the head of the trough and then seaward over the western trough edge. The propagation speed of the leading edge of the warm tongue during the five-day interval is about  $25 \text{ cm s}^{-1}$ , and is consistent with the mean current measurements around the trough. Also note that Chiniak Trough, to the east of Kiliuda, had a similar resident of warm water. Several other satellite IR images were examined that did not have quite the clarity and contrast of these, but did indicate warm water extending across the shelf in the vicinity of Kiliuda and Chiniak Troughs.

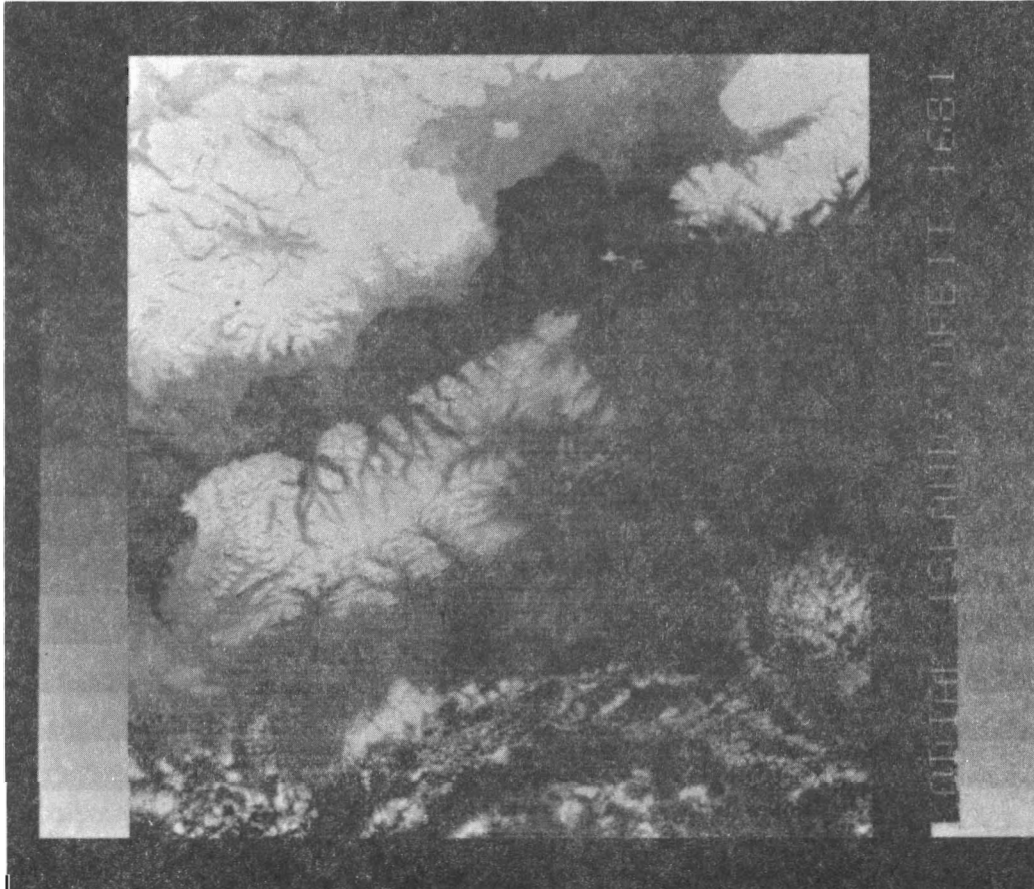


Plate I. Infra-red image taken on February 22, 1979 by the NIMBUS-7 Coastal Zone Color Scanner. Kodiak Island is the whiter area in the center. White areas indicate cloud or snow cover. Warm water is indicated by darker shades and cool water by lighter shades. A tongue of warmer water extends shoreward toward the middle of Kodiak Island; its location is over the eastern edge of Kiliuda Trough (c.f. Fig. 1).



Plate II. Infra-red image taken on February 23, 1979 by the NIMBUS-7 Coastal Zone Color Scanner. Kodiak Island is the whiter area in the center. White areas indicate cloud or snow cover. Warm water is indicated by darker shades and cool water by lighter shades. One day later than Plate I, the warm water intrusion has turned westward near the head of Kiliuda Trough.



Plate III. Infra-red image taken on February 27, 1979 by the NIMBUS-7 Coastal Zone Color Scanner. Kodiak Island is the whiter area in the center. White areas indicate cloud or snow cover. Warm water is indicated by darker shades and cool water by lighter shades. Four days later than Plate II, the warm water has nearly completed a loop around the perimeter of Kiliuda Trough and extends seaward along the western through edge. The leading edge has moved at about  $20\text{-}25 \text{ cm s}^{-1}$  (c.f. Fig. 4).

### C. Local Wind Measurements

Concurrent with the current meter deployments, local wind measurements were made by the NOAA Meteorological buoy, EB-46, near the shelf break and within 35 km of the mooring array. Wind speed data were converted to wind stress with the quadratic drag formulation used by Mayer *et al.* (1979). Figure 4 shows the wind stresses averaged over nearly the same intervals as the current meter deployments. The summer stress was less than one-fifth the magnitude of the winter stress, and the direction was to the northeast so that the along-shelf windstress components were reversed between the winter and summer periods measured.

This large seasonal variation in local wind stress did not influence the mean cyclonic flow pattern on the central Kodiak shelf, which suggests that mechanisms other than local wind forcing must dominate the mean shelf currents. Nevertheless, there were some variations in magnitude at the near-shore stations, K6 and K8, where the summer mean current magnitudes were about 70% of the winter values. At the remaining stations, winter/summer variations in mean current magnitude were insignificant. This evidence suggests that the near-shore current magnitudes are seasonally modulated by the wind field (although flow direction is unchanged) while mid- and outer-shelf currents are not likewise affected. Below, results from the modeling studies are interpreted in a way which will give more insight into the effects of the winds on the shelf flow.

#### D. Time Series

Figure 5 shows 35 hr low-pass filtered winter time series of the 25 m depth currents resolved along mean flow axes (moorings K6-K10), bottom pressure (moorings K8-K10 only) and wind stress at EB-46. Again, one should note the difference between the comparatively stable flow at stations K6, K7 and K8, on the perimeter of the vortex, and the highly variable, rotary nature of the flow at K9 and K10, near the axis of the vortex. These time series also show a few significant events in the wind stress, bottom pressure and along isobath current which will be discussed in a later chapter.

#### E. CTD data

Numerous CTD surveys were conducted over the Kodiak shelf and Alaskan Stream during the course of the study. These data were calibrated with bottom water samples, edited and one-meter averaged for analysis. Some of the data have been used by Schumacher *et al.* (1979) and Reed *et al.* (1980). These hydrographic observations are not fully analyzed here, but are drawn upon or referenced in support of other observations or conclusions.

Figure 6 displays density ( $\sigma\text{-T}$ ) profiles from the axis of Kiliuda Trough, near mooring K10, typical of winter (early spring), summer, and fall stratification. Fall is the peak runoff period in the Gulf of Alaska (Chapter 1), creating a seasonal maximum in stratification as demonstrated by the curve for November; but even then the stratification is very weak. In comparison, the Hudson Shelf Valley (see Introduction) has an order of magnitude greater stratification

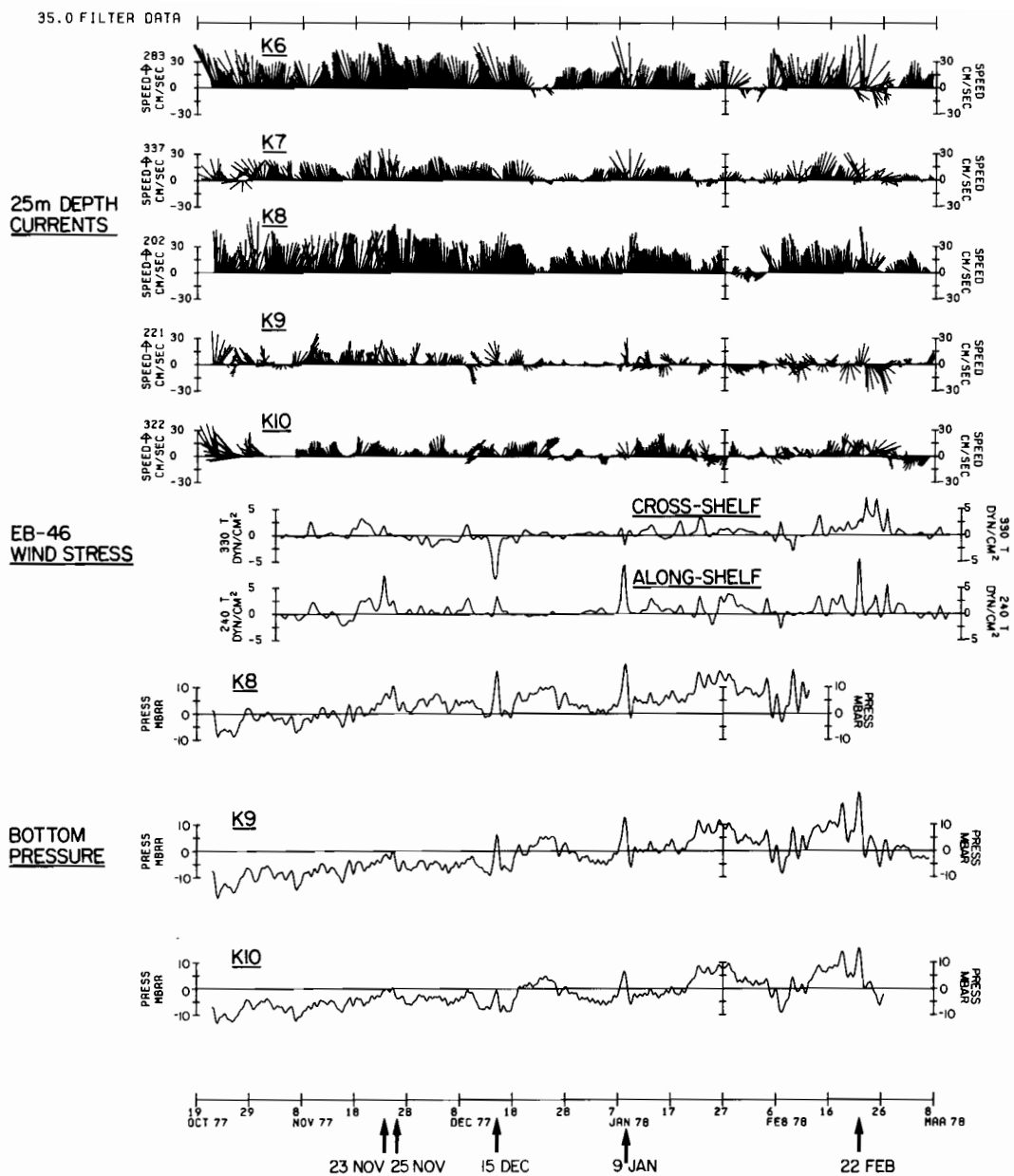


Figure 5. Time series of 35 hour low-pass filtered data during the winter deployment. From top to bottom: 25 meter depth current vectors for stations K6-K10 resolved along individual mean flow axes; cross-shelf ( $330^{\circ}$ T) and along-shelf ( $240^{\circ}$ T) wind stress at EB-46; bottom pressure variations (millibars) at stations K8, K9, K10.

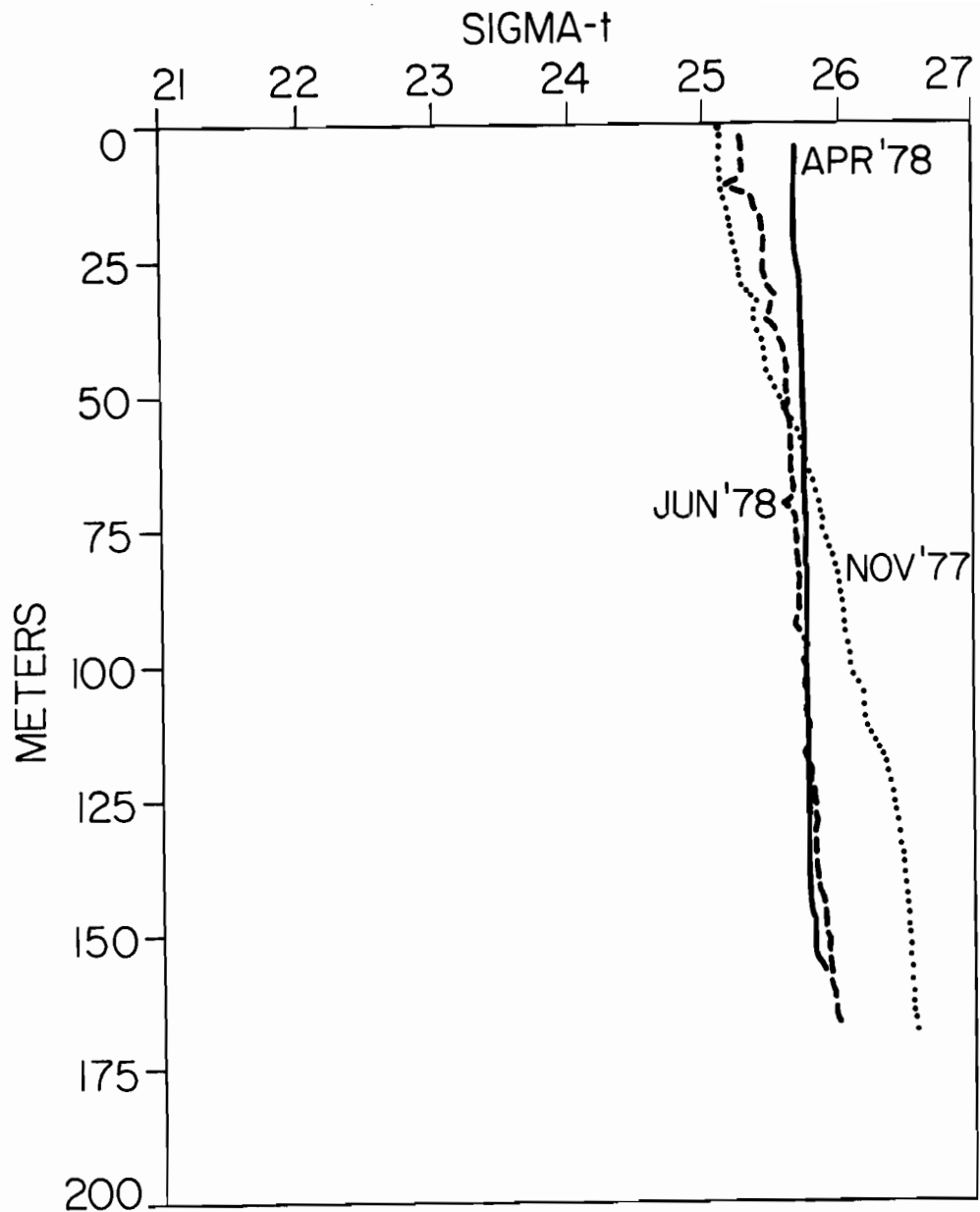


Figure 6. Sigma-t profiles from the axis of Kiliuda Trough (near mooring K9) showing typical seasonal extremes of stratification. The maximum in the fall coincides with peak runoff to the Gulf of Alaska.

$(\partial\sigma_t/\partial z)$  in summer and in the winter is of the same order, but larger, than the peak stratification of the Kiliuda Trough shown here. The relatively weak stratification of the Kiliuda Trough means small baroclinic effects on the flow and allows for a barotropic model to be applied to the Kodiak shelf.

### Chapter 3: Theoretical Discussion

#### A. The Taylor-Proudman Column

The data in the previous section demonstrate two important characteristics of flow over the Kodiak shelf. The flow pattern 1) shows a strong tendency for along isobath flow in the vicinity of Kiliuda Trough, and 2) does not exhibit a significant seasonal variation from winter to summer. The purpose of this chapter is to develop an appropriate theoretical basis to determine the extent of the topographic effects on the flow and its driving mechanisms.

The current pattern around Kiliuda Trough may be interpreted as a Taylor-Proudman column on the shelf. The Taylor-Proudman column is a well-known phenomenon of rotating fluid dynamics (see e.g., Greenspan, 1968) in which steady, inviscid, constant density flow cannot vary in the direction of the axis of rotation. Therefore, horizontal flow does not vary vertically and if encountering an obstacle at the bottom must, at all depths, move around the obstacle, forming a stationary vertical column over the obstacle. This is equivalent to stating that barotropic, geostrophic flow must follow isobaths. The effect can be modified by fluid stratification, non-linearity and viscosity.

Stratified Taylor-Proudman theory has been examined for ocean applications by Hogg (1973), Huppert (1975) and Huppert and Bryan (1976). A non-dimensional stratification parameter,  $S^{\frac{1}{2}}$  (see Table 2), measures the baroclinic effect in quasi-geostrophic theory. For steady (e.g., Huppert, 1975) and unsteady (e.g., Rhines, 1977) stratified quasi-geostrophic flow interacting with topography, a

vertical scale for exponential decay,  $\lambda^{-1} = D/S^{1/2}$ , where D is the depth scale, has been identified. Thus for small  $S^{1/2}$ , the decay scale is large relative to the depth scale and baroclinic shear is small. Table 2 shows a range of  $S^{1/2}$  and  $\lambda^{-1}$  computations representing seasonal extremes of stratification obtained from CTD measurements over the axis of Kiliuda Trough (c.f. Figure 6). Only during the periods of peak stratification was  $\lambda^{-1}$  on the order of the trough axis depth ( $\sim 200$  m); usually it was much greater. The current meter data (Figure 4) show that flow was quite uniform with depth except possibly near the middle of the trough vortex where the depth was greatest and the mean flow weakest. Hide (1971) introduced a veering term  $\sigma^{-1} = D \frac{\partial \phi}{\partial z} \sim S$  (not  $S^{1/2}$ ) where  $\phi$  is the horizontal angle the current vector has with an arbitrary axis. The values of S given in Table 2 would indicate little turning with depth except, again, near the trough axis where  $\Delta\phi$  may be as great as  $(.8)^2$  rad.  $\sim 40^\circ$ . Considering also the comparatively weak stratification over the Kodiak shelf relative to nearby coastal waters where baroclinic flows have been observed, the data and scaling estimates indicate that barotropic theory will be sufficient to evaluate flow over the Kodiak shelf if one keeps in mind that the results will be subject to weak modification due to stratification. (This modification would show the topographically controlled near bottom flow pattern to grow less distinct with distance from the bottom.)

Table 2: Scales and scaling parameters appropriate to the Kiliuda Trough region of the Kodiak Shelf.

---

$U \sim 5 \text{ to } 20 \text{ cm s}^{-1}$	velocity scale
$L \sim 20 \text{ km}$	length scale (trough width)
$f \sim 1.2 \times 10^{-4} \text{ sec}^{-1}$	Coriolis
$A_V \sim 10^2 \text{ cm}^2 \text{ s}^{-1}$	vertical eddy viscosity
$A_H \sim 10^5 \text{ cm}^2 \text{ s}^{-1}$	horizontal eddy viscosity
$D \sim 200 \text{ meters}$	depth scale (trough axis)

$\varepsilon = \frac{U}{fL} \sim .02 \text{ to } .08$	Rossby number
$\frac{E_V}{2} = \frac{A_V}{fD^2} \sim 2 \times 10^{-3}; E_V^{\frac{1}{2}} \sim .06$	vertical Ekman number
$\frac{E_H}{2} = \frac{A_H}{fL^2} \sim 2 \times 10^{-4}$	horizontal Ekman number
$N = \frac{g}{\rho} \frac{\partial \rho}{\partial z}^{\frac{1}{2}} \sim 3.5 \times 10^{-3} \text{ to } 9.5 \times 10^{-3} \text{ s}^{-1}$	Brunt-Väisälä frequency
$S^{\frac{1}{2}} = \frac{ND}{fL} \sim .29 \text{ to } .80$	stratification parameter
$\lambda^{-1} = \frac{fL}{N} \sim 250\text{m to } 700\text{m}$	vertical e-folding scale

---

## B. The Vorticity Equation

Flow over the Kodiak shelf will be studied with a barotropic vorticity equation. It is a form of an equation commonly used in geophysical fluid dynamic studies and the derivation given below is a standard one and not to be construed as this author's own work. It is presented here to orient the reader to the important dynamics and scales. The identification and use of important scaling factors and the subsequent simplification to a form appropriate to the Kodiak shelf are part of the new contributions of this study. A much more complete derivation of the full vorticity equation is given in Pedlosky (1979) chapters 3 and 4. The salient points are given below and the notation used is borrowed from that text.

A right-handed cartesian system is used with the y-axis oriented southwestward along the major bathymetric trend of the Kodiak shelf system. The x-axis is positive shoreward and the origin is located at a reference depth,  $D$ , below the mean sea level (Figure 7). In this study  $D$  is representative of the shelf break depth and the depth of the Kiliuda Trough axis. It is mathematically convenient to locate the origin at the shelf break in the numerical model (Chapter 4) and at the coast in the analytical model (Chapter 5).  $H$  is the local depth; thus  $H = D + \eta - h_B$ , where  $h_B$  is the height of the bottom above the reference level, and  $\eta$  is the sea level displacement. The variable  $h$  is the height of the sea-level above the reference level;  $h = D + \eta$ .

Assuming the fluid to be barotropic and hydrostatic, the horizontal momentum and continuity equations in conventional cartesian notation are:

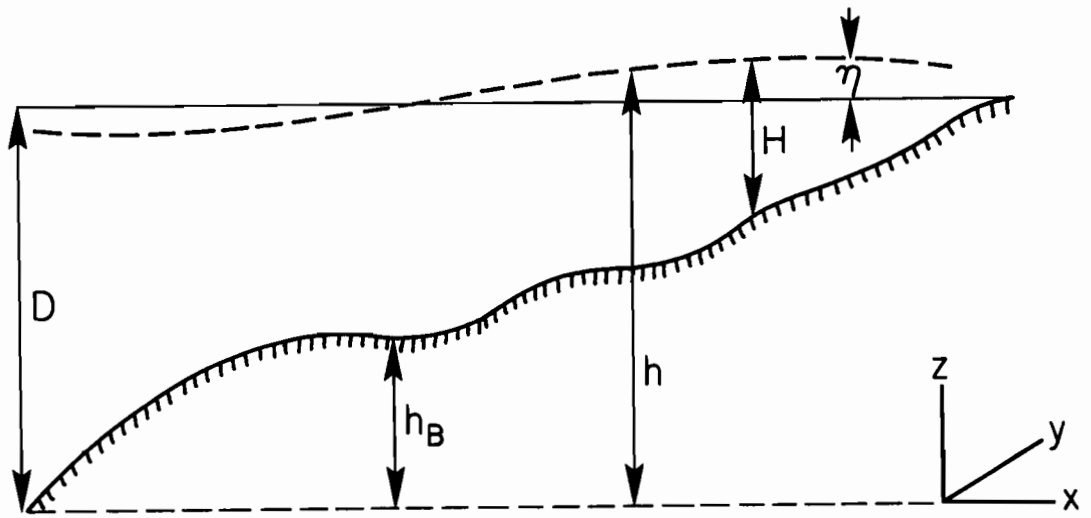


Figure 7. Schematic of the shelf profile, coordinate system and variables used in the text. The y-axis is oriented southwestward along the Kodiak Shelf.

$$\frac{\partial u}{\partial t} + u \frac{\partial u}{\partial x} + v \frac{\partial u}{\partial y} - fv = -g \frac{\partial \eta}{\partial x} + A_H (\nabla^2 u) + A_V \frac{\partial^2 u}{\partial z^2} \quad (3.1a)$$

$$\frac{\partial v}{\partial t} + u \frac{\partial v}{\partial x} + v \frac{\partial v}{\partial y} + fu = -g \frac{\partial \eta}{\partial y} + A_H (\nabla^2 v) + A_V \frac{\partial^2 v}{\partial z^2} \quad (3.1b)$$

$$\frac{\partial u}{\partial x} + \frac{\partial v}{\partial y} + \frac{\partial w}{\partial z} = 0 \quad (3.1c)$$

where  $u, v, w$  are velocity components in the  $x, y, z$  directions,  $f$  is the Coriolis parameter,  $g$  is gravitational acceleration,  $A_H$  and  $A_V$  are the horizontal and vertical kinematic eddy viscosities and  $\nabla^2 = \frac{\partial^2}{\partial x^2} + \frac{\partial^2}{\partial y^2}$ . Scaling the independent variables  $[x, y, z, t]$  by  $[L, L, D, T]$  and the dependent variables  $[u, v, w, \eta]$  by  $[U, U, U \frac{D}{L}, fUL/g]$  the equations can be expressed in terms of non-dimensional variables as follows:

$$\varepsilon_T \frac{\partial u}{\partial t} + \varepsilon(u \frac{\partial u}{\partial x} + v \frac{\partial u}{\partial y}) - v = -\frac{\partial \eta}{\partial x} + \frac{E_H}{2} (\nabla^2 u) + \frac{E_V}{2} \frac{\partial^2 u}{\partial z^2} \quad (3.2a)$$

$$\varepsilon_T \frac{\partial v}{\partial t} + \varepsilon(u \frac{\partial v}{\partial x} + v \frac{\partial v}{\partial y}) + u = -\frac{\partial \eta}{\partial y} + \frac{E_H}{2} (\nabla^2 v) + \frac{E_V}{2} \frac{\partial^2 v}{\partial z^2} \quad (3.2b)$$

$$\frac{\partial u}{\partial x} + \frac{\partial v}{\partial y} + \frac{\partial w}{\partial z} = 0 \quad (3.2c)$$

where  $\varepsilon_T = \frac{1}{fT}$ ,  $\varepsilon = \frac{U}{fL}$  (Rossby number),  $E_H = \frac{2A_H}{fL^2}$  and  $E_V = \frac{2A_V}{fD^2}$  (horizontal and vertical Ekman numbers) and all variables are now non-dimensional.

The form of the vertical Ekman number is convenient because the Ekman layer thickness,  $\delta_E$ , is given by

$$\delta_E = \left(\frac{2Av}{f}\right)^{\frac{1}{2}} = D E_v^{\frac{1}{2}} \quad (3.3)$$

Furthermore, the x-direction transport of the bottom Ekman layer,  $U_E$ , induced by an interior geostrophic flow,  $v$ , in the y-direction is equal to: (Pedlosky, p. 181)

$$U_E = -v \frac{E_v^{\frac{1}{2}}}{2} \quad (3.4)$$

Table 2 gives scales and scaling parameters appropriate to the Kodiak shelf. For the general case, we will assume  $\epsilon_T \sim \epsilon$ . It is clear that  $\epsilon; \frac{E_v}{2}; \frac{E_H}{2} \ll 1$  so the lowest order flow is geostrophic, and the flow can be assumed inviscid, with  $\frac{\partial}{\partial z} \rightarrow 0$ , except in the surface and bottom boundary layers.

In non-dimensional terms, the bottom is at  $z = h_B/D$  and the free surface at  $z = h/D = 1 + \frac{fUL}{gD} \eta = 1 + \epsilon F \eta$ , where  $F = \frac{f^2 L^2}{gD}$ . Integrating the continuity equation between these limits yields

$$\left(\frac{h-h_B}{D}\right) \left(\frac{\partial u}{\partial x} + \frac{\partial v}{\partial y}\right) = w \Big|_{z = \frac{h_B}{D}} - w \Big|_{z = \frac{h}{D}} \quad (3.5)$$

At the bottom,  $w$  is given by (Pedlosky, p 215)

$$w \Big|_{z = \frac{h_B}{D}} = \left(u \frac{\partial}{\partial x} + v \frac{\partial}{\partial y}\right) \frac{h_B}{D} + \frac{1}{2} E_v^{\frac{1}{2}} \zeta \quad (3.6)$$

where  $\zeta = \frac{\partial v}{\partial x} - \frac{\partial u}{\partial y}$  is the relative vorticity. The first term on the right in (3.6) is the vertical motion due to flow over topography and the second term is the bottom Ekman boundary layer pumping (a friction coefficient times the curl of the velocity). At the free surface, ignoring Ekman pumping due to wind stress curl,  $w$  is:

$$w \Big|_{z = \frac{h}{D}} = \frac{1}{D} \frac{\partial h}{\partial t} = \varepsilon F \frac{\partial \eta}{\partial t} + \varepsilon F \left( u \frac{\partial}{\partial x} + v \frac{\partial}{\partial y} \right) \eta \quad (3.7)$$

(Pedlosky, p. 221)

Based on the scales in Table 2, the approximation is made that:

$$\frac{E_H}{2} ; \frac{E_V}{2} \ll \frac{E_V^{\frac{1}{2}}}{2} \sim \varepsilon \ll 1$$

Substituting (3.6) and (3.7) into (3.2a), (3.2b) and (3.5) yields:

$$\varepsilon \left( \frac{\partial u}{\partial t} + u \frac{\partial u}{\partial x} + v \frac{\partial u}{\partial y} \right) - v = - \frac{\partial \eta}{\partial x} \quad (3.8a)$$

$$\varepsilon \left( \frac{\partial v}{\partial t} + u \frac{\partial v}{\partial x} + v \frac{\partial v}{\partial y} \right) + u = - \frac{\partial \eta}{\partial y} \quad (3.8b)$$

$$\varepsilon F \frac{\partial \eta}{\partial t} + \left( u \frac{\partial}{\partial x} + v \frac{\partial}{\partial y} \right) \left( \varepsilon F \eta - \frac{h_B}{D} \right) + \left( 1 + \varepsilon F \eta - \frac{h_B}{D} \right) \left( \frac{\partial u}{\partial x} + \frac{\partial v}{\partial y} \right) = \frac{1}{2} E_V^{\frac{1}{2}} \zeta \quad (3.8c)$$

Next, the dependent variables are expanded in powers of  $\varepsilon$ :

$$u = u_0 + \varepsilon u_1 + \varepsilon^2 u_2 + \dots$$

$$v = v_0 + \varepsilon v_1 + \varepsilon^2 v_2 + \dots$$

$$\eta = \eta_0 + \varepsilon \eta_1 + \varepsilon^2 \eta_2 + \dots$$

Because  $\varepsilon$  is small  $1 \gg \varepsilon \gg \varepsilon^2 \dots$ , and because  $\varepsilon$  is arbitrary, terms of like order in  $\varepsilon$  must balance. To lowest order,  $O(1)$ :

$$v_0 = \frac{\partial \eta_0}{\partial x} \quad (3.9a)$$

$$u_0 = - \frac{\partial \eta_0}{\partial y} \quad (3.9b)$$

$$(u_o \frac{\partial}{\partial x} + v_o \frac{\partial}{\partial y}) \frac{h_B}{D} = (1 - \frac{h_B}{D}) (\frac{\partial u_o}{\partial x} + \frac{\partial v_o}{\partial y}) = 0 \quad (3.9c)$$

By virtue of (3.9a) and (3.9b), the right side of (3.9c) is zero. These equations state that the flow is, to lowest order, geostrophic and confined to flow along isobaths.

A more dynamically relevant equation can be derived if the Rossby number is considered large enough to break the rigid constraint of equation (3.9c). This is done by assuming  $\nabla h_B/D \sim \epsilon$  as a general case as long as the result will degenerate to (3.9c) for  $\nabla h_B/D \gg \epsilon$  (Pedlosky, 1979, Chapter 3). A new variable,  $\eta_B$ , of order 1 is introduced such that:

$$\epsilon \eta_B = \frac{h_B}{D} \quad (3.10)$$

With this, the  $O(\epsilon)$  balances are:

$$\frac{\partial u_o}{\partial t} + u_o \frac{\partial u_o}{\partial x} + v_o \frac{\partial u_o}{\partial y} - v_1 = - \frac{\partial \eta_1}{\partial x} \quad (3.11a)$$

$$\frac{\partial v_o}{\partial t} + u_o \frac{\partial v_o}{\partial x} + v_o \frac{\partial v_o}{\partial y} + u_1 = - \frac{\partial \eta_1}{\partial y} \quad (3.11b)$$

$$F \frac{\partial \eta_o}{\partial t} + (u_o \frac{\partial}{\partial y} + v_o \frac{\partial}{\partial x}) (F \eta_o - \eta_B) + \frac{\partial u_1}{\partial x} + \frac{\partial v_1}{\partial y} = \frac{r}{2} \zeta_o \quad (3.11c)$$

$$\text{where } r = \frac{E^{\frac{1}{2}}}{v} ; \zeta_o = \frac{\partial v_o}{\partial x} - \frac{\partial u_o}{\partial y}$$

Equations (3.11a) and (3.11b) can be cross-differentiated and substituted to (3.11c) to eliminate  $u_1$ ,  $v_1$  and  $\eta_1$  and yield the following quasi-geostrophic potential vorticity equation

$$\left( \frac{\partial}{\partial t} + u_o \frac{\partial}{\partial x} + v_o \frac{\partial}{\partial y} \right) (\zeta_o - F\eta_o + \eta_B) + \frac{r}{2} \zeta_o = 0 \quad (3.12)$$

In the strictly inviscid limit, where  $r \ll 1$  (i.e.  $\varepsilon_T; \varepsilon \gg E_V^{1/2}$ ), it can be shown that, to  $O(\varepsilon^2)$ , the dimensionalized version of (3.12) is equivalent to the more familiar inertial potential vorticity conservation relation:

$$\frac{D}{Dt} \left( \frac{\zeta+f}{H} \right) = 0 \quad (\text{Pedlosky, p. 91})$$

Henceforth, we will consider the steady state version of (3.12), and introduce the geostrophic streamfunction  $\psi = \eta_o$  and  $\nabla^2 \psi = \zeta_o$ . The coefficient  $F = \frac{f^2 L^2}{g D} = \frac{L^2}{R^2}$  where  $R$  is the barotropic Rossby radius.  $F$  is a relative measure of the vorticity induced by displacement of the free surface. For a continental shelf,  $F \ll 1$ , which is a rigid lid approximation, and terms of  $O(F)$  can be neglected. Equation (3.12) is now rewritten:

$$\left( \frac{\partial \psi}{\partial x} \frac{\partial}{\partial y} - \frac{\partial \psi}{\partial y} \frac{\partial}{\partial x} \right) \frac{h_B}{D} + \varepsilon \left( \frac{\partial \psi}{\partial x} \frac{\partial}{\partial y} - \frac{\partial \psi}{\partial y} \frac{\partial}{\partial x} \right) \nabla^2 \psi + \frac{1}{2} E_V^{1/2} \nabla^2 \psi = 0 \quad (3.13)$$

It can be seen that the approximation (3.9c) can be recovered from (3.13) for  $\nabla (h_B/D) \gg \varepsilon; E_V^{1/2}$ .

### C. The Potential Vorticity and Ekman Pumping approximations.

Equation (3.13) represents a vorticity balance between three terms: the vorticity induced by flow across isobaths which is of

order  $\nabla(h_B/D)$ , a vorticity advection term of order  $\epsilon$ , and a bottom boundary layer pumping term of order  $\frac{E_v^{1/2}}{2}$ . The topographic term is generally the largest on the shelf. The small deviations between streamlines and isobaths may be balanced by the advective term or pumping terms, or both, depending on the relative scaling of  $\epsilon$  and  $\frac{E_v^{1/2}}{2}$ . For  $\frac{E_v^{1/2}}{2} \gg \epsilon$ , the balance is:

$$\left(\frac{\partial\psi}{\partial x}\frac{\partial}{\partial y} - \frac{\partial\psi}{\partial y}\frac{\partial}{\partial x}\right) \frac{h_B}{D} + \frac{1}{2} E_v^{1/2} \nabla^2\psi = 0 \quad (3.14)$$

and for  $\epsilon \gg \frac{1}{2} E_v^{1/2}$

$$\left(\frac{\partial\psi}{\partial x}\frac{\partial}{\partial y} - \frac{\partial\psi}{\partial y}\frac{\partial}{\partial x}\right) \left(\frac{h_B}{D} + \epsilon\nabla^2\psi\right) = 0 \quad (3.15)$$

The first of these, (3.14), is a linear vorticity balance in common use in quasi-geostrophic modeling on complex shelves (where it is usually in a dimensional form using bottom layer thickness in place of  $\frac{1}{2}E_v^{1/2}$  and pressure as the dependant variable; e.g., Galt, 1980; Hsueh, 1980; Han *et al.*, 1980; Mayer *et al.*, 1982). It basically states that positive (negative) vorticity must exist at a point if flow is toward deeper (shallower) water. Equation (3.15), on the other hand, represents the conservation along a streamline of the quantity  $\frac{h_B}{D} + \epsilon\nabla^2\psi$ , the potential vorticity. This relation states that relative vorticity must increase (decrease) downstream if flow is toward deeper (shallower) water. Put another way, (3.14) states that the maximum relative vorticity occurs over the maximum topographic

gradient, whereas (3.15) states that the maximum vorticity gradient occurs over the maximum topographic gradient. It seems, then, that the two effects are spatially out of phase to some extent.

The modeling studies of Galt (1980) made use of (3.14) as a generalized linear formulation to be applied to a variety of coastal settings. (It can also be generalized further to include baroclinicity). He applied his barotropic model to several case studies including the Kodiak shelf. On the other hand, the potential vorticity conservation relation (3.15) will be used here in the present study. The scaling factors (Table 2) show that  $\varepsilon \sim \frac{1}{2}E_V^{\frac{1}{2}}$ , so that (3.15) is no less valid than (3.14) for the Kodiak shelf. There is, therefore, an opportunity to compare results of these two formulations, as will be shown below.

Equation (3.15) is used here because the data strongly suggested potential vorticity conservation with cyclonic flow around a deep trough. Inertial effects can be important on shelves, such as Kodiak, with large vertical scale bathymetric features of short length scales giving a comparatively large Rossby number. In this case the Rossby number is small enough for the lowest order momentum balance to remain geostrophic while remaining large enough for inertial terms to be important to the ageostrophic components of the momentum and vorticity balances. As in the cases mentioned above, anticyclonic flow around shallow banks indicates potential vorticity conservation whereby relative vorticity becomes more anticyclonic along streamlines where flow is toward shallower water. The data presented above from the

Kiliuda Trough suggest the same mechanism with a Taylor-Proudman column of cyclonic relative vorticity associated with greatest depth.

Equation (3.15) was derived by assuming  $h_B/D$  is small, or  $O(\epsilon)$ . As such it is a valid approximation for the lowest order flow since it approaches

$$\left( \frac{\partial \Psi}{\partial x} \frac{\partial}{\partial y} - \frac{\partial \Psi}{\partial y} \frac{\partial}{\partial x} \right) \frac{h_B}{D} = 0 \quad (3.16)$$

for  $h_B/D \rightarrow 0(1)$  (Pedlosky, 1979, p. 91). This is the well known result that, with large topographic relief, geostrophic flow follows depth contours. The expression for potential vorticity,  $\epsilon \nabla^2 \Psi + h_B/D$ , however, is valid only for small  $h_B/D$ . Therefore, equation (3.15) is only an approximation for potential vorticity conservation (in dimensional variables with  $\zeta$  as relative vorticity and  $H$  as depth):

$$\left( u \frac{\partial}{\partial x} + v \frac{\partial}{\partial y} \right) \frac{f + \zeta}{H} = 0 \quad (3.17)$$

If this expression is non-dimensionalized and expanded in powers of  $\epsilon$ , it is found that equation (3.15) retains some  $O(\epsilon)$  terms while neglecting others where  $h_B/D \rightarrow 0(1)$ . Nevertheless, in that limit, the potential vorticity is so dominated by the topographic balance (3.16) that the effect would hardly be noticeable. The main advantage of using (3.15) over (3.17) is that it avoids the singularity of  $H \rightarrow 0$  near the coast and facilitates the numerical computation while still adequately approximating the lowest order flow.

## Chapter 4: Topographic Effects on the Kodiak Shelf Flow

### A. The Numerical Potential Vorticity Model

In the foregoing chapter, the choice of the inertial potential vorticity equation (3.15) was made because the data indicate potential vorticity conservation. In this chapter, results from a numerical model of the Kodiak Shelf employing (3.15) are given. It is shown that with realistic scaling, the flow patterns evident in the current meter observations can be accurately reproduced.

Equation (3.15), with (3.10), states that potential vorticity,  $\nabla^2\psi + \eta_B$ , is conserved along a streamline. An equivalent expression is:

$$\nabla^2\psi + \eta_B = K(\psi) \quad (4.1)$$

which states that the potential vorticity is a function of  $\psi$ . The function  $K(\psi)$  is a value that must be determined for each streamline.

Equation (4.1) was applied to the Kodiak shelf by employing a numerical finite differencing technique. The details of the numerical scheme are given in the appendix and a schematic of the model is shown in Figures 8 and 9. For convenience, the y-axis was located at the seaward boundary and was made a streamline to take into account the kinematic effect of the Alaskan Stream. Velocity scales (Table 2) were chosen to be typical of currents on the shelf which would be considerably weaker than in the core of the stream. The shoreline was assumed a streamline where  $\psi = 0$ . The sea-level decrease from the coast seaward and consequent geostrophic flow entering from the right

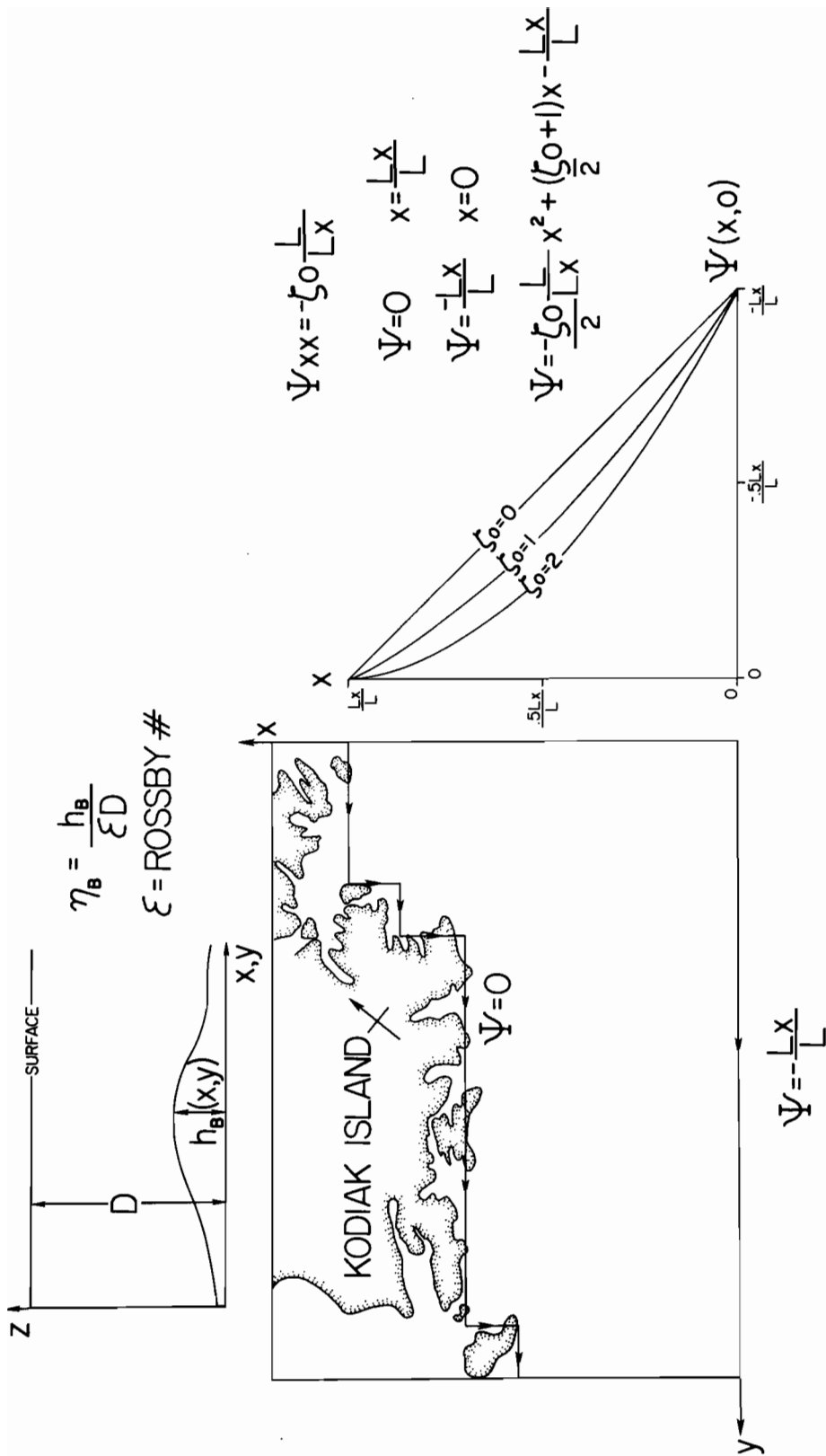


Figure 8: Schematic of the numerical model and boundary conditions. See text for definitions of variables.

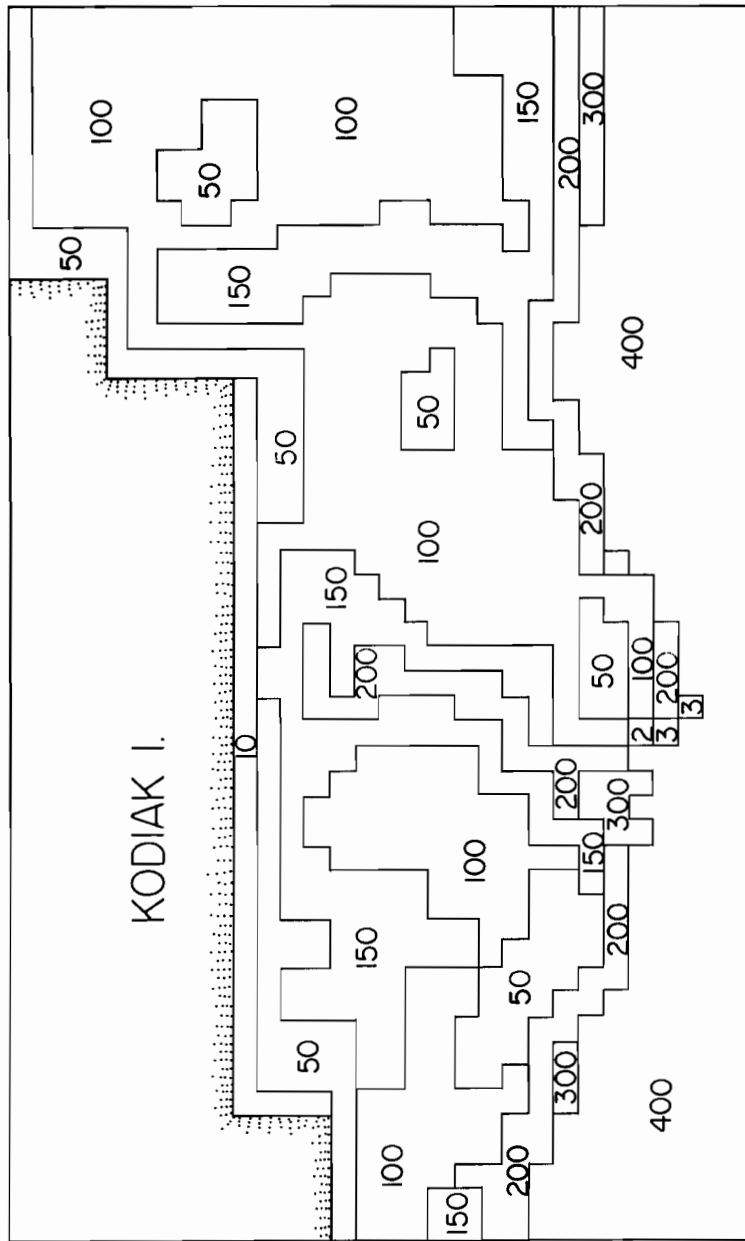


Figure 9. Schematic of the rectangular grid pattern for bathymetry in the numerical model. Depths are in meters.

was assumed based on the regional circulation. (In the next chapter this will be discussed quantitatively.) The x-axis is the upstream (right-hand) boundary where a cross-shelf distribution of  $\psi$  was imposed so that the function  $K(\psi)$  could be determined. For simplicity, the stronger flow of the Alaskan Stream, which remains seaward of the shelf break, was not included in this boundary condition on  $\psi$ . The exact form of this  $\psi$  distribution was not qualitatively important, as shown below. A parabolic function was used assuming  $\frac{\partial^2 \psi}{\partial y^2} = 0$  and  $\frac{\partial^2 \psi}{\partial x^2} = -\zeta_0 \frac{L}{L_x}$ , where  $L$  is the length scale (Table 2) and  $L_x$  is the dimensional shelf width along the x-axis. The resulting boundary condition along the x-axis ( $y=0$ ) is:

$$\psi = \frac{-\zeta_0}{2} \frac{L}{L_x} x^2 + \left(\frac{\zeta_0}{2} + 1\right)x - \frac{L_x}{L} x \quad (4.2)$$

and, from this:

$$\frac{\partial \psi}{\partial x} = -\zeta_0 \frac{L}{L_x} x + \frac{\zeta_0}{2} + 1 \quad (4.3)$$

From (4.3), the boundary condition defines the cross-shelf profile of velocity entering the right hand side of the model.  $\zeta_0$  represents a scaled relative vorticity of the flow and can range from 0 to 2 with no counter flow imposed at the coast. Furthermore,  $\frac{\partial \psi}{\partial x}$  is unity midway along the x-axis, at  $x = \frac{L_x}{2L}$ , meaning that the velocity scale,  $U$ , represents the cross-shelf averaged along-shelf velocity at the upstream boundary.

## B. Model Results: The Along-Isobath Flow Limit

The Rossby number,  $\varepsilon$ , was determined for the model by choice of a velocity scale with the length scale fixed at  $\sim 20$  km (Kiliuda Trough width). Only small Rossby numbers validate the quasigeostrophic theory and, as expected, the model predicts a strong tendency for flow along isobaths when velocity scales of  $U = 5, 10, \text{ and } 20 \text{ cm s}^{-1}$  ( $\varepsilon = .02, .04, .08$ ) were employed (Figures 10a,b,c). These speeds are typical of direct current observations (Figure 4). As the theory predicts, flow with the smaller Rossby numbers shows the greatest topographic effect and tends to form a cyclonic vortex over the trough.

The parameter  $\zeta_0$  is the amount of relative vorticity along the upstream boundary and the effect of varying  $\zeta_0$  from 0 to 2 is evident in Figures 11a,b. Clearly this parameter does not qualitatively effect the imprint of the topography on the flow. The quantitative differences between these examples is discussed in the context of larger scale forcing in the next chapter.

It is evident from Figure 10 that with decreasing  $\varepsilon$ , the flow also tends to become more of a jet-like current confined to the region of greatest topographic relief. This result owes to the small Rossby number limit of streamlines closely following isobaths. Where isobaths converge, so will streamlines, causing stronger flow over steeper topography. This effect is quantitatively demonstrated by employing, in dimensional terms, the lowest order balance:

$$\frac{\partial \psi}{\partial x} \frac{\partial h_B}{\partial y} - \frac{\partial \psi}{\partial y} \frac{\partial h_B}{\partial x} = 0 \quad (4.4)$$

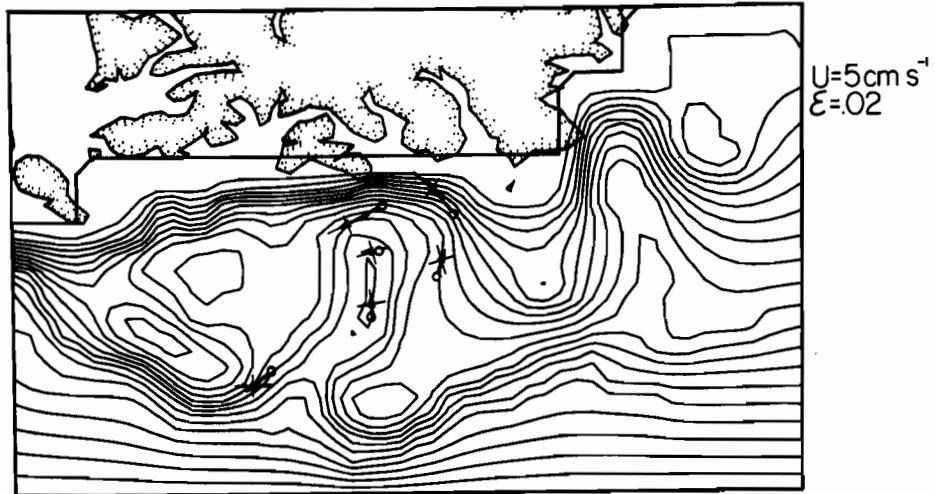


Figure 10a. Streamlines for a Rossby number determined from  $U = 5$   $\text{cm s}^{-1}$  ( $\epsilon = .02$ ) and  $\zeta_0 = 1$ . Streamline spacing midway along the right hand boundary represents the velocity scale. Mean 25 meter depth winter currents are superimposed.

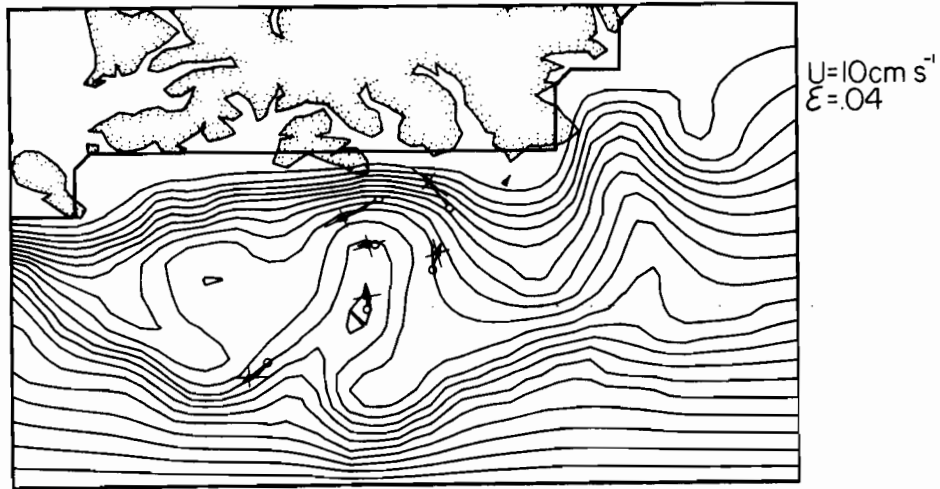


Figure 10b. Streamlines for a Rossby number determined from  $U = 10$ ,  $\text{cm s}^{-1}$  ( $\epsilon = .04$ ) and  $\zeta_0 = 1$ . Streamline spacing midway along the right hand boundary represents the velocity scale. Mean 25 meter depth winter currents are superimposed.

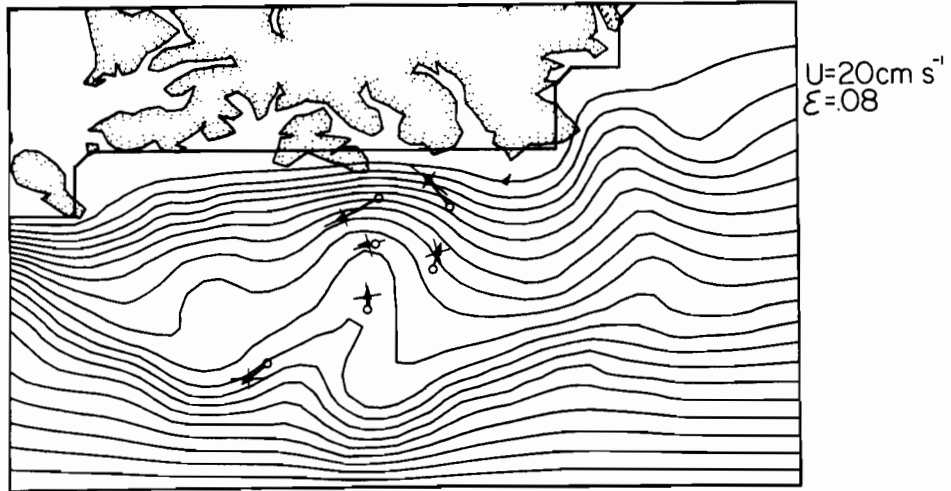


Figure 10c. Streamlines for a Rossby number determined from  $U = 20$ ,  $\text{cm s}^{-1}$  ( $\epsilon = .08$ ) and  $\zeta_0 = 1$ . Streamline spacing midway along the right hand boundary represents the velocity scale. Mean 25 meter depth winter currents are superimposed.

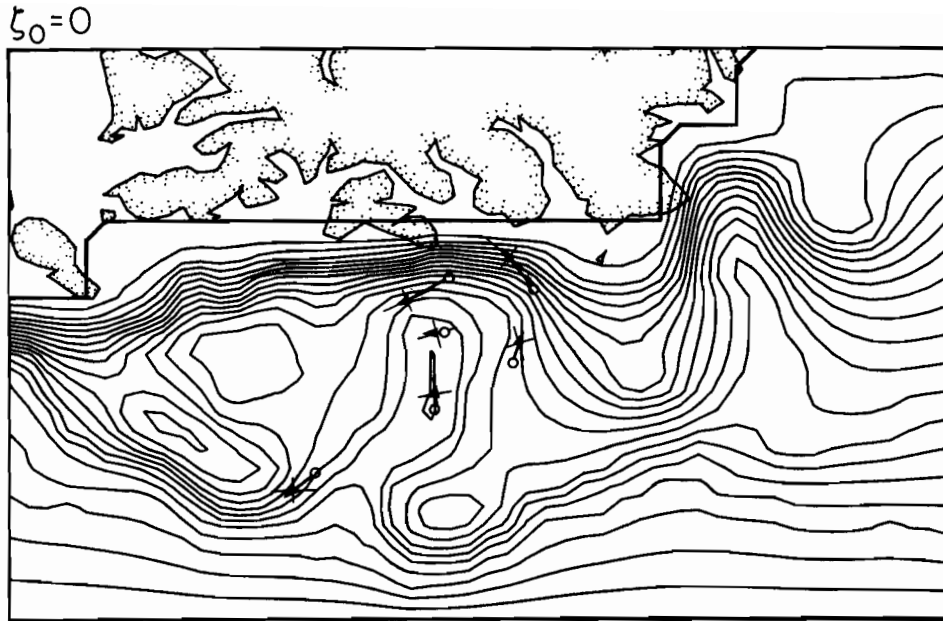


Figure 11a. Same as 10a except that  $\zeta_0=0$ , or no relative vorticity along the upstream boundary.

$\zeta_0 = 2$

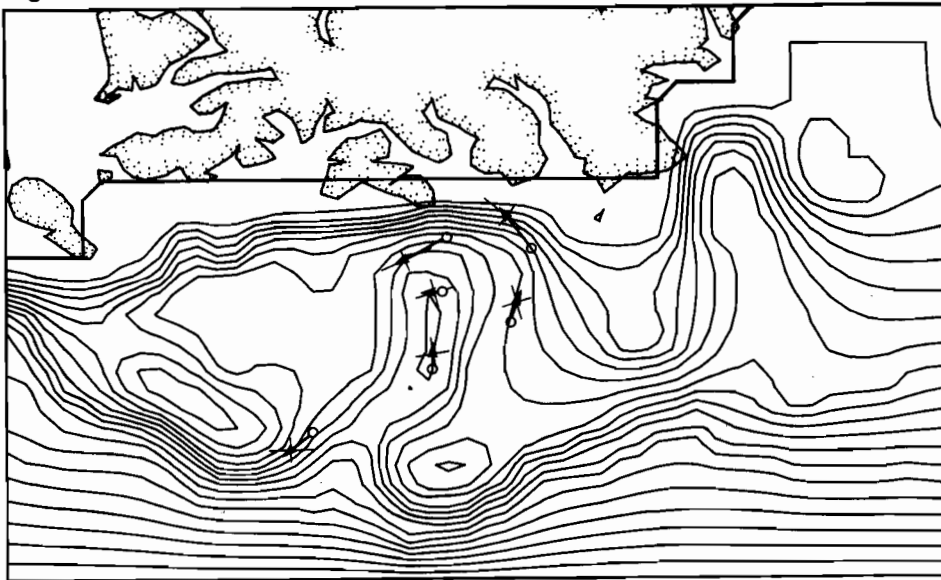


Figure 11b. Same as 10a except that  $\zeta_0 = 2$ , representing inflow along the upstream boundary that is maximum at the shelf break and zero at the coast.

where  $\Psi$ ,  $x$ , and  $y$  are now dimensional variables. Equation (4.4)

requires that  $\Psi = \Psi(h_B)$  and

$$u = -\frac{\partial \Psi}{\partial y} = -\frac{\partial \Psi}{\partial h_B} \frac{\partial h_B}{\partial y} \quad \text{and} \quad v = \frac{\partial \Psi}{\partial x} = \frac{\partial \Psi}{\partial h_B} \frac{\partial h_B}{\partial x} \quad (4.5)$$

In vector notation

$$\vec{v} = \frac{\partial \Psi}{\partial h_B} \vec{k} \times \vec{\nabla}_{h_B} \quad (4.6)$$

and

$$\left| \vec{v} \right| = \frac{\partial \Psi}{\partial h_B} \left| \vec{\nabla}_{h_B} \right| \quad (4.7)$$

where  $\left| \right|$  indicates vector magnitude and  $\vec{k}$  is the vertical unit vector. Thus, along a streamline, the current magnitude should be proportional to the local gradient of depth.

For moorings K6, K7, and K8 the values of  $\left| \vec{\nabla}_{h_B} \right|$  were estimated over intervals of 5, 10, and 15 km and averaged (Table 3). The values of  $\left| \vec{v} \right| / \left| \vec{\nabla}_{h_B} \right|$  were then computed from the mean currents and are shown to be quite close, ranging between  $3.0$  and  $4.2 \times 10^3 \text{ cm s}^{-1}$ . Averaging these values indicates that  $\partial \Psi / \partial h_B \sim 3.5 \times 10^3 \text{ cm s}^{-1}$ .

Since

$$\frac{\Delta \Psi}{\Delta x} \cong \frac{\Delta \Psi}{\Delta h_B} \frac{\Delta h_B}{\Delta x} \quad (4.8)$$

the cross-shelf average of the along-shelf flow at the upstream

Table 3. Values of local topographic gradient averaged over 5, 10, 15 km and their ratios with mean current at stations K6, K7 and K8.

	$\left  \vec{\nabla} h_B \right  \times 10^3$		
Current meter stations:	<u>K6</u>	<u>K7</u>	<u>K8</u>
Distance (km)			
5.	10.0	0.8	4.8
10.	7.0	2.2	6.5
<u>15.</u>	<u>4.7</u>	<u>4.5</u>	<u>11.3</u>
average	7.2	2.5	7.5
$\left  \vec{v} \right  \text{ cm s}^{-1}$	21.5	10.6	25.1
$\left  \vec{v} \right  / \left  \vec{\nabla} h_B \right  \times 10^{-3} \text{ cm s}^{-1}$	3.0	4.2	3.3
$\left  \vec{v} \right  / \left  \vec{\nabla} h_B \right $ average for all three stations = $3.5 \times 10^3 \text{ cm s}^{-1}$			

boundary of the model can be estimated using  $\Delta h_B \cong 200$  m and  $\Delta x \cong 150$  km to yield  $\frac{\Delta \Psi}{\Delta x} \cong 4.7$  cm s<sup>-1</sup>. This implies that  $\sim 5$  cm s<sup>-1</sup> is an appropriate velocity scale for the shelf flow. As evidenced in Figure 10, the model and data are in good agreement with this scaling. Of the three velocity scales shown, the streamline pattern matched the observed currents best for the  $U = 5$  cm s<sup>-1</sup> case. Currents of appropriate speeds around the trough were reproduced by the model owing to the tendency of the streamlines to be concentrated by the topography. This result implies that a very weak cross-shelf-averaged along-shelf flow ( $\sim 5$  cm s<sup>-1</sup>) will support the stronger along-isobath current observed around the trough.

The above estimates give added credibility to the numerical model used in this study. They imply that the model is successful because it produces the lowest order balance (4.4) from the governing potential vorticity equation (3.15) with an appropriately small Rossby number.

### C. Comparison with the Ekman Pumping Equation

In Chapter 3, equation (3.14), was discussed as perhaps being suitable for this study because it has been applied in several other models of shelf flow with topography. Henceforth, (3.14) will be referred to as the Ekman pumping equation since it is a balance of vorticity induced by flow across isobaths against Ekman pumping in the bottom boundary layer. It is clear that if  $\frac{1}{2}E_v^{\frac{1}{2}}$  is also appropriately small that the lowest order balance (4.4) will again emerge and results from the two approaches should be very similar. Han (1982, personal communication) has indicated that, in applying Galt's (1980) model to the Hudson Shelf Valley currents, when the bottom layer thickness parameter (equivalent to  $E_v^{\frac{1}{2}}$ ) was decreased the modeled currents become more confined to isobaths.

Galt (1980) applied his model of the Ekman pumping equation to the Kodiak Shelf, which presents an opportunity for comparison. Figure 12 reproduces the barotropic velocity field from Galt's (1980) model. It is driven by a cross-shelf sea-level slope imposed at the upstream boundary, as is the model presented above. It is clear that the topography again exerts a large influence on the mean flow pattern. There are, however, noticeable differences between the two models (see Figure 10) which reflect the different nature of the governing equations.

It was discussed in Chapter 3 that Ekman pumping requires relative vorticity be present over a sloping bottom. Where currents cross isobaths toward deeper water, the relative vorticity should be positive (counter-clockwise) and greatest where the bottom slope is

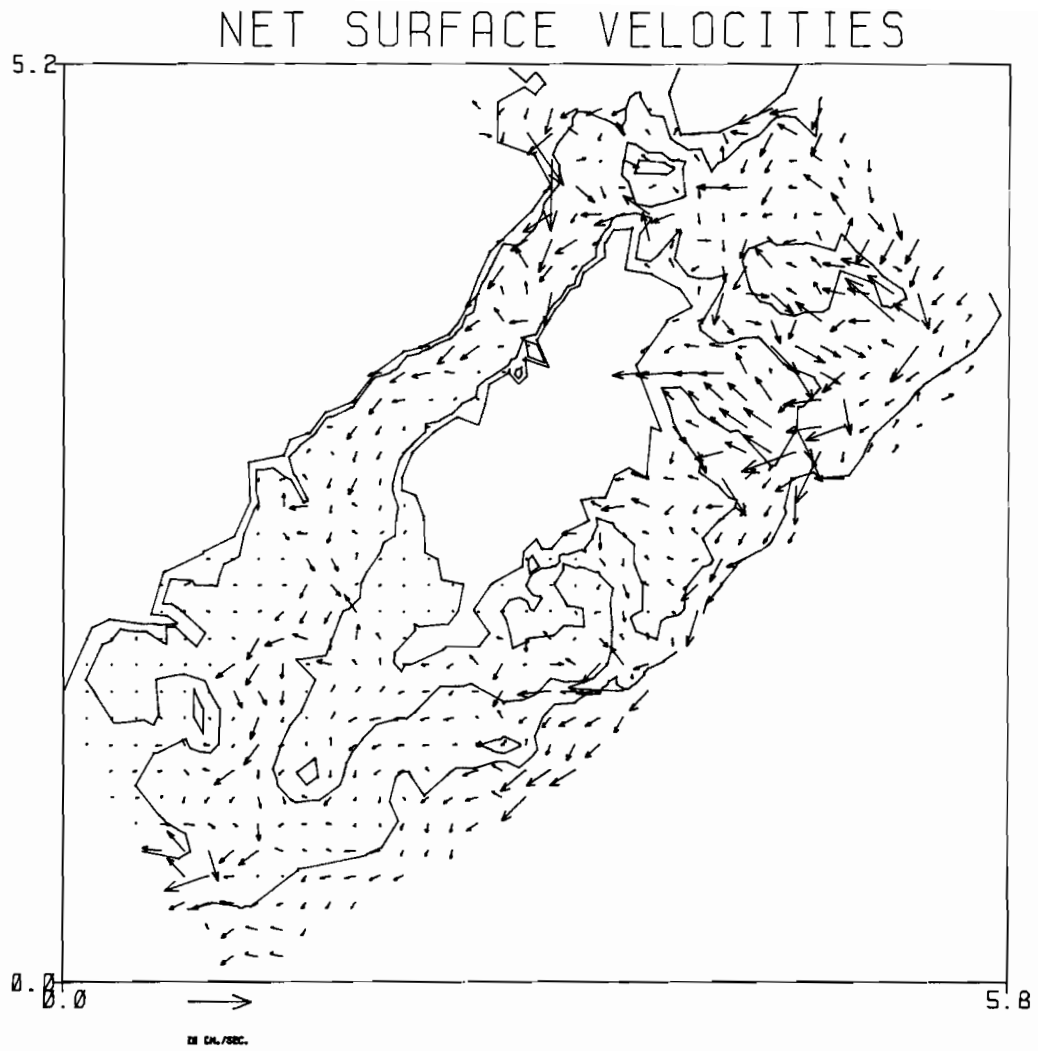


Figure 12. Barotropic velocity vectors from the numerical model of Galt (1980) which used the Ekman pumping equation (see text). (Courtesy of J. A. Galt.)

steepest. Consequently, along-shelf flow encountering the eastern edge of Kiliuda Trough would be deformed so as to produce positive vorticity over the trough edge. This, in turn, would induce seaward down-channel flow along the trough axis, as evident in Figure 12.

The potential vorticity equation (3.15), modeled in Figures 10 and 11, requires that the vorticity be associated with maximum depth rather than depth gradient. This creates a vortex centered over the trough axis not the trough edge. The data support this model, especially the trough axis stations, K9 and K10 (Figure 4), which indicate generally up-channel flow.

In both models under discussion, the magnitude of the terms that measure the departure from strict along isobath flow are scaled by  $\frac{1}{2}E_v^{\frac{1}{2}}$  in the Ekman pumping relation and by  $\epsilon$  in the potential vorticity relation. Figure 12 was generated from the Ekman pumping relation with  $\frac{1}{2}E_v^{\frac{1}{2}}$  equal to 0.25 (Galt, 1982, personal communication). This is comparable to the  $\epsilon = .02$  used in the potential vorticity model here. Therefore, the disagreement between the models is not due to a disparity in these parameters.

The difference between the model results is more likely due to the behavior of the various terms and geometry of the flow. The geometry of the problem is important because the flow conforming to isobaths forms the positive vortex defacto when the flow on the Kodiak Shelf is generally southwestward. With decreasing Rossby number, the model shows that the vortex actually becomes more pronounced. Both equations under discussion are abbreviations of the more general equation (3.13) which can be presented cryptically as

$$T + P + E = 0$$

where  $T$  is the topographic term,  $P$  the potential vorticity advection and  $E$  the Ekman pumping. The term  $T$  will be positive if flow is toward shallow water,  $P$  will be positive when flow is along an increasing relative vorticity gradient and  $E$  is proportional to the local relative vorticity. By virtue of the fact that the flow follows the topography around the trough, the relative vorticity is maximum at the trough axis and near zero along the trough edge. This causes  $E$  to be very small along the trough edge, favoring the balance  $T + P = 0$ . A model including  $E$  but ignoring  $P$  would simulate flow turning down-channel as indicated by Figure 12. In short, the along-isobath flow constraint favors the balance  $T + P = 0$  because  $E$  is naturally small. The balance  $T + E = 0$  does not allow the flow to follow isobaths as closely as the data indicate it should. The inclusion of relative vorticity advection terms ( $P$ ) in modeling this complex shelf is justifiable and the use of (3.15) instead of (3.14) is physically more realistic for this case study.

#### D. Comparison with the Hudson Shelf Valley

The geographic setting of the Hudson Shelf Valley (HSV) is similar to that of Kiliuda Trough. Both are oriented cross-shelf, the coastal orientation is NE-SW and the mean along-shelf flow is similarly southwestward. The Ekman pumping equation has been applied to address the topographic effects of the HSV by Hsueh (1980), Han *et al.* (1982) and Mayer *et al.* (1982). As with Galt (1980), these models

predict down-channel flow in the absence of wind forcing when the shelf flow is southwestward. Mayer et al. (1982) show that the long term mean flow is up-valley and that it is accounted for by the along-axis pressure field being reversed in deeper water (>40 m) because of the density field. They further show that the up-valley flow is enhanced by a northeastward wind stress, due to coastal Ekman divergence, even when the wind stress is not strong enough to reverse the flow on the shelf. A southwestward wind stress, however, augments the shelf flow and the barotropic along-axis pressure gradient in the HSV to generate down-valley flow.

On the Kodiak Shelf, the predominant wind stress is southwestward and yet up-valley mean flow is indicated by the data. The HSV is both narrower, shallower and more highly stratified than the Kiliuda Trough. For the HSV,  $\epsilon \sim E_v^{3/2} \sim 0.15$ , which are almost an order of magnitude larger than for Kiliuda. Since these terms measure the departure from strict along-isobathic geostrophic flow (Chapter 3), an ageostrophic along-axis flow in response to an along-axis pressure gradient (Han et al., 1980) should be more important to the dynamics of the HSV than it would be for the Kiliuda Trough.

#### E. Chapter Summary

In this chapter the smaller scale features (20-50 km) in the steady currents over the Kodiak Island shelf were studied with a barotropic numerical potential vorticity model. Measured mean currents on the shelf were accurately reproduced by the model under proper scaling, the dominant effect of the rugged bathymetry is

steering the flow was demonstrated. The model farther demonstrates the existence of a steady cyclonic vortex over the Kiliuda Trough, which is here interpreted as a Taylor Proudman column. The strength of the mean flow is shown to vary along a streamline in proportion to the local topographic gradient. This is required by the limit of along-isobath flow, whereby streamlines are converged along with isobaths over steep topography.

The appropriateness of the potential vorticity formulation used here was discussed in comparison with a linear vorticity equation balancing the topographic term and bottom Ekman pumping. The potential vorticity model, which requires greater vorticity over deeper water, was more successful at reproducing the currents measured in the vicinity of Kiliuda Trough because of the cyclonic circulation established by flow following topographic contours around the trough.

## Chapter 5: The Alaskan Stream Driven Mean Shelf Flow

### A. Statement of the Problem

The numerical model in the foregoing chapter was solved using an inflow condition across the right hand boundary. This mean along-shelf flow was presumed to be part of the year round southwestward regional shelf circulation described in Chapter 1. The larger scale shelf dynamics are now studied to account for this flow. An analytical model is presented to support the hypothesis that the mean shelf currents are largely induced by the Alaskan Stream. This is an attractive model for the Northwest Gulf of Alaska because it helps account for the lack of seasonal variability in the outer shelf currents in the presence of large seasonal variations in wind stress, as discussed in Chapters 1 and 2.

Particular use is made of existing theory, namely the "Arrested Topographic Wave" model given by Csanady (1978) (hereinafter referred to as ATW). It is a simple, well studied linear equation, analogous to the classic heat equation, which has proved to be a useful model for shelf studies when appropriate boundary conditions are applied. New solutions to this equation are introduced below which are developed from boundary conditions appropriate to shelves bounded on the seaward side by a strong oceanic boundary current.

In the original work, Csanady (1978) did discuss the forcing of shelf currents by the oceanic circulation with an externally applied along-shelf sea level gradient. This solution reveals some relevant physics of the Alaskan shelf currents and is therefore given a

detailed discussion below. However, it is not completely satisfactory for this case study. First, the necessary along-shelf pressure gradient, sloping down to the southwest, cannot be reliably demonstrated by some external mechanism. Secondly, Csanady (1978) did not address the potential effect of a strong western boundary current on the adjacent shelf flow.

Shaw (1982) analyzed the flow on the shelf driven by an along-shore thermohaline current over the slope. However, he only addressed the along-shelf pressure gradient set up by this baroclinic current and found it to be two orders of magnitude too small to account for shelf currents with the ATW model. He also addressed the forcing of shelf flow by deep ocean currents with a vorticity equation for the bottom pressure field. In his formulation, the bottom pressure field is the surface pressure field reduced by the baroclinic field and is a characteristically weak signal in the wind driven ocean circulation (i.e., the concept of a level of no motion). He shows that the continental slope effectively insulates the deep ocean pressure field from the shelf. In this context, his discussions relate more to boundary conditions for the deep ocean flow than for shelf flow.

The effect that a strong baroclinic boundary current over the continental slope would have on the cross-shelf pressure gradient at the shelf break has not been addressed. Nevertheless, Shaw's (1982) formulation does allow for such an analysis and is used below to estimate the strength of a shelf break geostrophic current caused by the Alaskan Stream. This shelf break current then becomes the boundary condition for the shelf problem.

The new solution to the ATW equation introduced here incorporates the cross-shelf pressure gradient at the shelf break caused by a boundary current such as the Alaskan Stream. Although it has similar properties to the earlier result by Csanady, it demonstrates that flow on the shelf can be caused by the cross-shelf, rather than the along-shelf, pressure gradient imposed at the shelf break by the oceanic circulation over the continental slope.

Solutions including coastal wind stress are also given. In Chapter 7 comparisons are made with the East Florida Shelf and South Atlantic Bight, which are shelves bordered by the Gulf Stream.

#### B. The Large Scale Along-Shelf Averaged Vorticity Balance

Before presenting any solutions, the applicability of the ATW model to the Northwest Gulf of Alaska shelf must be examined. An important assumption in Csanady's (1978) formulation was uniform bathymetry in the along shelf direction. In contrast, the Kodiak shelf flow is strongly controlled by deep cross-shelf features. The governing equation (3.13), derived in Chapter 3, is horizontally isotropic and nonlinear owing to these small along-shelf length scales. The length of the Northwest Gulf of Alaska shelf system, on the other hand, which extends from the Kenai Peninsula to the Aleutian Islands (Figure 1), is many times longer than these topographic and flow features. It seems more appropriate, therefore, that the large scale dynamics should be governed by a more simple anisotropic vorticity balance. Such a balance, namely the ATW equation, can be reduced from equation (3.13) by making a few liberal assumptions and

performing an along-shelf average. In this way, the ATW equation is proposed here to model the cumulative dynamics over a long segment of the shelf where along-shelf topographic variations of short length scale are significant.

For this application, it is convenient to consider the following substitutions:

$$h_B = \hat{h}_B^*(x) + h_B'(x) g(y) \quad (5.1a)$$

$$\psi = \hat{\psi}^*(x) + \hat{\psi}(y) + \psi'(x) g(y) \quad (5.1b)$$

The dominant cross-shelf varying nature of  $\psi$  and  $h_B$  is represented by  $\hat{\psi}^*(x)$  and  $\hat{h}_B^*(x)$ . The function  $\hat{\psi}(y)$  is assumed to be slowly varying, that is  $\frac{\partial \hat{\psi}}{\partial y} \ll \frac{\partial \psi}{\partial y}$ . It is included because a mean along-shore pressure gradient is anticipated to be important in the dynamics. Superimposed on these is the variability over small along-shelf scales. The function  $g(y)$  is assumed to be quasi-periodic, similar to a sinusoid, to represent the bank-trough nature of the topography, and is also part of the expression for  $\psi$  since streamlines closely conform to isotbaths (Chapter 4). It is therefore assumed that

$$\overline{g} \approx \overline{\frac{dg}{dy}} \approx 0 \quad (5.2a)$$

and that

$$\overline{g \frac{dg}{dy}} \approx \overline{g \frac{d^3g}{dy^3}} \approx \overline{\frac{dg}{dy} \frac{d^2g}{dy^2}} \approx 0 \quad (5.2b)$$

The over bar represents an along-shelf average over a very long segment of the shelf. These approximations are due to the alongshore averaging scale being much greater than the scale of  $g(y)$  and to the property of  $g(y)$  that even and odd derivatives are nearly out of phase (i.e., quasi-sinusoidal).

With these substitutions and assumptions, (3.13) can be along-shelf averaged to yield:

$$-\overline{\frac{\partial \hat{\psi}}{\partial y} \frac{\partial \hat{h}_B/D}{\partial x}} + \varepsilon \left( \overline{\frac{\partial \hat{\psi}}{\partial x} \frac{\partial^3 \hat{\psi}}{\partial y^3}} - \overline{\frac{\partial \hat{\psi}}{\partial y} \frac{\partial^3 \hat{\psi}}{\partial x^3}} \right) + \frac{E_v^{1/2}}{2} \left( \overline{\frac{\partial^2 \hat{\psi}}{\partial x^2}} + \overline{\frac{\partial^2 \hat{\psi}}{\partial y^2}} \right) = 0 \quad (5.3)$$

Since  $\frac{\partial \hat{h}_B/D}{\partial x}$  is  $O(1)$  while  $\frac{1}{2}E_v^{1/2}$  and  $\varepsilon$  are  $\ll 1$ , there is no balance in this equation unless  $\overline{\frac{\partial \hat{\psi}}{\partial y}}$  is  $O(\varepsilon)$  or  $O(\frac{1}{2}E_v^{1/2})$ . This implies that the non linear terms are  $O(\varepsilon^2)$  or  $O(\varepsilon \frac{1}{2}E_v^{1/2})$  thus much less than  $\frac{1}{2}E_v^{1/2}$  and that  $\overline{\frac{\partial^2 \hat{\psi}}{\partial y^2}} \ll \overline{\frac{\partial^2 \hat{\psi}}{\partial x^2}}$ . Consequently

$$\frac{1}{2} E_v^{1/2} \overline{\frac{\partial^2 \hat{\psi}}{\partial x^2}} - \overline{\frac{\partial \hat{\psi}}{\partial y} \frac{\partial \hat{h}_B}{\partial x}} = 0 \quad (5.4)$$

Since  $\hat{\psi}(y)$  is slowly varying, it is safe to assume that  $\overline{\frac{\partial \hat{\psi}}{\partial y}} \approx \frac{\partial \hat{\psi}}{\partial y}$ . With this, a new streamfunction,  $\hat{\psi}$ , can be identified to satisfy

$$\frac{1}{2} E_v^{1/2} \frac{\partial^2 \hat{\psi}}{\partial x^2} - \frac{\partial \hat{\psi}}{\partial y} \frac{\partial \hat{h}_B/D}{\partial x} = 0 \quad (5.5)$$

as long as it has the form:

$$\tilde{\psi} = \hat{\psi}^*(x) + \hat{\psi}(y) \quad (5.6)$$

If  $\frac{\partial}{\partial x} \frac{\hat{h}_B^*}{D} = s$ , a constant, then (5.5) can be written, dropping the "v"

$$\kappa \frac{\partial^2 \psi}{\partial x^2} - \frac{\partial \psi}{\partial y} = 0 \quad (5.7)$$

where

$$\kappa = \frac{E^{1/2} v}{2s} \quad (5.8)$$

Equation (5.7) is the ATW equation which Csanady (1978) derived for a shelf with no along-shelf topographic variations. The differences in notation between (5.7) and Csanady's version should be mentioned to avoid confusion. Csanady's version is in dimensional terms with sea-level as the dependent variable. His velocity variables are vertically averaged and therefore include the boundary layer transports. In the non-dimensional notation used here,  $\psi$  is the geostrophic streamfunction as well as the zeroth order sea-level anomaly ( $\psi = \eta_0$ ), and velocity components are geostrophic. The boundary layer transports can be accounted for by integrating the solutions. His linear drag coefficient,  $r$ , is here equivalent to  $\frac{1}{2} f \delta_E$ . Csanady also showed that equation (5.7) is analogous to the heat diffusion equation where the y-axis represents time,  $\psi$  temperature,  $\frac{\partial \psi}{\partial x}$  heat flux and  $\kappa$  thermal diffusivity. The sign of the second term is positive in Csanady's formulation because of the different bottom slope terms used. Csanady determined the depth gradient ( $\partial H / \partial x$ ), whereas the notation used here is for the gradient of the height of the bottom above a reference level ( $\partial \hat{h}_B / \partial x$ ), as shown

in Figure 7. Csanady (1978) defined the "forward" direction as that which is analogous to time in the heat conduction equation and is the direction of propagation of shelf disturbances. The positive y-axis points "forward" in the notation used here, and in Csanady's it is the negative y-axis.

For a coastal boundary condition, Csanady (1978) used (converted to the present notation):

$$\frac{\partial \psi}{\partial x} = \frac{2\tau_o}{f\delta_E U} \tau_y \quad (5.9)$$

where  $\tau_y$  is the nondimensional along-shelf windstress,  $\tau_o$  is the kinematic wind stress scale,  $\delta_E$  is given by equation 3.3 and  $U$  is the velocity scale. This boundary condition follows from three assumptions: the alongshore current,  $v$ , is in geostrophic balance with the cross-shelf pressure gradient, the bottom stress is given by a linear drag law and that, very near shore, the along-shelf momentum is dominated by surface (wind) and bottom stresses.

### C. The Arrested Topographic Wave and Along-shelf Pressure Gradient

For this and all subsequent discussions on solutions to the ATW equation the origin of our coordinate system (Figure 7) is at the coast ( $x = 0$ ). The shelf break is at  $x = -\ell$ , where horizontal distances have been scaled by the shelf width, so that  $\ell \sim 1$ .

To study the forcing by an external along-shelf pressure gradient, Csanady assumed the following boundary conditions:

$$\frac{\partial \psi}{\partial x} = 0 \quad x = 0 \quad \text{coast} \quad (5.10a)$$

$$\frac{\partial \psi}{\partial y} = \gamma \quad x = -\ell \quad \text{shelf edge} \quad (5.10b)$$

$$\psi = 0 \quad y = 0 \quad (5.10c)$$

(Initial condition very far upstream.)

The coastal condition derives from (5.9) assuming no wind stress. At the shelf break, a constant along-shelf sea level slope,  $\gamma$ , is imposed by the oceanic pressure field. The solution given by Csanady was from Carslaw and Jaeger (1959) and in the present notation is:

$$\begin{aligned} \psi = \gamma y + \frac{\gamma(x^2 - \ell^2)}{2\kappa} + \frac{16\gamma\ell^2}{\kappa\pi^3} \sum_{n=0}^{\infty} \frac{(-1)^n}{(2n+1)^3} \exp[-\kappa(2n+1)^2\pi^2 y/4\ell^2] \\ \times \cos[(2n+1)\pi x/2\ell] \end{aligned} \quad (5.11)$$

The transient terms under the summation decay exponentially and far downstream of the arbitrary origin,

$$\psi = \gamma y + \frac{\gamma(x^2 - \ell^2)}{2\kappa} \quad (5.12)$$

and the along-shelf velocity is thus

$$\frac{\partial \psi}{\partial x} = \gamma \frac{x}{\kappa} = \frac{\partial \psi}{\partial y} \frac{x}{\kappa} \quad (5.13)$$

A physical interpretation of this solution is that the along-shelf pressure gradient drives a weak cross-shelf geostrophic flow. This flow, crossing isobaths, must induce relative vorticity which, with  $v = 0$  at the coast, requires the current to increase in magnitude seaward. The along-shelf flow is directly linked to the along-shelf

pressure gradient by equation (5.13). Consequently, before this mechanism can be used to explain the southwestward mean shelf flow in the Northwest Gulf of Alaska, an along-shelf sea-level gradient (sloping down to the southwest) must first be demonstrated.

Csanady (1978) also used the Arrested Topographic Wave model to study the along-shelf sea-level gradient set up by local or non-local wind stress. In that result, a sea-level gradient is generated sloping upward in the direction of the wind stress. If the wind is affecting only a segment of the coastline, there will be a reverse gradient along the portion of the coast which lies down-wind of the wind forced zone (Csanady, 1978, Figure 6). It is conceivable that along-shelf winds in the north and northeast Gulf of Alaska could induce the necessary sea-level set up in the northwest gulf. This mechanism, however, would be subject to the large seasonal variations in wind-stress and outer shelf currents, which are directly proportional to the along-shelf pressure gradient by equation (5.13), should reflect this seasonal modulation. Since this variability is not evident in the outer shelf current meter data near Kodiak, this forcing mechanism for the along-shelf sea-level gradient is probably not important here.

Sturges (1974) suggested that a boundary current flow across latitude circles could be accompanied by an along-stream sea-level slope owing to the geostrophic balance. That is, if (in standard dimensional terms):

$$fLv = g(\eta_C - \eta_0) \quad (5.14)$$

where  $L$  is the width of the current,  $\eta_C$  is sea level on the coastal side of the stream and  $\eta_0$  that on the oceanic side, then flow towards smaller  $f$  must be accompanied by greater  $Lv$  or  $\eta_0$ , or lesser  $\eta_C$  or some combination thereof.

This process is examined here more thoroughly by taking the  $y$ -derivative of (5.14) and rearranging terms to yield:

$$\frac{\beta Lv}{g} = \frac{\partial \eta_C}{\partial y} - \frac{\partial \eta_0}{\partial y} - \frac{f}{g} \frac{\partial}{\partial y} (Lv) \quad (5.15)$$

where  $\beta = \frac{\partial f}{\partial y} \sim -1 \times 10^{-13} \text{ cm}^{-1} \text{ s}^{-1}$  (negative due axis orientation).

The order of magnitude scales for the Alaskan Stream are  $L \sim 100 \text{ km} = 10^7 \text{ cm}$  and  $v \sim 100 \text{ cm s}^{-1}$ , which makes the  $\beta$ -term, on the left hand side of (5.15), about  $-10^{-7}$ .

Shay and Hickey (1983) used these scales and, by neglecting the last two terms in (5.15), proposed that the  $\beta$ -term generated a  $\partial \eta_C / \partial y$  of an appropriate direction and magnitude to drive the along-shelf flow according to equation (5.13). Nevertheless, the importance of the neglected terms remains uncertain. Sturges (1974) took into account a  $\partial \eta_0 / \partial y \sim 10^{-7}$  term in analyzing the effect of the Gulf Stream on coastal sea level, but found the last term in (5.15), a transport term, to be negligible. For the Alaskan Stream this transport term may also be significant. In the most recent extensive survey, volume transports relative to 1500 db varied along-stream from  $\sim 11$  to  $\sim 16 \text{ Sv}$  (Wright, 1981). From the above scaling, an along-shore transport variation of  $\frac{\partial}{\partial y} (Lv) \sim 1 \text{ cm s}^{-1}$  will yield a term large enough to balance the  $\beta$ -term ( $\sim 10^{-7}$ ). This converts to  $\frac{\partial}{\partial y} (Lv)$

$\sim 10^8 \text{ cm}^2 \text{ s}^{-1}/1000 \text{ km}$ , or about 10% of the transport ( $Lv \sim 10^9 \text{ cm}^2 \text{ s}^{-1}$ ) over the length scale of the stream. Based on the data presented by Wright (1981) this term should be significant. It cannot be demonstrated that the latter two terms in (5.15) can be ignored. A simple balance of the first two terms in (5.15), therefore, should not be used to conclude that  $\partial\eta_C/\partial y$  is externally imposed on the Kodiak shelf by the Alaskan Stream through this  $\beta$ -plane effect as suggested by Shay and Hickey (1983).

A steric sea level gradient may exist due to the mass distribution of the Pacific Sub-Arctic Gyre circulation. However, an analysis of the historical hydrographic data base to address this question is not available and would be beyond the scope of this project. Nevertheless, one can deduce from the geopotential anomaly distribution of the Alaskan Stream shown in Figure 2 that no large steric along-shelf sea level gradient is evident from that survey. In comparison, a detailed analysis of the steric pressure field from Cape Hatteras to Nova Scotia by Csanady (1979) concluded that the thermohaline contribution to the mean along-shore pressure gradient along the east coast is relatively minor.

It appears doubtful that any external mechanism for imposing the required alongshelf pressure gradient can be determined with certainty. Nevertheless, one would intuitively expect that such a gradient should exist given the predominant southwestward flow on the shelf. The real issue here is not whether the gradient exists, but whether it drives the shelf flow. Some other mechanism may drive the flow and the along-shelf pressure gradient may be required by the

dynamics as a result of the flow, not as the cause. It is shown in the following sections that this is indeed the situation for this case study by attributing the flow to effects of the Alaskan Stream boundary current.

#### D. The Alaskan Stream as a Boundary Condition

Aside from the lack of a demonstrated driving force, the solution discussed above does have some relevant properties. Equation (5.13) provides for increasing magnitude of the current with distance from the coast. This is generally descriptive of the shelf flow, given the presence of the Alaskan Stream over the continental slope. However, a different interpretation to that above of the dynamics intrinsic to Equation (5.13) can be made: The shelf break flow exists because of the Alaskan Stream; the current decreases shoreward over the shelf to zero at the coast, providing for a constant along-shelf pressure gradient.

The governing ATW equation (5.7) can be solved in a manner which accounts for this. The along-shelf current is given an arbitrary value at the shelf break and set to zero at the coast. Formally, this requires:

$$\frac{\partial \psi}{\partial x} = 0 \quad \text{at } x = 0 \quad (\text{coast}) \quad (5.16a)$$

$$\frac{\partial \psi}{\partial x} = V \quad \text{at } x = -\ell \quad (\text{shelf edge}) \quad (5.16b)$$

$$\psi = 0 \quad \text{at } x = 0 \quad (\text{initial condition very far upstream}) \quad (5.16c)$$

The solution is (from Carslaw and Jaeger, p. 112):

$$\psi = \frac{-\kappa V y}{\ell} - V \ell \left\{ \frac{3x^2 - \ell^2}{6\ell^2} - \frac{2}{\pi^2} \sum_{n=1}^{\infty} \frac{(-1)^n}{n^2} \exp(-\kappa n^2 \pi^2 y / \ell^2) \cos n\pi x / \ell \right\} \quad (5.17)$$

For large  $y$ , this approaches

$$\psi = \frac{-\kappa V y}{\ell} - V \ell \left( \frac{3x^2 - \ell^2}{6\ell^2} \right) \quad (5.18)$$

and

$$\frac{\partial \psi}{\partial x} = -V \frac{x}{\ell}; \quad \frac{\partial \psi}{\partial y} = -\frac{\kappa V}{\ell} \quad (5.19)$$

so that

$$\frac{\partial \psi}{\partial x} = \frac{\partial \psi}{\partial y} \frac{x}{\ell} \quad (5.20)$$

Since (5.20) is identical to (5.13), the relationship between  $\frac{\partial \psi}{\partial x}$  and  $\frac{\partial \psi}{\partial y}$  is the same in this solution as in Csanady's. Another similarity is that, at large  $y$ ,  $\frac{\partial \psi}{\partial y}$  is constant across the shelf. The important difference is that, in this solution, an along-shelf oceanic boundary current at the shelf break induces a parallel flow on the adjacent shelf. The boundary conditions (5.16) on the ATW equation (5.7) create a vorticity over the shelf which requires a balancing cross-isobath flow,  $\frac{\partial \psi}{\partial y}$ . Therefore, the along-shelf sea-level slope is a secondary effect, not the primary driving mechanism.

The advantage of this interpretation is that it eliminates the necessity of establishing, by measurement or inference, the existence of an along-shelf sea-level slope. While this is very difficult, the existence of the Alaskan Stream is irrefutable. It makes more sense to describe a model which links the shelf flow to this well documented

oceanic boundary current than to an elusive along-shelf pressure gradient. This gradient cannot be neglected, however, since it is fundamental to these dynamics. It simply does not need to be considered a driving force for the along-shelf currents.

Figures 13 and 14 depict the along-shelf profile of sea level, or streamfunction, for the gravest mode of the two solutions (5.17) and (5.11) respectively. The similarity between them for large  $y$  is clear, and the same physical processes are obviously involved. With zero current at the coast as a boundary condition, along-shelf currents must be accompanied by an along-shelf pressure gradient, and vice-versa.

Figure 15 depicts streamlines for the asymptotic limit given by equation (5.18). The parabolic nature of the solution is obvious, with the contours turning into the coast as required by the coastal boundary condition (5.16a). Again, it should be noted that these are contours of geostrophic streamfunction, or equivalently, lowest order sea-level anomaly. Mass balance at the coast is accomplished in the bottom Ekman layer, as will be shown below. At the seaward edge of the shelf the streamlines become more parallel to the coast and more closely spaced as the along-shelf current increases with distance off shore. The cross-shelf geostrophic current, or along-shelf pressure gradient, remains constant throughout.

#### E. An Additional Solution with Arbitrary Depth

Without compromising the results just discussed, an additional step can be made in generalizing this problem for an arbitrary cross-

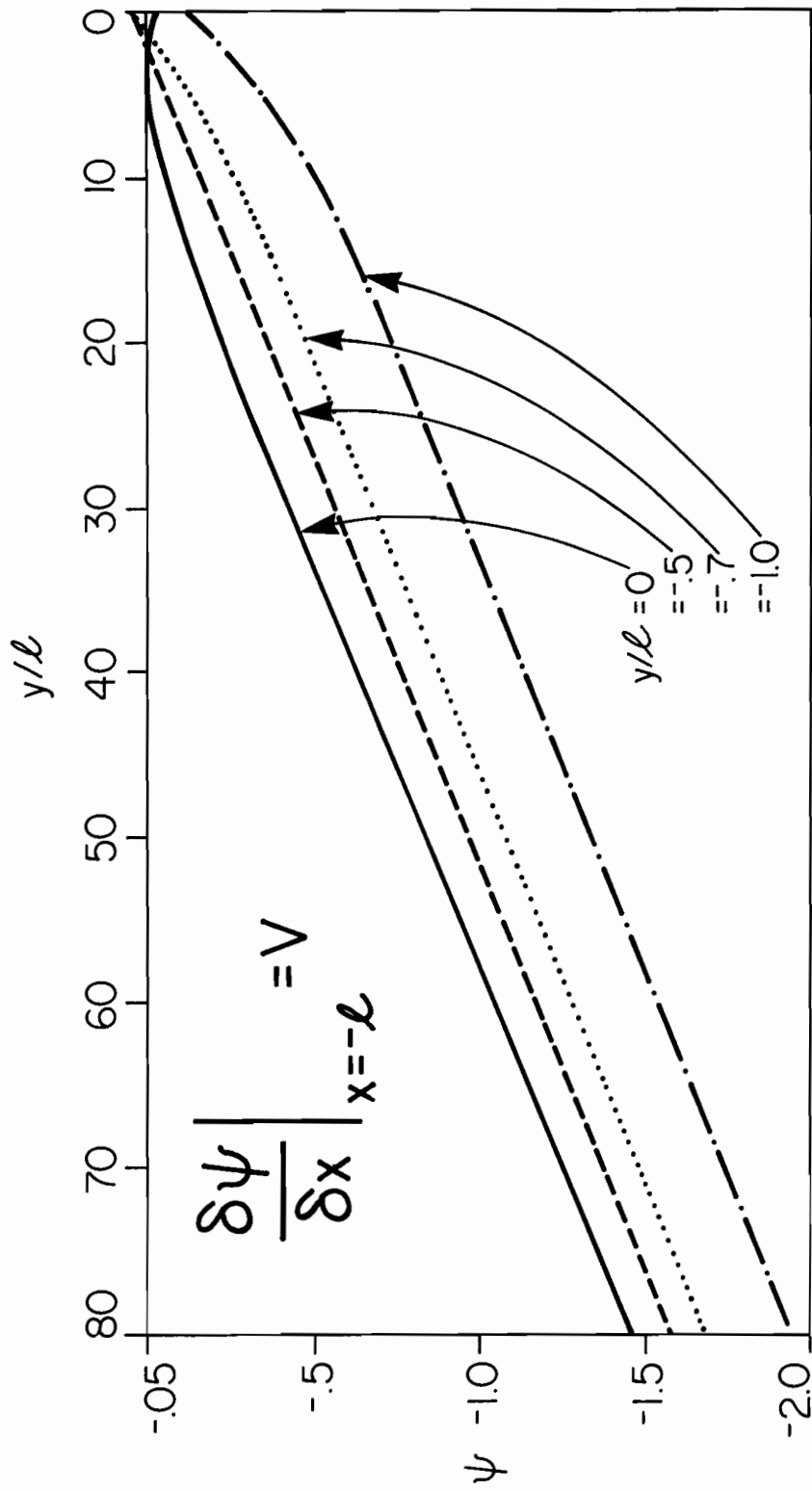


Figure 13. The gravest mode ( $n=1$ ) for the solution 5.17 in which the shelf flow is driven by a shelf break current.

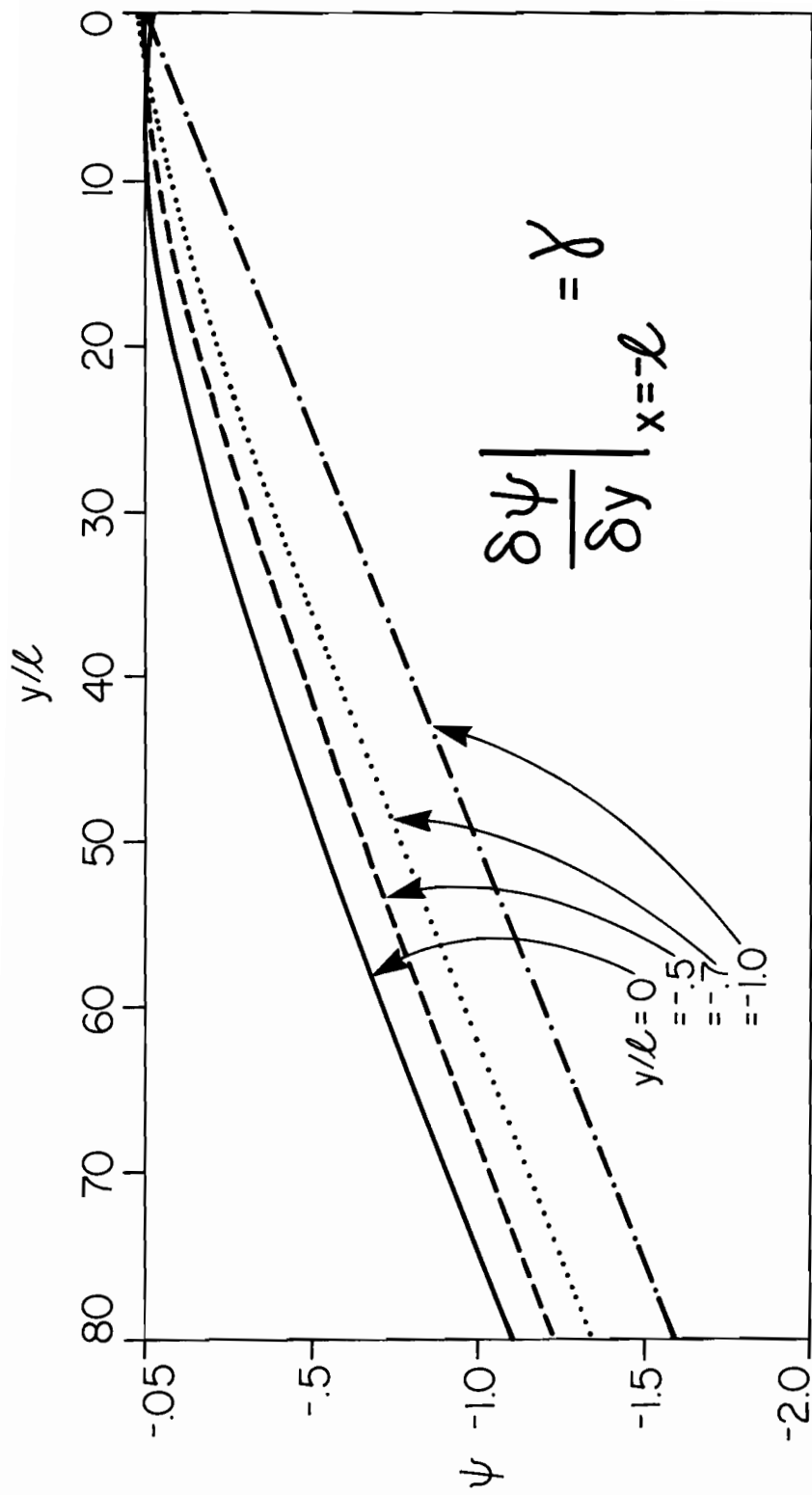


Figure 14. The gravest mode ( $n=0$ ) for the solution 5.11 (originally by Csanady, 1978) in which the shelf flow is driven by an along-shelf pressure gradient.

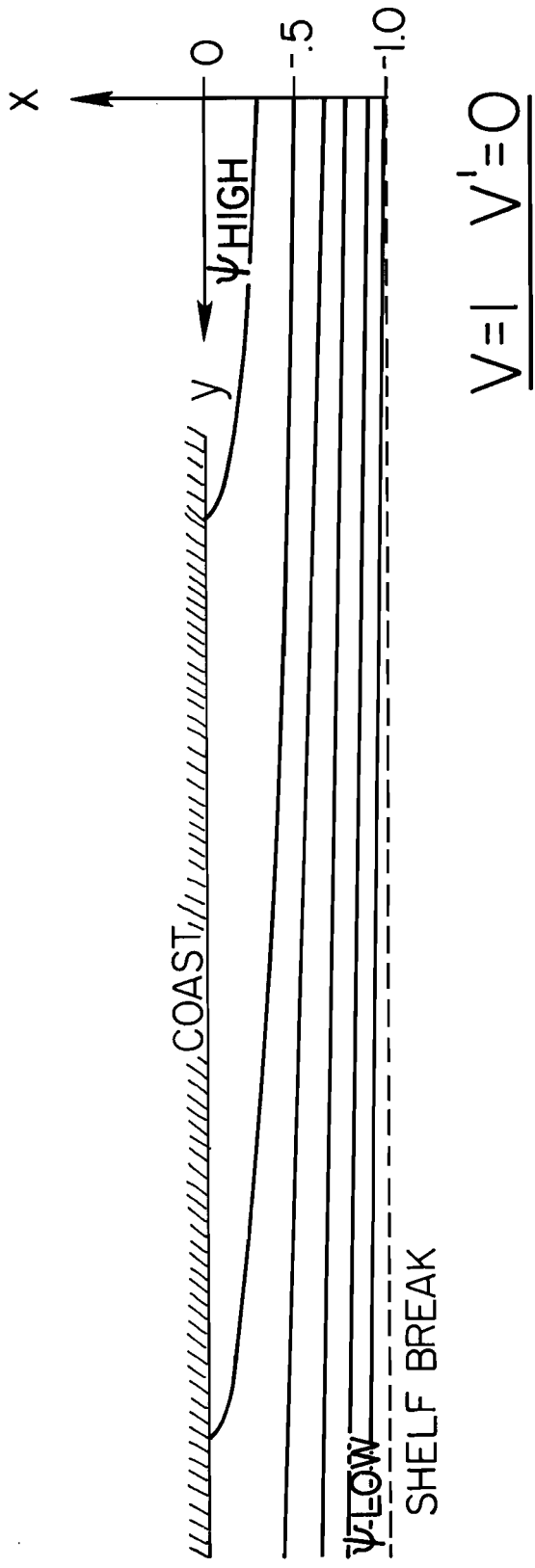


Figure 15. Streamline pattern for the asymptotic limit Equation 5.18 in which the shelf flow is driven by a positive current,  $V$ , at the shelf break.

shelf depth profile and boundary conditions (5.16). In the above examples, a linearly sloping bottom was assumed and the resultant cross-shelf profile of  $v$  was also linear (equations 5.13 and 5.19). This implies that depth and  $v$  may be, in general, linearly related. For an arbitrary bottom  $h_B(x)/D$ , a solution to (5.5) can be assumed as follows:

$$\psi(x) = By + A \left( \int \frac{h_B(x)}{D} dx - x \right) + \Sigma [\text{terms neglected}] \quad (5.21)$$

The second term in the parentheses arises from knowing that  $\frac{h_B}{D} = 1$  at  $x = 0$  and  $\frac{h_B}{D} = 0$  at  $x = -\ell$ . The terms under the summation are not rigorously sought because they are assumed to approach zero for large  $y$ . Therefore we are, in effect, assuming *a priori* that  $\frac{\partial \psi}{\partial y} = \text{constant}$ . Taking the derivative:

$$\frac{\partial \psi}{\partial x} = A \left( \frac{h_B}{D} - 1 \right) \quad (5.22)$$

At  $x = -\ell$ ,  $\frac{\partial \psi}{\partial x} = V$  and  $h_B/D = 0$ , therefore

$$A = -V \quad (5.23)$$

and

$$\frac{\partial^2 \psi}{\partial x^2} = -V \frac{\partial}{\partial x} \frac{h_B}{D} \quad (5.24)$$

Substituting this into (5.5) gives:

$$B = -\frac{1}{2} E \frac{1}{V} V \quad (5.25)$$

The final solution for  $\psi$  at large  $y$  is

$$\psi = -\frac{1}{2} E \frac{1}{v} V y - V \left[ \int \frac{h_B(x)}{D} dx - x \right] \quad (5.26)$$

with

$$\frac{\partial \psi}{\partial x} = -V \left( \frac{h_B}{D} - 1 \right) = V \frac{H}{D} \quad (5.27)$$

and

$$\frac{\partial \psi}{\partial y} = -\frac{1}{2} E \frac{1}{v} V \quad (5.28)$$

Equation (5.27) is identical to (5.19) when  $\frac{h_B}{D} = 1 + \frac{x}{\ell}$ , i.e., a linearly sloping bottom. Therefore, (5.27) is a more general solution and shows that the alongshore velocity,  $\frac{\partial \psi}{\partial x}$ , is a linear function of depth when the alongshore pressure gradient is assumed constant.

Equation (5.28) gives the along-shelf sea-level slope and, in the context used here, the weak cross shelf geostrophic flow that must exist to balance the relative vorticity in the governing equation (5.5). If (5.28) is vertically integrated, the geostrophic transport is:

$$\int_{\frac{h_B}{D}}^1 -\frac{\partial \psi}{\partial y} dz = \frac{1}{2} E \frac{1}{v} V \left( 1 - \frac{h_B}{D} \right) = \frac{1}{2} E \frac{1}{v} V \quad (5.29)$$

This is the negative of the transport of the bottom boundary layer (Equation 3.4) and the cross-shelf flux is in a two-dimensional balance.

#### F. The Alaskan Stream and Shelf Break Currents

The model presented above is based on the same governing equation as the Arrested Topographic Wave (Csanady, 1978). In this new solution, however, boundary conditions are applied which take into account the cross-shelf pressure gradient due to the Alaskan Stream, and the solution shows that the along-shelf flow is driven by the stream, current magnitude increases seaward and the along-shelf pressure gradient arises as a secondary effect.

It must be pointed out that the model presented here is barotropic while the driving current, the Alaskan Stream, is baroclinic. The core of the surface current, relative to 1500 db, is between the 1000 and 2000 meter isobaths (Chapter 1). Bottom currents are very weak at these depths and the vorticity balance of the ATW equation would not hold with such weak bottom Ekman pumping. Near the shelf break, however, no consistent baroclinic flow can be deduced from the dynamic method inshore of about the 300 meter isobath (Chapter 1). This indicates that the flow is nearly barotropic relative to these depths.

If this barotropic model applies, there must be a transition from a bottom depth controlled barotropic flow at the shelf break to the deeper baroclinic oceanic boundary current. Proceeding shoreward from the core of the stream, the bottom will penetrate the vertical zone of strong surface flow and the barotropic nature represented by this model will become more important. In general, shelf break currents measured at about the 200 meter isobath in the northwest gulf are typically  $\sim 20 \text{ cm s}^{-1}$ . This would indicate, from the above model, that

at mid-shelf (depth  $\sim 100$  meters) the velocity is typically  $10 \text{ cm s}^{-1}$ . The potential vorticity model in Chapter 4 fit the data well with  $5\text{-}10 \text{ cm s}^{-1}$  speed scales, cross-shelf averaged, though the fit is somewhat better for the weaker speed. As a consequence, a  $\sim 20 \text{ cm}^{-1}$  flow at the shelf break coupled to a  $\sim 100$  to  $150 \text{ cm s}^{-1}$  surface current relative to  $1500 \text{ db}$  at the core of the stream seems reasonable.

Figure 16 shows isotacs of the baroclinic current in the Alaskan Stream off Kodiak, relative to  $1500 \text{ db}$  (from Wright, 1981). An  $\sim 20 \text{ cm s}^{-1}$  shelf break current is consistent with these data. To illustrate how the shelf break current is maintained by the Alaskan Stream, we will examine a simple vorticity balance for the stream in a  $\beta$ -plane. The  $\beta$ -effect in this case will be balanced by the bottom stress curl, which can be integrated across the stream to estimate the shelf break current. To proceed, we apply the vorticity equation for the bottom velocity used by Shaw (1982). With all variables dimensionalized and omitting local wind stress curl, Shaw's vorticity equation is:

$$r \frac{\partial v_b}{\partial x} - f \frac{\partial H}{\partial x} u_b + \beta V = 0 \quad (5.30)$$

where  $u_b$  and  $v_b$  are the bottom geostrophic velocity components,  $r$  is a linear drag coefficient with dimensions of velocity,  $V$  is the sum of the barotropic, ( $V_B$ ) and baroclinic ( $V_C$ ) meridional transports,  $\beta = \frac{\partial f}{\partial y}$ , conventional  $y$ -north and  $x$ -east coordinates are temporarily used and  $\frac{\partial H}{\partial y} = 0$ .

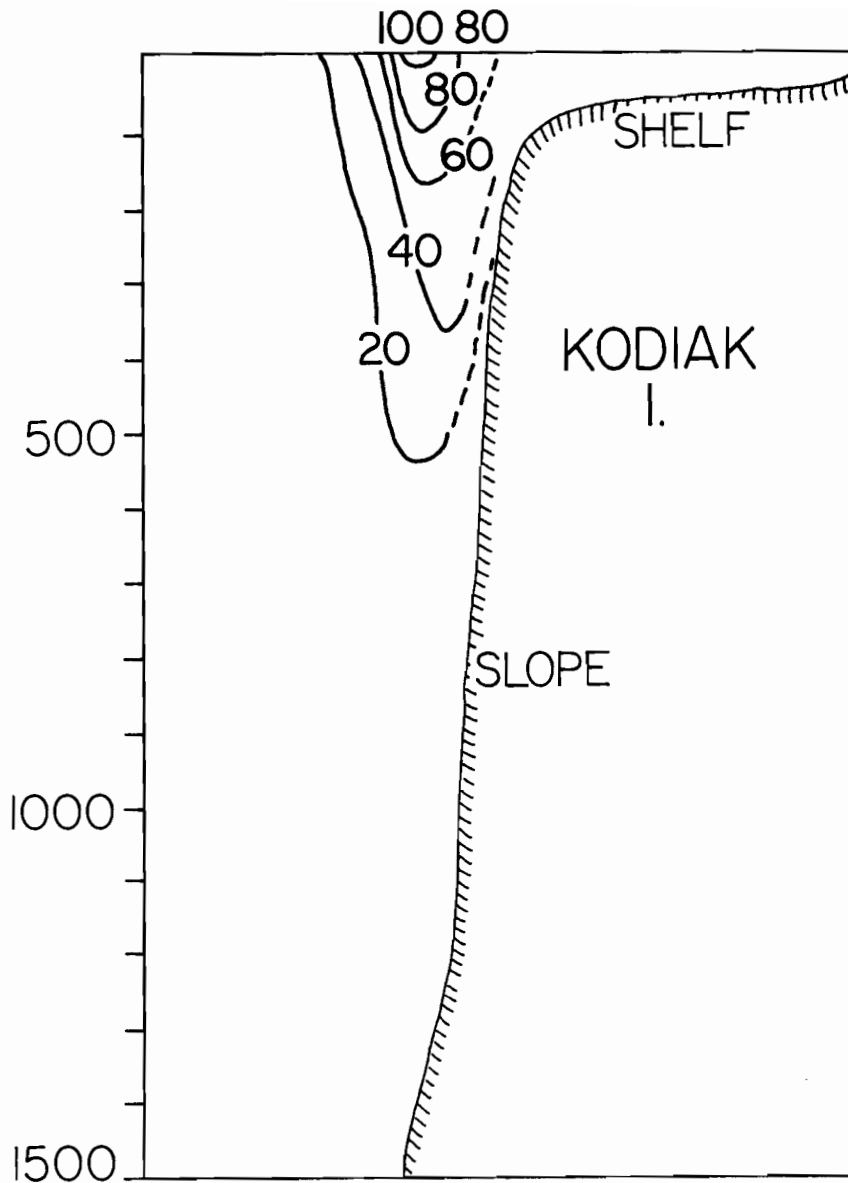


Figure 16. Isotacs of flow in the Alaskan Stream adjacent to Kodiak, relative to 1500 db, 13-15 February, 1980. (Contoured from the data from Wright, 1981.)

Simple scale analysis will show that as H shoals to ~100 m (shelf depths) this balance approaches

$$r \frac{\partial v_b}{\partial x} - f \frac{\partial H}{\partial x} u_b = 0 \quad (5.31)$$

which is the ATW equation.

Shaw also shows that with negligible along-shelf bottom density variations

$$\frac{\partial}{\partial x} (f u_b) + \frac{\partial}{\partial y} (f v_b) = 0 \quad (5.32)$$

In his notation,  $V_B = H v_b$  and  $U_B = H u_b$ . With these relations the second term in equation (5.30) is:

$$-f \frac{\partial H}{\partial x} u_b = -f \frac{\partial U_B}{\partial x} - f \frac{\partial V_B}{\partial y} - \beta H v_b \quad (5.33)$$

Then, if the divergence of the barotropic transport in (5.33) is small, (5.30) becomes:

$$r \frac{\partial v_b}{\partial x} + \beta V_c = 0 \quad (5.34)$$

In this expression the vorticity induced by strong meridional transport in a  $\beta$ -plane is balanced by bottom Ekman pumping, which is proportional to the relative vorticity of the bottom velocity.

We will now apply (5.34) to the Kodiak Island/Northwest Gulf of Alaska shelf under study here. The southwest oriented y-axis causes  $\beta$

to be negative. (A term  $\frac{\partial f}{\partial x} U_c$  would also appear but can be considered negligible compared to  $\beta V_c$ .)

Equation (5.34) can be integrated laterally, along  $x$ , across the continental slope. With  $x_1$  the seaward side and  $x_2$  the shelf break,

$$r v_b \Big|_{x_2} - r v_b \Big|_{x_1} = -\beta \int_{x_1}^{x_2} V_c dx = -\beta T_c \quad (5.35)$$

where  $T_c$  is the volumetric baroclinic transport and  $\beta < 0$ .

The bottom velocity field seaward of the western boundary current should be small;  $v_b \Big|_{x_1} \sim 0$ . The Alaskan Stream transport is  $\sim 12$  Sv (Reed et al., 1980) and using typical values of  $r$  between .05 and  $0.1 \text{ cm s}^{-1}$ , the shelf break velocity is estimated to be between  $12 \text{ cm s}^{-1}$  and  $24 \text{ cm s}^{-1}$ . These values agree favorably with direct measurements of shelf break currents discussed in Chapter 1 and indicated in Figure 16.

#### G. Solutions that Include Coastal Winds

It is worth examining two other solutions to the arrested topographic wave equation (5.7). The first is a simple case of wind forcing using the coastal boundary condition (5.9) and assuming no current at the shelf break. Introducing the variable  $\xi$  and boundary conditions such that:

$$\xi = x + l \quad (5.36a)$$

$$\frac{\partial \psi}{\partial \xi} = V' \text{ at } \xi = l \text{ (coast)} \quad (5.36b)$$

$$\frac{\partial \psi}{\partial \xi} = 0 \text{ at } \xi = 0 \text{ (shelf edge)} \quad (5.36c)$$

the solution at large  $y$  reduces to

$$\psi = \frac{kV'y}{\ell} + V'\ell \frac{3\xi^2 - \ell^2}{6\ell^2} \quad (5.37)$$

where  $V'$  represents the wind stress and equals the right-hand side of (5.9). Equation (5.37) is identical to (5.18) except for the change in sign of  $\ell$ . From (5.36a), (5.37) becomes:

$$\psi = \frac{kV'y}{\ell} + V' \left( \frac{3x^2 + 6x\ell + 2\ell^2}{6\ell} \right) \quad (5.38)$$

Note that the sign of  $\frac{\partial\psi}{\partial y}$  is determined by  $V'$ , therefore sea-level rises along-shelf in the direction of the wind-stress. This contrasts with the solution (5.18) in which sea level slopes down in the direction of a shelf break current.

Since the governing equation is linear, the solutions (5.18) and (5.38) may be superimposed to show the result of both shelf break current and coastal wind stress forcing. This results in:

$$\psi = \frac{ky}{\ell} (V' - V) + \frac{(V' - V)(3x^2) + V'(6x\ell + 2\ell^2) + V\ell^2}{6\ell} \quad (5.39)$$

Therefore:

$$\begin{aligned} \frac{\partial\psi}{\partial x} &= (V' - V) \frac{x}{\ell} + V' & (5.40) \\ &= V' \text{ at } x = 0 \text{ (coast)} \\ &= V \text{ at } x = -\ell \text{ (shelf edge)} \end{aligned}$$

and

$$\frac{\partial \psi}{\partial y} = (V' - V) \frac{k}{\ell} \quad (5.41)$$

Note that when coastal wind stress and the shelf break current act in the same direction,  $\partial\psi/\partial y$  tends to vanish.

Figures 17, 18, 19 show contours of sea level or geostrophic streamfunction ( $\psi = \eta_0$ ) for some examples of the solution (5.39). In Figure 17,  $V = 0$ , and the flow is forced solely by a coastal wind stress  $V'$ . Note that this pattern is simply a reflection of Figure 15, which has  $V' = 0$  and shows solely the effect of the shelf break boundary condition of  $\partial\psi/\partial x = V$ . Figure 18 shows the effect of a positive shelf break current and an opposing wind stress of equal magnitude;  $V = -V'$ . Sea level is depressed at the coast and at the shelf break and there is a current reversal mid-shelf. In the last example, Figure 19,  $V = V'$ , in which case the current is uniform across the shelf and there is no along-shelf sea level slope.

The constraint of transport conservation in the cross-shelf plane can also be demonstrated for this solution, as follows: the equation for the bottom in the constant slope cases is:

$$\frac{h_B}{D} = 1 + sx; \quad s = 1/\ell \quad (5.42)$$

Then from (5.8), equation (5.41) becomes

$$\frac{\partial \psi}{\partial y} = \frac{1}{2} E \frac{k}{V} (V' - V) \quad (5.43)$$

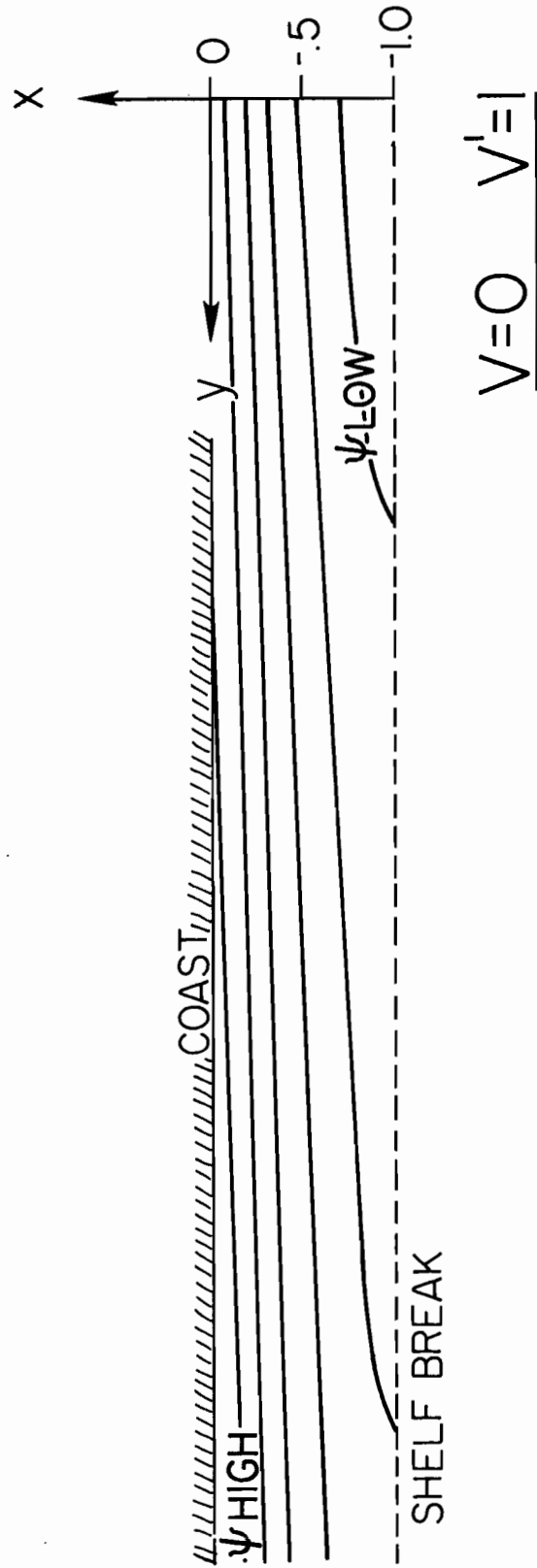


Figure 17. Streamline pattern for equation 5.39 with a positive wind stress ( $V'=1$ ) and no shelf break current ( $V=0$ ). Note that this pattern is a simple reflection of Figure 15.

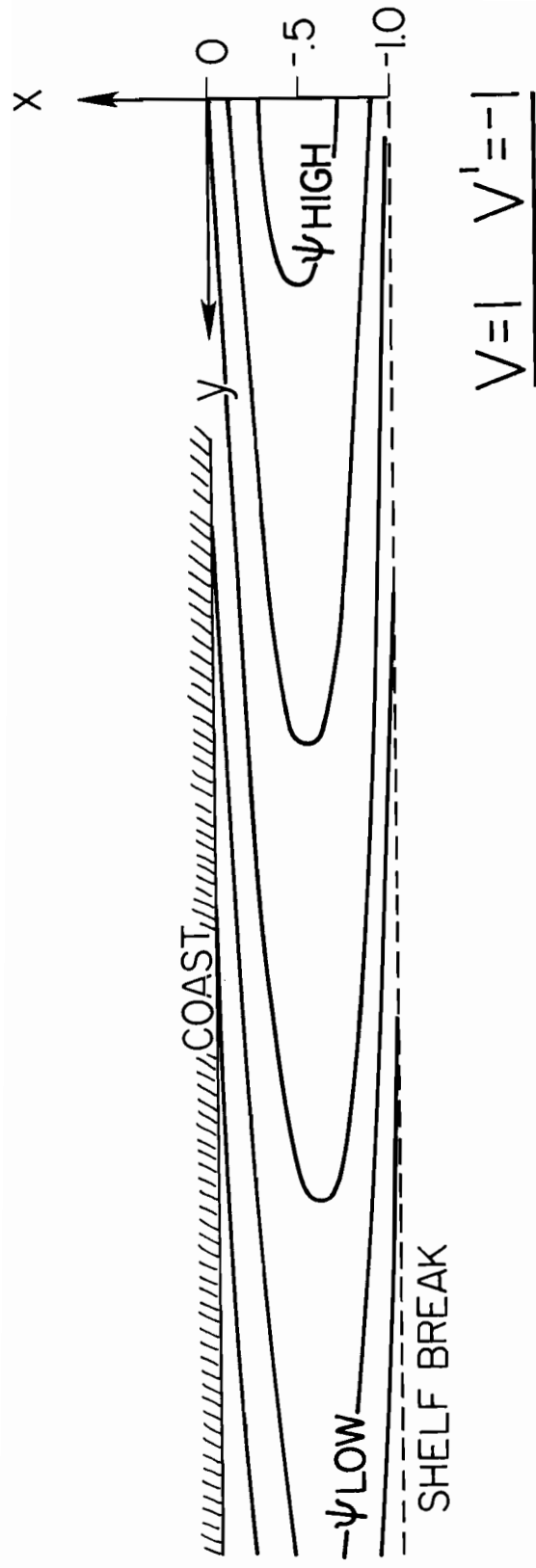


Figure 18. Streamline pattern for equation 5.39 with a positive shelf break current ( $V=1$ ) and an opposing wind stress ( $V'=-1$ ).

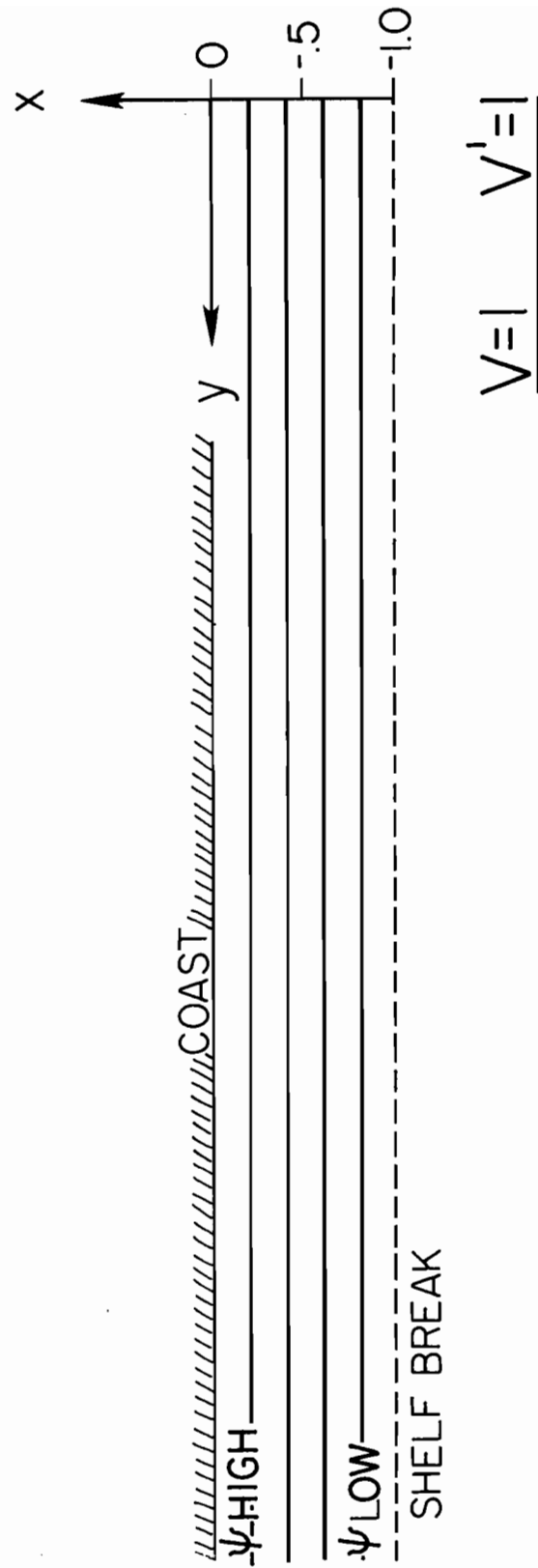


Figure 19. Same as 18 except that the wind stress is in the same direction as the shelf break current ( $V=V'=1$ ).

The geostrophic transport is, with (5.42):

$$\begin{aligned} \int_{\frac{h_B}{D}}^1 -\frac{\partial \psi}{\partial y} dz &= -\frac{1}{2} E^{\frac{1}{2}} \frac{1}{V} (V' - V) \left(1 - \frac{h_B}{D}\right) \\ &= \frac{1}{2} E^{\frac{1}{2}} \frac{1}{V} (V' - V) \frac{x}{\ell} \end{aligned} \quad (5.44)$$

The bottom boundary layer transport is, from (3.4) and (5.40)

$$U_E \text{ (bottom)} = -\frac{1}{2} E^{\frac{1}{2}} \frac{1}{V} [(V' - V) \frac{x}{\ell} + V'] \quad (5.45)$$

The surface wind driven transport is given, in this notation, by Pedlosky (1979) p. 218 as

$$\begin{aligned} U_E \text{ (surface)} &= E^{\frac{1}{2}} \frac{\tau_o \tau_y}{f \delta_E U} \\ &= \frac{1}{2} E^{\frac{1}{2}} \frac{1}{V} V' \end{aligned} \quad (5.46)$$

From equations (5.44), (5.45) and (5.46) the interior geostrophic and boundary layer cross-shelf transports are in balance. When  $V' = V$ , the interior cross-shelf geostrophic transport vanishes and mass balance is accomplished in the boundary layers alone.

#### H. Residual Flow from Tidal Current Rectification

This discussion of the mean flow on the Kodiak Shelf should not be concluded without addressing the residual flow that can result from rectification of tidal currents by topography. In the northern hemisphere, such currents flow along isobaths with shallow depth to the right of flow direction and come about through non-linear processes, and vorticity and momentum conservation where there are strong cross-isobath tidal currents. The magnitude of this residual current

depends, in part, on the tidal current amplitude and topographic gradient. The dominant tidal current in the Kiliuda Trough region is the  $K_1$  with amplitudes of  $\sim 15 \text{ cm s}^{-1}$ .

Two recent papers on this topic give equations to estimate the tidal residual current. Robinson (1981) derived the following simplified expression for the major component:

$$\bar{v} = 1.5 \times 10^{-5} \frac{\Delta h}{h} E \quad (5.48)$$

where  $E$  is the tidal excursion length and  $\frac{\Delta h}{h}$  is the fractional depth change over the distance  $E$ . In a different model, Loder (1980) derived this expression:

$$\bar{v} = \frac{H_d U_d^2 f \partial H / \partial x}{2\omega^2 H^2} \left( 3 \frac{H_d}{H} - 2 \right) \quad (5.49)$$

where  $H_d$  is the depth on the deep side of a topographic feature and  $H$  that on the shallow side,  $U_d$  is the tidal current amplitude on the deep side and  $\omega$  is tidal frequency. If the bathymetric scales and tidal current data from the Kiliuda Trough/Albatross Bank vicinity are applied to these relationships, the resultant residual current estimate in both cases is about 4 or 5  $\text{cm s}^{-1}$ .

Recalling the results from Chapter 4, it was found that  $\sim 5 \text{ cm s}^{-1}$  was an appropriate velocity scale for the shelf. At first glance, then, the tidal residuals seem to be important. However, one must also recall from Chapter 4 that the velocity scale represented a cross-shelf average and that the flow in the vicinity of the trough was considerably greater; 20 to 25  $\text{cm s}^{-1}$ , owing to the local

topographic steepness. The tidal residuals computed here reflect those same steep topographic gradients of the trough perimeter and are significantly weaker than the measured mean currents (Chapter 2).

Loder's (1980) model was designed specifically to predict residual flow around Georges Bank (New England shelf), particularly along the steep northern edge. He predicted a mean eluerian velocity of  $23 \text{ cm s}^{-1}$  which agrees well with the  $\sim 30 \text{ cm s}^{-1}$  observations of Magnell *et al.* (1980) and Butman *et al.* (1982). Recently, Butman (1982) has estimated that about 50% of the residual current at a station on the southern flank can be attributed to this mechanism. On the other hand, observations of the sub-tidal variability in currents along the northern flank by Magnell *et al.* (1980) cast some doubt on Loder's theory. One would expect some modulation of the residual current with changing tidal current amplitude. Magnell *et al.* found significant correlation, at one specific site and depth, between the along-isobath subtidal filtered current and tidal current amplitude. These low frequency fluctuations, however, were in the meteorological forcing band (3-10 days) and the correlation was highest with along-isobath tidal currents, not the cross-isobath. Furthermore, the fortnightly variation, which was evident in the cross-isobath tidal current amplitude, was not evident in the residual current or the along-isobath tidal current amplitude. Magnell *et al.* (1980) concluded that a barotropic bottom interaction theory, such as Loder's (1980), does not account for their observed variability of tidal current amplitude on wind-driven time scales.

The along-isobath currents at the perimeter of Kiliuda Trough do not show any indication of a bi-weekly variability (Figure 5). The unfiltered bottom pressure data from stations K8, K9, K10 (not shown) have a significant spring-neap signal but when compared to the filtered currents in Figure 5 there is no obvious visual correlation. This observation, in conjunction with the points made above, leads to the conclusion that tidally driven residual currents are of secondary importance to the Kodiak Shelf mean flow.

#### I. Chapter Summary

Several ideas have been introduced in this chapter in order to explain the mean flow over the Kodiak and adjacent shelf areas. It was suggested that the Arrested Topographic Wave model of Csanady (1978) represents the cumulative dynamics over a long segment of the shelf by along-shelf averaging the smaller scale topographic effects. A new solution to the ATW equation was introduced which shows that shelf currents are driven by the cross-shelf sea level gradient at the shelf break, which, in turn, is caused by the oceanic boundary current, the Alaskan Stream. The magnitude of the along-shelf current is proportional to local depth ( $H$ ) as long as the along-shelf pressure gradient is constant and the current is assumed zero at the coast (i.e., there is no wind forcing). A solution including coastal wind forcing is also given to assess the simultaneous effects of forcing by both shelf break currents and wind stress. These solutions attribute the outer shelf currents primarily to the oceanic boundary current and not to wind forcing. The observed lack of seasonal variability in

outer shelf currents and in the Alaskan Stream but not in wind stress supports this theory.

Discussion is made of the importance of the alongshelf pressure gradient to the dynamics. While it is a necessary ingredient to the vorticity and momentum balances, it may arise on account of the flow being driven by some other mechanism rather than be the driving mechanism itself. In this study, the presence of the swift Alaskan Stream boundary current is shown to have a significant impact on the shelf flow. The vorticity dynamics of the baroclinic boundary current produce a parallel current at the shelf break, which acts as a boundary condition for the shelf flow in terms of a geostrophic cross-shelf pressure gradient. The flow pattern that results from the solution derived with this boundary condition is the same as one which is forced by an along-shelf pressure gradient, when that along-shelf gradient is equal to the one that arises on account of the above solution. It appears that the two mechanisms, forcing by a shelf break current or by an along-shelf pressure gradient, may be indistinguishable, except in a case such as this, where the shelf break flow is clearly related to an oceanic boundary current.

## Chapter 6: Flow Variability

### A. Seasonal Variability

In the previous two chapters this study has been treated as two problems; one on a small scale and one on a large scale. The small scale problem of Chapter 4 dealt with the lowest order effects of the bank-trough topography on the Kodiak shelf, with an along-shelf length scale of 20-50 km. Chapter 5 addressed the large scale dynamics of the Northwest Gulf of Alaska shelf region with an along-shelf scale of >1000 km. The mean shelf flow was determined to be southwestward year-round, owing to the Alaskan Stream. This allowed the supposition of inflow through the right-hand boundary in the numerical model of the small scale effects presented in Chapter 4.

In this chapter, some aspects of the flow variability will be discussed assuming quasi-steady conditions and applying some of the steady state results of the preceding chapters. This will be done by examining how variations in the regional, or large scale, circulation will affect the boundary conditions and therefore the flow pattern of the numerical model. In this way, features of the observed variability in the current meter record can be conceptually accounted for.

Throughout the foregoing discussions, the apparent lack of seasonal variability in flow has been emphasized. This description pertains primarily to the outer shelf currents and to the Alaskan Stream, which are strongly coupled in the northwest gulf. The inner shelf domain throughout the northern gulf coastal region is strongly affected by seasonally variable wind forcing and coastal runoff (see again Chapter 1). How these seasonal changes are manifested on the

Kodiak shelf can be assessed conceptually by varying the boundary conditions of the numerical model in Chapter 4 to reflect changes in the large scale shelf circulation as prescribed by the results of Chapter 5.

Equation (5.40) shows that when coastal wind forcing is applied in the same direction as the shelf break currents, the vorticity in the along-shelf current is reduced. The reader is now referred back to Figures 11a and 11b. In the first figure, inflow across the right-hand boundary was given no vorticity ( $\zeta_0 = 0$ ). This exemplifies the mean winter condition of the larger scale shelf flow subject to the seasonal westward wind stress if the wind driven coastal current was equal in magnitude to the shelf break current. In the second figure, the  $\zeta_0 = 2$  case corresponds to the condition of  $\frac{\partial \psi}{\partial x} = 0$  at the coast ( $x = L_x/L$  in equation 4.3). This exemplifies the summer condition of negligible wind forcing.

Qualitatively, the lowest order topographic effect on the mean flow pattern is no different in these two cases. Quantitatively, however, the first figure (11a) shows a higher density of streamlines between the trough vortex and the shore. In each figure a streamline can be identified passing just inshore of middle current meter station (K9) of the three stations aligned with the trough axis. The number of streamline intervals between this streamline and the coast is 14 in the first diagram and 10 in the second, so that the streamline density in the first figure is a factor of 1.4 greater than in the second. The streamline densities near the mid shelf moorings are not significantly different between these figures.

These model examples agree well with the data in Figure 4. The near shore currents at stations K6 and K8 were significantly greater in winter than in the summer. The winter/summer ratios for K6 (25 and 70 meter depths) and K8 (same) are, respectively; 1.38, 1.77, 1.40 and 2.05. The greater values for the 70 meter depth can easily be attributed to slightly greater baroclinicity during summer. At K7, the 25 meter depth currents had a ratio of 1.18. (The winter means at stations K9 and K10 were substantially weaker than the square root of the variance and are therefore not compared.) In all, this agreement between model and data is very good and illustrates how these models account for the observed seasonal variability.

#### B. Statistical Analysis; Empirical Orthogonal Functions (EOF)

The data in Figure 5 show considerable variability on time scale from days to weeks, typical of current meter observations on the continental shelf. Such variability is usually attributed to wind forcing by synoptic storms, coastal trapped waves or wave-like or eddy-like fluctuations in oceanic currents near the continental margin. Some of these variations can also be examined using the model results. Before doing so, however, it is useful to examine some of the statistical properties of the data to illustrate the complexity of the flow on the Kodiak Shelf.

Cross correlations between various moorings were poor for both the along-shelf and cross-shelf currents, indicating poor spatial coherence over relatively small distances. However, when the currents

were resolved along the principal axes for each mooring (Figures 4 and 5), cross-correlations were greatly improved, indicating coherent variability in the topographically trapped flow pattern around Kiliuda Trough.

This can be shown more explicitly with the use of empirical orthogonal function (EOF) analysis (also known as multivariate or principal axis analysis). This technique has a demonstrated utility in oceanographic data interpretation by decomposing any number of coincident input time series into an equal number of modes. These modes are uncorrelated time series ranked in order of their variance and are purely statistical. Nevertheless, their spatial and temporal patterns can often represent certain dynamic modes derived theoretically. A classic example of such an EOF analysis was done for vertical modes in shelf currents by Kundu *et al.* (1975). A dynamical/empirical comparison, however, is limited to a system where the dynamic modes are uncorrelated and are in effect throughout the period of observation. When dynamic interpretations are difficult, the EOF modes may still be analyzed in terms of their statistical properties.

Input data for this application are time series of scalar quantities, such as velocity components. Each EOF mode is composed of a weighted sum of the input series, where the weights are called eigenvectors. Each input series has an eigenvector for each EOF mode, expressed as follows

$$E_n(t) = \sum_m \alpha_{n,m} V_m(t) \quad (6.1)$$

where  $E_n(t)$  is the  $n^{\text{th}}$  EOF mode and  $\alpha_{n,m}$  is the eigenvector for the  $n^{\text{th}}$  mode and  $m^{\text{th}}$  input series  $V_m(t)$ . The input series can also be reconstructed from the modes by the relation

$$V_m(t) = \sum_n \alpha_{n,m} E_n(t) \quad (6.2)$$

The size of the eigenvector,  $\alpha_{n,m}$ , tells how important the  $n^{\text{th}}$  mode is to the  $m^{\text{th}}$  input series and vice-versa. The sign determines whether  $V_m(t)$  and  $E_n(t)$  are positively or negatively correlated.

The sum of the variances of the modes equals the sum of the variances of the inputs. For a current meter data set, the total variance equals the sum of the (u, v) component variances. Therefore, for a system of five current meters, the total variance is the sum of the ten component variances. If an EOF analysis is done with these ten component inputs, each u and v from each mooring will have an eigenvector for each mode representing its weight, or contribution to that mode. These component eigenvectors can be added vectorially to give the magnitude and direction of variability for each mooring which contributes to each mode, making it possible to examine the mode of variance of the flow pattern near the Kiliuda Trough taking into account both current magnitude and direction at each location.

The pattern of these eigenvector vectors for the first EOF mode is shown in Figure 20 and the values are listed in Table 4. This analysis used the 25 meter depth currents from moorings K6 through K10. The first mode contains 47% and 37% of the total variance for the winter and summer deployments, respectively. The mean flow streamlines from the numerical model results of Chapter 4 are

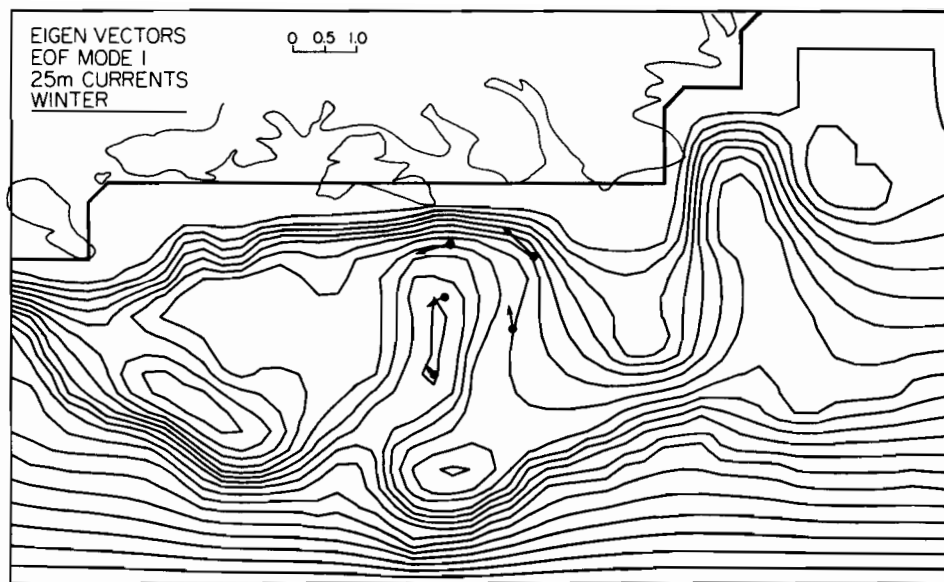


Figure 20a: Eigen vector pattern for the first EOF mode of the 25 meter depth currents during the winter mooring. Mean flow streamlines from the numerical model (Chapter 4) are superimposed.

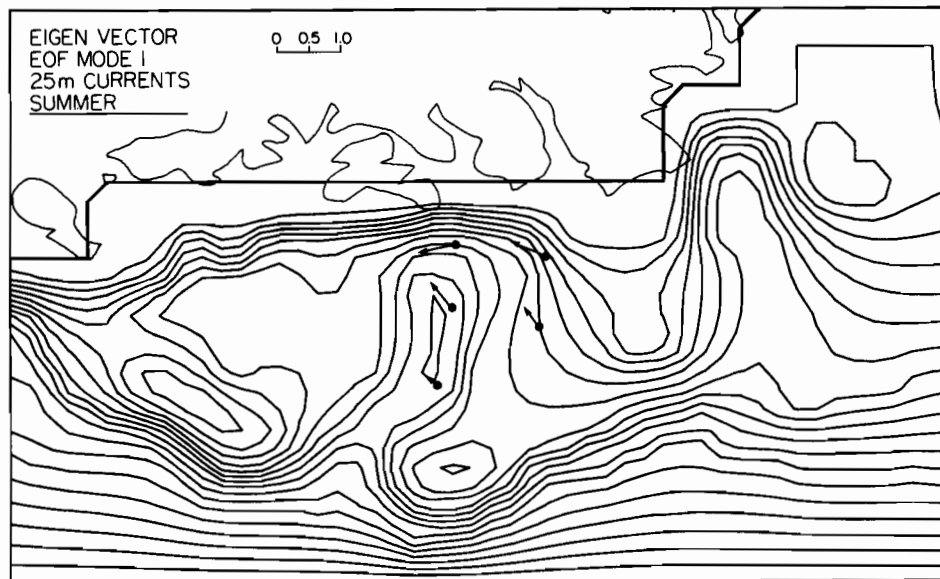


Figure 20b: Same as 20a except using summer current meter data.

superimposed on these figures to show that the dominant mode of variance for the array follows a horizontal pattern which is nearly identical to the mean flow pattern. Therefore the first EOF mode may be interpreted as representing the coherent spin-up or intensification of the vortex or loop current trapped over the Kiliuda Trough. This strong dynamic effect of the topography leaves the higher EOF modes to account statistically for the remaining variance, yielding a confusion of patterns which are difficult to interpret dynamically and are therefore not shown.

Table 4

First EOF mode of 25 meter depth winter currents. See text for description.

Mooring I.D.	component east	eigenvectors north	eigenvector direction (°T)	vectors magnitude
K6	-.646	-.010	269	.646
K7	-.271	.215	308	.346
K8	-.263	-.503	208	.568
K9	-.112	-.325	199	.344
K10	-.153	.011	274	.153

The EOF analysis was also applied to the bottom pressure data at stations K8-K10 (winter only), were arrayed along the axis of Kiliuda Trough. The eigenvectors of the bottom pressure EOF modes are plotted in Figure 21. The second mode (~2.5% of the variance) represents a cross-shelf or along-trough pressure gradient as seen with the aid of

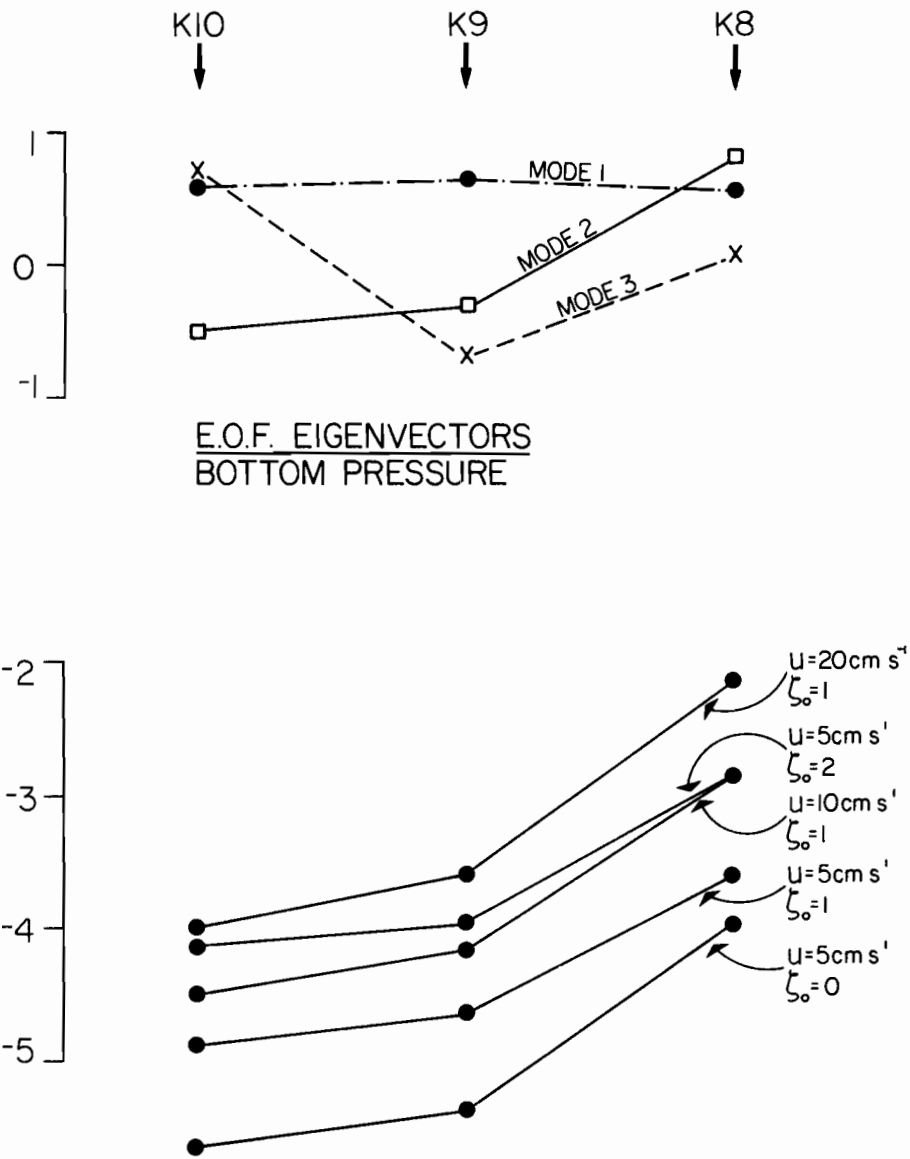


Figure 21: Horizontal distributions of the first and second EOF modes of bottom pressure (top) and the pattern of stream values at stations K8 - K10 (bottom) taken from the model examples in Figures 10 and 11.

equation (6.1), which indicates that mode 2 is computed, effectively, by subtracting the bottom pressure time series at K9 and K10 from K8.

In the theoretical formulation of Chapter 3 the streamfunction was defined as being the lowest order sea-level anomaly, which, in the barotropic case, is equivalent to bottom pressure. The stream line patterns developed in Chapter 4 are useful, therefore, in interpreting the second EOF mode of bottom pressure. Figure 21 also shows an assemblage of numerical stream values at each of the station locations, K8-K10, taken from the model examples of Figures 10 and 11. Their pattern is strikingly similar to bottom pressure EOF mode 2, indicating that the variability represented by bottom pressure mode 2 is related, geostrophically, to the variability in the flow around the trough vortex. The correlation of the first EOF mode of the currents with the second bottom pressure mode was  $r \approx 0.67$ .

The first EOF mode of bottom pressure has an even distribution of eigenvectors (Figure 21), and contains more than 96% of the total bottom pressure variance. It therefore represents a spatially uniform pressure signal or variations on a scale much larger than the length of the array. The correlation between this mode and the first mode of currents was  $r \approx -.42$  but not significant at the 95% level. The sign of the correlations indicates that a decreasing current is weakly associated with a rise in sea-level. The possibility that the first mode signal is related to atmospheric pressure owing to a poor isostatic response in sea-level appears ruled out because the correlation between mode 1 and Kodiak atmospheric pressure (not shown) was insignificant.

### C. Response to Synoptic Atmospheric Storms

Figure 22 illustrates the time series of the current meter and bottom pressure EOF modes under discussion. For comparative purposes, both along- and cross-shelf wind stress components at EB-46 and bottom pressure at K9 are again shown. There are several pulse-like events evident in the bottom pressure and current meter time series which are associated with the strong wind stress events of 23 November, 15 December, 9 January and 22 February, when the local wind stress exceeded  $5 \text{ dynes cm}^{-2}$ .

Generally, shelf currents respond most efficiently to the along-shelf wind component. The responses shown in Figure 11, however, were not consistently related to the along-shelf wind stress component, especially the 15 December event, during which the predominant wind stress component was directed off-shore. Nevertheless, there appears to be a consistent pattern. The largest responses in current meter and bottom pressure data were related to storm events which brought strong along-shelf winds to the north-northeastern coastal areas of the Gulf of Alaska.

A case by case study can be made by analyzing the surface synoptic weather maps of Figure 23 which show the regional meteorological conditions during the wind stress peaks measured at EB-46. The 23 November storm (upper left) was centered well to the south of Kodiak bringing the measured westward wind stress on the shelf. The winds in the northern apex of the gulf were weak and variable. On 24 November the storm weakened substantially; by 25 November, it merged with another low to the east and this brought more intense along-shelf

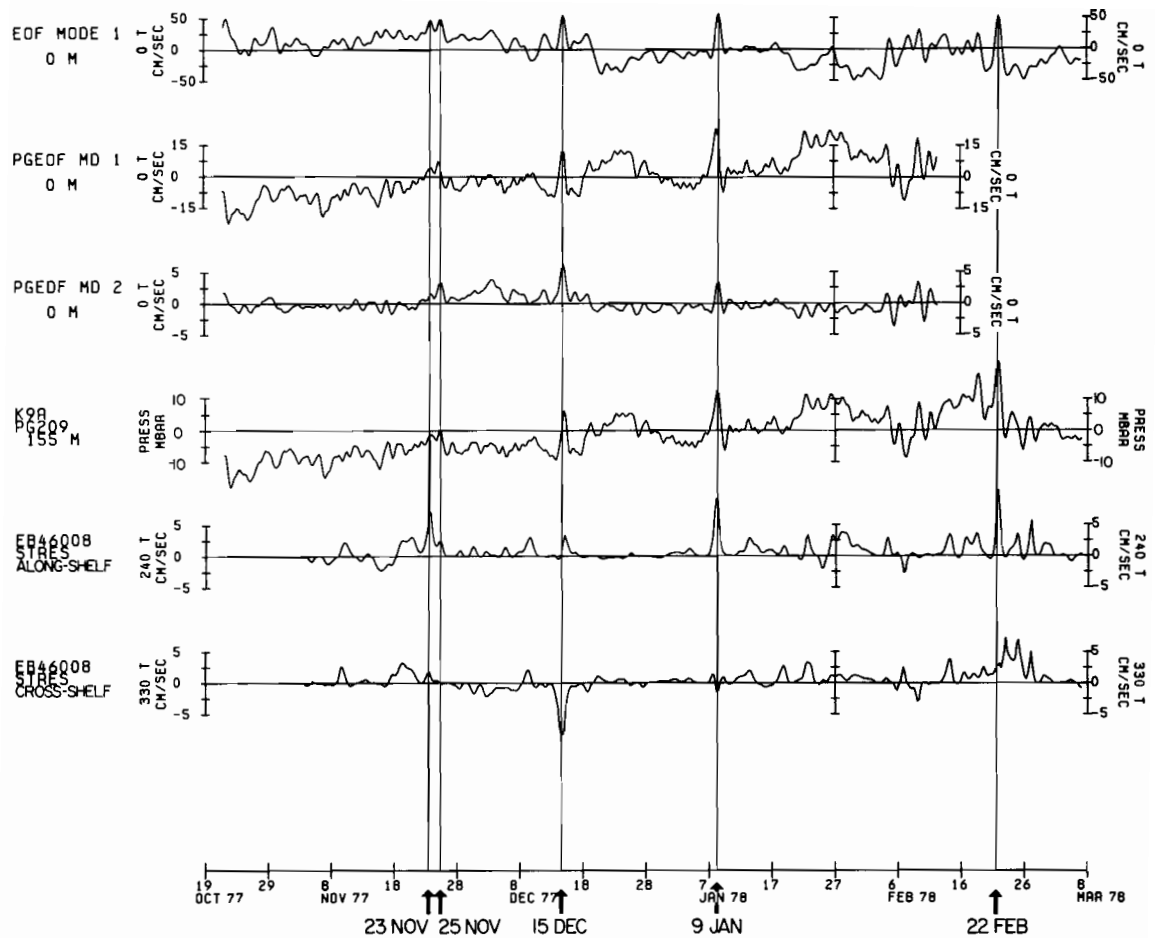


Figure 22: Time series of winter data shown from top to bottom as: The first EOF mode of currents, first and second EOF modes of bottom pressure, bottom pressure at mooring K9, and the along- and cross-shelf wind stress components at EB-46. Vertical lines indicate significant storm events discussed in the text. K9 is included to show the bottom pressure response to the February storm.

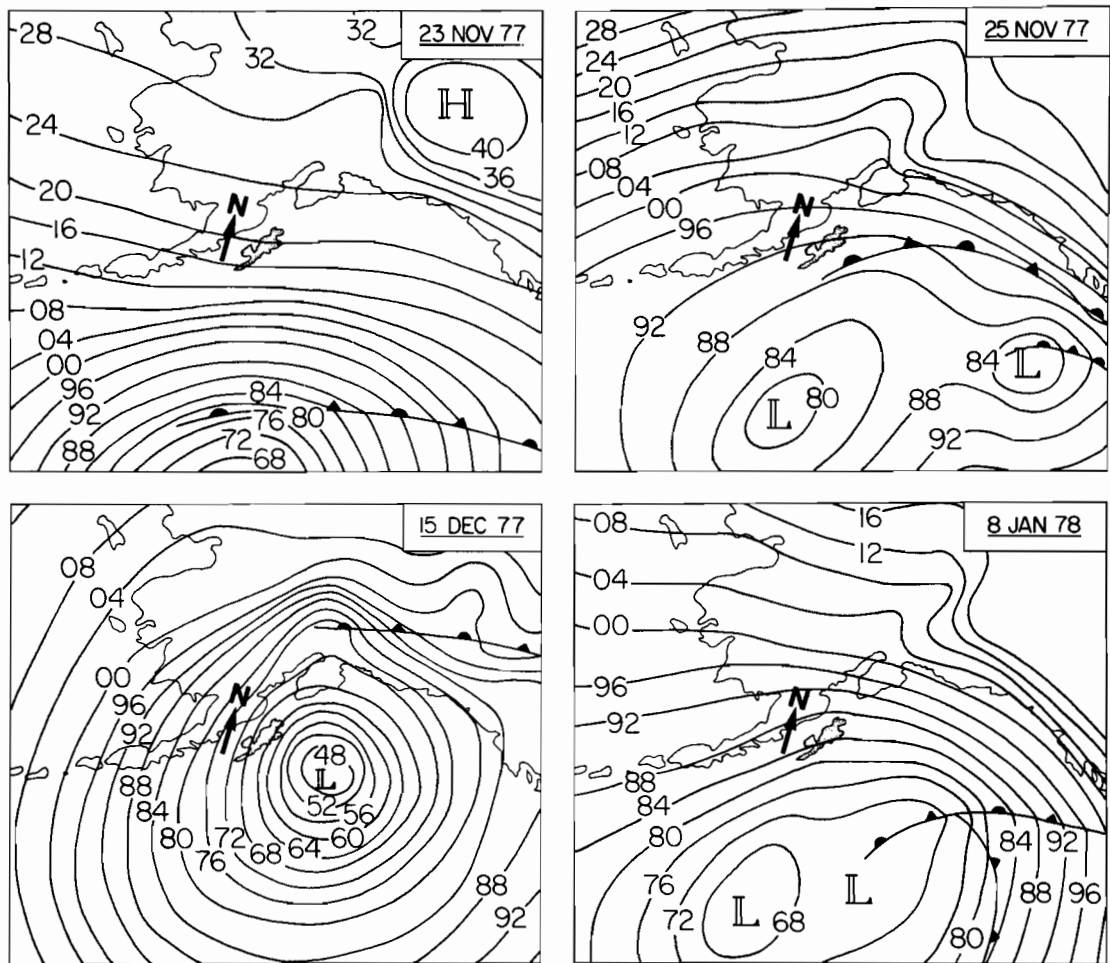


Figure 23. Synoptic weather maps over the Gulf of Alaska showing the severe storms discussed in the text. Contours are in millibars (00=1000).

winds to the north-northeastern gulf (upper right). The measured wind stress at EB-46 (Figure 22) agrees with this scenario with a smaller peak indicated on 25 November. On 15 December an intense (946 mb) low was centered just to the southeast of Kodiak (lower left). This brought strong offshore winds to the Kodiak shelf but also strong along-shelf winds around the north-northeastern gulf. The third storm event (8 January; lower right, Figure 23) caused strong along-shelf winds in the north-northeastern gulf as well as the measured along-shelf wind at Kodiak. There was no weather map conveniently available for the 22 February storm. However, a map of storm tracks (Mariners Weather Log, July 1978) shows that the storm center moved due north across Kodiak.

In comparing the wind stress data, the current and bottom pressure modes and the weather maps, it is evident that the coastal wind conditions to the east of Kodiak are as or more critical than the local along-shelf winds in determining the response of currents and bottom pressure on the Kodiak shelf. For example, EB-46 along-shelf wind stress on 23 November was about a factor of three greater than on 25 November, while the bottom pressure modes showed a larger response on 25 November and the first mode of currents had similar peaks on both dates. More impressive is the 15 December event: large distinctive pulses in all the EOF series, which signify pulses in sea level and current around the Kiliuda Trough, were coincident with a wind stress pulse directed in the sea-ward cross-shelf direction. There was a smaller pulse in the along-shelf wind stress but it was no greater than other along-shelf wind stress events in the record which

did not accompany large pulses in current and bottom pressure data. During the 8 January event, the winds were along-shelf at Kodiak (EB-46) as well as in the north-northeastern gulf. Nevertheless, the responses in EOF modes of Figure 22 were not significantly larger than on the 15 December storm.

The implication of these observations is that the current and bottom pressure signals on the Kodiak shelf are most sensitive to the regional flow conditions as these respond to the path of a storm. Beardsly and Butman (1974) report similar enhanced response to storms which brought along-shelf winds over a considerable stretch of the mid Atlantic Bight coast. The model results of earlier chapters may again be applied to examine this concept. Since the radius of curvature of the perimeter of the Gulf of Alaska is many times larger than the shelf width, the coastline can be considered straight. When an intense cyclone transits the northern gulf, the isobars of atmospheric pressure can lie parallel to the coast over considerable along-shelf distances ( $\sim 1000$  to  $2000$  km) as, for example, in Figure 23. One can compare this case with the analytical solutions of Chapter 5, equation (5.40), wherein the large-scale cross-shelf sea level slope,  $\frac{\partial \psi}{\partial x}$ , should show an increase during the presence of a coastal wind,  $V'$ , as compared to when  $V' = 0$ . This response is evident in both the first and second bottom pressure EOF modes. Bottom pressure increases at each station but to a lesser extent with increasing distance from shore (see again Figure 5).

The flow pattern on the Kodiak Shelf remains highly distorted by the lowest order topographic effects. It is useless, therefore, to

decompose the current meter data into conventional along and cross-shelf components, as determined by the alignment of the coast, and to disregard the local bathymetry. The EOF analysis identified a mode representing fluctuations in the flow pattern around the Kiliuda Trough which shows a positive response to the major wind events under discussion (Figure 22). From the results of the numerical model in Chapter 4, increasing the velocity and decreasing the vorticity of the upstream boundary condition will intensify the currents around the trough. Such boundary condition changes would be caused by the large scale wind pattern associated with these intense storms.

The major events in the record of Figure 22 would be difficult to explain with any model which only took into account the local wind stress as measured at EB-46 because the response to this local along-shelf wind stress is inconsistent. Only by applying the results of Chapters 4 and 5 can a consistent descriptive account be made for the data, by examining the large scale, or regional response to a storm and analysing how these conditions should affect the local situation on the Kodiak shelf.

## Chapter 7: Discussion of Other Shelf Domains

### A. Purpose

The description of the Kodiak shelf flow presented here has shown the dominant effect of the Alaskan Stream and the modulating effect of the wind stress. New solutions to the ATW equation, incorporating a shelf break current as a boundary condition, were introduced to accomplish this. The detailed theoretical discussions were given in Chapter 5. The purpose of this chapter will be to discuss three other well studied shelf domains in order to assess 1) the relevance of the theory to those other shelves and 2) the comparative uniqueness of the Kodiak shelf system. These three shelves are: The East Florida shelf and South Atlantic Bight, which together are bounded by the Gulf Stream; the Middle Atlantic Bight, believed to be forced by an along-shelf pressure gradient; and the Washington/Oregon shelf, comprising an eastern oceanic boundary.

### B. East Florida Shelf and South Atlantic Bight (S.A.B.)

The East Florida shelf is narrow, bounded to seaward by the swift Gulf Stream (or Florida Current) and has quite uniform along-shelf bathymetry. It therefore makes an excellent candidate for testing features of the model presented in Chapter 5.

One such feature is the ratio between the along and cross-shelf geostrophic current components,  $v/u$ , which is directly proportional to the local depth ( $H$ ). This is seen from combining Equations (5.27), (5.28) and (3.3) to form:

$$v/u = (\partial\psi/\partial x) / -(\partial\psi/\partial y) = 2H/\delta_E \quad (7.1)$$

(See also Figure 15.)

Lee (1975), in a study that links low frequency fluctuations in flow on the shelf to Florida Current spin-off eddies, presented progressive vector diagrams (PVD's) which are useful to interpret the net current. They show northward mean flow with a significant seaward cross-shelf component. If our coordinate system from Chapter 5 were shifted to the east Florida Shelf, the y-axis would point south, the x-axis shoreward and the origin would be at the coast. The boundary current,  $V$ , would be negative, causing a southward sea-level increase (equation 5.28) and seaward cross-shelf geostrophic flow, in agreement with the PVD's presented by Lee (1975).

The mooring was stationed in 30 meters of water for 43 days in early spring and for 15 days in summer. The combined mean current from both deployments was  $\sim 12 \text{ cm s}^{-1}$ . Deduced from the PVD's,  $v/u$  was  $\sim 4.6$  for the spring deployment and  $\sim 7.2$  for the summer with a net of  $\sim 5.7$ . With a water depth of 30 m at the mooring site and a typical Ekman layer thickness of  $\sim 10 \text{ m}$  (e.g. Mayer *et al.*, 1982; Hsueh and Peng, 1978),  $v/u$  is  $\sim 6$  according to Equation (7.1). The good comparison of these estimates between data and model prediction is very encouraging and suggests that the model is generally applicable.

The South Atlantic Bight, between Florida and Cape Hatteras, is a broad shelf bounded to seaward by the Gulf Stream. The oceanography of this region is reviewed by Pietrafesa *et al.* (1982), Lee and Brooks (1979), Lee *et al.* (1982) and by many authors in a special issue of J.G.R. (1983, 88, C3). In general the shelf can be divided into three

regimes (Blanton, 1982). The near shore regime (0-20 m) is dominated by mixing of freshwater discharge. Baroclinic flow is northward during the spring/summer and southward during the fall owing to the prevailing wind stress. This zone is distinct from the mid-shelf region (20-40 m) where the flow responds barotropically and in geostrophic balance with wind induced sea level at the coast. The outer shelf (40-100 m) is dominated by the Gulf Stream, where wave-like fluctuations induce upwelling and account for much of the subtidal variability of the outer shelf currents (Lee and Brooks, 1979). At mid-shelf the seasonal mean is 1 to 5 cm s<sup>-1</sup>, summer and winter, respectively. Prolonged southward flow events occur in late summer which are partly wind and partly density driven. North of Charleston, the Gulf Stream moves offshore and has less direct effect on shelf circulation. For the South Atlantic Bight the net flow is northward over most of the year, but from late summer to early winter, wind stress and inner shelf currents are southward forming a cyclonic gyre (Pietrafesa et al., 1982). Density forcing is also important over the southern portion of the inner shelf (Atkinson et al., 1981).

Recently, Atkinson et al. (1983) have discussed the climatology of S.A.B. waters. They cite a strong influence of the Gulf Stream on the mean northward flow in mid and outer shelf zones for both winter and summer, and a strong influence of transient wind stress in the mid-shelf region. They used data from a mid-shelf mooring to indirectly estimate the along-shelf sea level slope according to the method of Scott and Csanady (1976). Sea level sloped down to the north with a magnitude of  $1.67 \times 10^{-7}$  during winter/spring and

$0.67 \times 10^{-7}$  during summer/fall, in good agreement with Sturges' (1974) estimate of  $\sim 2 \times 10^{-7}$ . A simple along-shelf mean momentum balance of bottom stress vs. pressure gradient indicated a northward mean current also in good agreement with their observations. The authors attribute the mean flow to the sea level gradient and attribute the gradient to offshore oceanic conditions, without specifying what those conditions may be.

The along-shelf sea-level gradient along the east coast is believed to slope downward from the tropics to Cape Hatteras and can mostly be accounted for with our equation (5.15) (Sturges, 1974). Nevertheless, it is encouraging that the observed slope agrees with the model presented above in Chapter 5 when applied to the S.A.B. Equation (5.19) indicates that sea level slopes down in the direction of the shelf break current, and with a northward flowing Gulf Stream, this is consistent with Sturges' data.

Blaha (1982) has presented monthly mean coastal sea-level data from the Florida shelf to the South Atlantic Bight. The monthly mean along-shelf sea-level differences between stations indicate that north of Florida there is an autumn peak in downward-to-the-north gradient. Monthly mean wind stress data show a southward peak for the same period. Through equation (5.41) it can be seen that this southward wind stress would increase the sea-level gradient in agreement with the data. On the other hand, along the Florida shelf, Blaha's data show a reversal in this seasonal along-shelf sea-level trend but not in the wind stress. This was diminished by adjusting the sea-level

data for local coastal wind set-up and local surface heating, indicating these effects are also important.

The above observations indicate a strong similarity between the S.A.B. and Kodiak shelf dynamics as described by the model of Chapter 5. It is a steady state problem which addresses the large-scale mean or seasonally varying flow on a shelf bounded by an oceanic boundary current. For the Kodiak Shelf, this model serves to show why the current is generally southwestward year-round owing to the southwestward flowing Alaskan Stream.

The South Atlantic Bight is more stratified than the Kodiak shelf and a strong front separates the Gulf Stream from shelf waters. Nevertheless, the basic flow pattern conforms to the model in terms of equation (5.40). The shelf break current,  $V$ , can be considered constant year-round while the coastal condition,  $V'$ , fluctuates with seasonally averaged wind stress. When it is southward, as in the autumn, the inner shelf currents flow south causing cyclonic shear across the shelf. The mid-shelf is at about 50 m and it is shoreward of this that the flow response to wind and buoyancy forcing is greatest.

As with the South Atlantic Bight, the inshore waters of the Kodiak Shelf should be subject to seasonal variation correlated with wind stress. For the Northwest Gulf of Alaska the seasonal variations of wind stress bring strong westward stress in the winter changing to weak and variable stress in the summer. Thus, the inshore waters show a seasonal modulation in southwestward flow while the shelf break waters remain dominated by the less variable flow of the Alaskan

Stream. In contrast to the South Atlantic Bight the wind stress does not reverse in summer with sufficient strength or duration to reverse the flow on the inner shelf. It is better described as an "on-off" forcing which, during winter, serves to augment the ocean dominated flow. The manifestations of this seasonal variability on the Kodiak shelf, where the flow remains highly distorted by the lowest order topographic effects, was discussed in Chapter 6.

### C. The Middle Atlantic Bight (M.A.B.)

The M.A.B. is the broad shelf extending from Cape Hatteras north-eastward to Nova Scotia. The Gulf Stream leaves the shelf break south of Cape Hatteras, turning eastward across the Atlantic, and therefore does not impact the continental slope flow off the M.A.B. There is evidence of a weak southwestward baroclinic current over the continental slope, with a speed of  $\sim 20$  cm/s relative to 4000 db (Csanady, 1979). This may be the boundary flow of a weak subpolar gyre in the northwest Atlantic which is reproduced in the numerical model by Semtner and Mintz (1977).

Mean flow on the M.A.B. shelf is very similar to that on the Kodiak and Northwest Gulf of Alaska shelf area. It is southwestward year round with a mean of about  $5 \text{ cm s}^{-1}$  and outer shelf currents are generally stronger than on the inner shelf (Beardsley and Boicourt, 1981). Significant transient storm driven variability occurs. Coastal runoff is also significant to the near-shore currents and its seasonal variability is greater than that of the outer shelf currents

(Beardsley and Winant, 1979). These observations indicate a strong influence of the large scale oceanic circulation on the shelf flow.

There is considerable evidence that the mean flow is driven by a large scale along-shelf pressure gradient. Stommel and Leetmaa (1972) and Csanady (1976) applied models combining density (runoff) and wind forcing to the M.A.B. and both concluded that a mean sea surface slope of  $\sim 10^{-7}$ , downward to the southwest, must exist to account for the observed flow. Scott and Csanady (1976) measured this slope indirectly to be  $\sim 1.4 \times 10^{-7}$ . Beardsley and Winant (1979) argue that this may be high by as much as a factor of 5, but conclude that a slope of  $\sim 10^{-7}$  to  $\sim 10^{-8}$  is indicated. Csanady (1978) presented a solution to the ATW equation for shelf currents forced by an along-shelf pressure gradient (see above, Chapter 5) to account for the M.A.B. circulation. He further speculated that the sea surface slope was established by the deep ocean circulation. Beardsley and Winant (1979) concurred with this notion and presented evidence from the basin circulation model of the northwest Atlantic by Semtner and Mintz (1977), which reproduced a slope of  $\sim 0.9 \times 10^{-7}$  for the region coincident with the M.A.B. This pressure field was generated by the large scale wind stress and heat flow patterns over the North Atlantic, so Beardsley and Winant (1979) concluded that the M.A.B. shelf flow is a boundary component of the larger scale oceanic circulation.

The effect of the density field on the mean flow has also been studied. Csanady (1979) calculated the steric sea level field over the shelf and slope, using a reference level of 4000 db. He found that the thermohaline component did not make a significant contribu-

tion to the along-shelf pressure field and effects of the St. Lawrence river were confined to the Gulf of Maine. Shaw (1982) has offered a complex numerical model driven by along-isobath density gradients and concludes that winter cooling and density driven currents can account for much of the southwestward flow from winter to late summer. This flow exists independently of any external forcing.

Shaw gave added significance to this density driven flow in a separate analysis which showed that the continental slope effectively insulates the deep ocean bottom pressure field from the shelf. Wang (1982) has offered numerical solutions to the ATW equation assuming a homogeneous ocean over both the continental shelf and slope, and applying an along-shelf pressure field at the seaward edge of the continental slope. The modeled flow was confined to the slope region and did not penetrate onto the shelf, in basic agreement with Shaw's (1982) analysis.

These later results by Shaw (1982) and Wang (1982) cast doubt on the earlier conclusions about the importance of the oceanic circulation and an imposed along-shelf pressure gradient to driving the flow on the M.A.B. However, in both investigations, only the barotropic, or bottom pressure fields were considered and the apparent insulating effect of the continental slope must be evaluated with that limitation. The baroclinic boundary currents which exist over the slopes of western ocean margins were not taken into account. As shown in Chapter 5, this flow should be considered when evaluating the effect of the oceanic circulation on the shelf currents. The Semtner and

Mintz (1977) model, cited above as showing an along-shelf pressure gradient, is baroclinic.

Csanady's (1979) data showed a significant steric sea level drop across the continental slope, indicating an  $\sim 20 \text{ cm s}^{-1}$  baroclinic surface current relative to 4000 db. Although this is considerably weaker than the  $\sim 100 \text{ cm s}^{-1}$  Alaskan Stream found adjacent to the Kodiak Shelf, its presence could influence the cross-shelf pressure gradient at the shelf break, and therefore the shelf flow, in the manner proposed above in Chapter 5. This possibility should be investigated by those studying the M.A.B. circulation because of the uncertainties concerning the relative importance and mechanics of large scale forcing and buoyancy effects in setting up an along-shelf pressure field and driving the mean southwestward flow. Attributing the flow to the cross-shelf rather than the along-shelf pressure gradient at the shelf break, as was done in Chapter 5 for the Kodiak shelf, one may account for both the flow and the along-shelf pressure field of the M.A.B.

From these accounts, it is evident that the mean southwestward M.A.B. flow is forced in part by buoyancy effects and in part by the large scale oceanic circulation. The relative importance of these effects is still unknown and may vary cross-shelf, with the oceanic effects dominating the outer shelf. An along-shelf pressure gradient generated by the larger scale oceanic circulations appears to drive the flow, however, the nature of the oceanic forcing may be similar to that proposed here for Kodiak. This could be resolved if the analysis in Chapter 5, to estimate the shelf break current due to the oceanic

transport over the slope, is applied to the M.A.B. Clearly, the M.A.B. and Kodiak Shelves share many similarities. Both are NE/SW oriented, mean currents are southwest at  $5 \text{ cm s}^{-1}$ , both border cyclonic subarctic gyres and, by all studies so far, seem to be governed by the same basic vorticity balance for the mean flow.

#### D. Washington/Oregon Shelf

The shelf adjoining the Pacific Northwest coast of North America is part of an eastern ocean margin. The oceanic circulation lacks the intense boundary currents characteristic of western ocean boundaries (Stommel, 1948). Consequently, one should not expect an influence of a boundary current on the shelf flow here as compared with the studies discussed above.

Hickey (1979) thoroughly reviewed the shelf and slope circulation. There is significant transient variability in the two- to ten-day band, which may take the form of free (Cutchin and Smith, 1973) or forced (Allen, 1976) shelf waves. These fluctuations bring frequent reversals in current and are usually well-correlated with along-shelf wind stress and coastal sea level.

A seasonal flow variation is also prominent. Mean summer winds are southward, causing upwelling and southward flow. There is a near shore, baroclinic jet, on the order of the internal Rossby radius ( $\sim 20 \text{ km}$ ) in width. In the winter, the flow pattern is reversed, with the onset of mean northward wind stress, producing the northward flowing Davidson Current. The transition from winter to summer occurs rapidly all along the coast, usually within a day. During the summer,

a poleward undercurrent is found over the continental slope a few kilometers seaward of the shelf break at a depth of about 200 meters. This flow may be continuous from Baja California to Northern Washington. In winter, the core of the flow may rise and merge with the Davidson Current off Oregon and Washington. There is recent evidence of wintertime equatorward undercurrent over the slope off Washington (Werner and Hickey, 1983) may have a bearing on the dynamic importance of the along-shelf pressure field.

Steric sea level estimates by Sturges (1967) and Reid and Mantyla (1976) suggest that the long term mean sea level rises northward along Oregon and Washington. Enfield and Allen (1980) compiled long term statistics of adjusted (tide gauge height plus atmospheric pressure) sea level along most of the west coast and Alaska and Hickey and Pola (1983) combined these data with the earlier steric data to describe a seasonal trend in monthly mean sea level. Surface elevation rose to the north from October to June and then reversed slope to the south but less steeply from July to September. Hickey and Pola (1983) also showed that this seasonal pattern is consistent with local and non-local (i.e., elsewhere along the coast) wind forcing by applying solutions to the ATW equation given by Csanady (1978).

The importance of this along-shelf pressure gradient to shelf dynamics was analyzed by Werner and Hickey (1983). They identified three seasonal situations. In winter, the pressure gradient force is southward, opposing the mean wind stress. This is reversed in summer (July to September), when the pressure gradient force is northward and wind stress is southward. During spring, when the wind reverses from

northward to southward, both the wind stress and pressure gradient force are southward, causing the rapid transition in flow mentioned above as well as a stronger southward current. The pressure gradient is diminished and then reversed by the seasonal wind stress so that by summer they are again in opposition.

Modeling studies by Werner and Hickey (1982) succeeded in reproducing the essential features of the shelf and slope currents, including the slope undercurrents. Most importantly, these features were not reproduced when wind forcing alone was applied. The inclusion of an external along-shelf pressure gradient force was essential. In the vertically integrated along-shelf momentum balance the wind stress, bottom stress and pressure gradient dominated (except during the spring transition when local acceleration was also important). This steady balance, along with a cross-shelf geostrophic balance, are the bases (through cross differentiation) for the ATW equation (Csanady, 1978). Therefore the same momentum and vorticity relations discussed in the other case studies are important to this shelf as well.

Several features distinguish this shelf from the others. Of interest here is the lack of an oceanic boundary current which is so important for the Kodiak and S.A.B. cases and suggestive for the M.A.B. Therefore, the role of oceanic forcing does not include the shelf break current boundary condition mechanism. However, the large scale ocean dynamics do induce a mean along-shelf pressure gradient to the Pacific Northwest shelf which, coupled with seasonal wind stress, heavily influences the flow pattern. The pressure gradient varies

seasonally, driven by coastal wind forcing and to a lesser extent by deep ocean mechanisms such as heating and advection (Hickey and Pola, 1983). In addition, wind stress, shelf and slope currents undergo seasonal reversals. This contrasts with the Kodiak and M.A.B. shelves where the descriptor "year-round" applies to the mean flow and with the S.A.B. where only the inner shelf currents are subjected to wind and runoff controlled seasonal variability.

In summary, the Washington/Oregon shelf is predominantly a wind driven regime. The influence of oceanic forcing to the shelf is indirect through minor seasonal adjustments to the along-shelf pressure field. The seasonally varying along-shelf pressure field is important to the dynamics, second only to the wind, and is forced primarily by the wind through local and non-local mechanisms.

## Chapter 8: Summary

### A. Results

This study has sought to describe and explain the mean flow pattern over the central Kodiak Island shelf. The field study consisted of one winter and one summer four-month long current meter deployments of a five station array in the vicinity of a shallow bank and deep canyon or trough. An additional four-month winter mooring nearby but during a different year was also considered. Together, these data show that the mean flow is dominantly barotropic and constrained to follow the complex bathymetric pattern. Because the mean shelf flow is southwestward with the coast on the right, the currents form a cyclonic vortex as they pass around the perimeter of the deep Kiliuda Trough. The flow pattern constitutes an example of a Taylor-Proudman column on a shelf.

The presence of the cyclonic vortex over the trough implies potential vorticity conservation whereby an increase in depth along a streamline is balanced by an increase in relative vorticity. A simple potential vorticity equation was applied to the shelf with a numerical model. With the proper scaling velocity ( $\sim 5 \text{ cm s}^{-1}$ ) this model was in excellent agreement with the mean flow data. The scaling is appropriate to a lowest order balance of  $\vec{U} \cdot \vec{\nabla} H = 0$ , or flow along isobaths. One consequence of this balance is that stronger currents will occur in areas of steep topography as streamlines following isobaths converge.

These results were compared with another modeling study (Galt, 1980) which applied a vorticity balance including bottom Ekman

boundary layer pumping but not the inertial terms fundamental to this potential vorticity model. The present study gave a better rendition of the mean flow pattern. The bottom Ekman pumping was shown to be naturally small in the more general vorticity balance when the flow closely follows isobaths, thus favoring the potential vorticity formulation.

The topographically trapped flow pattern was identical in both the summer and winter data sets, indicating that it is a year-round feature. The numerical model accounts for the flow pattern by assuming an inflow across the right-hand (eastern) boundary which is a consequence of the regional shelf circulation. To account for the small seasonal variability in the data in spite of an order of magnitude seasonal variability in wind stress, the southwestward mean flow was dynamically linked to the strong Alaskan Stream boundary current which flows southwestward year-round along the continental slope.

It was shown that the shelf dynamics over large along-shelf scales could be accounted for by a simple vorticity balance, the Arrested Topographic Wave equation, derived by Csanady (1978). Csanady offered several solutions to the equation but none which apply to this study. New solutions were derived using boundary conditions representing the dominant current at the shelf break. It was shown that the presence of the shelf break current alone could drive an along-shelf current on the adjacent shelf, that the current magnitude would be proportional to the local depth and that an along-shelf sea level gradient would be generated which slopes downward in the flow direction.

The shelf break current which drives this flow was shown to be associated with the oceanic boundary current along the continental slope, the Alaskan Stream. A simplified planetary vorticity balance in the stream was integrated laterally to compute the shelf break current, showing it to be proportional to the stream transport and consistent in magnitude with observations.

A coastal boundary condition which takes into account wind forcing was applied to find a solution to the Arrested Topographic Wave equation subject to both wind forcing and the shelf break current. The resultant alteration to the basic large scale flow was then used to assess the effect on the boundary conditions of the numerical model. In this way the observed seasonal and storm forced variability in the data were accounted for.

To assist in these interpretations, Empirical Orthogonal Function (EOF) analyses were performed on the data. The first EOF mode for the currents accounted for nearly 50% of the variance and represented the fluctuations in the cyclonic flow around the topographically trapped vortex. EOF analysis of bottom pressure produced a second mode related geostrophically to the flow pattern and a first mode related to sea level variability on a larger spatial scale. Several pulse-like fluctuations in these modal time series were coincident with intense storms but could not be well accounted for if only the local along-shelf wind stress near Kodiak was considered. When the events were examined on a large spatial scale, it was found that the greatest responses consistently occurred when the storm tracks brought along-

shelf winds over a long section of the northern Gulf of Alaska coastline.

## B. Implications

These results show that the Kodiak Shelf is, oceanographically speaking, a component of the outer shelf of the northwestern Gulf of Alaska shelf domain. The southwestward year-round mean flow is driven primarily by the Alaskan Stream. A seasonal modulation is evident in the nearshore currents due to the regional wind stress variability, but there is no seasonal change in the basic topographically trapped flow pattern over the central shelf.

A qualitative description of the mean circulation of the northern Gulf of Alaska shelf emerges from these results. The outer shelf currents are dominated by the counter-clockwise oceanic gyre circulation. Forcing of the inshore waters is in part driven by the regional wind pattern and in part by coastal runoff. These three mechanisms reinforce one another to create a coastal flow which is also counter-clockwise around the gulf perimeter. This flow is sustained year round and is seasonally modulated by the runoff and wind stress. This was contrasted with the South Atlantic Bight where the summer coastal flow owing to runoff and wind stress opposes the Gulf Stream.

The ideas and methods put forward in this study have adequately accounted for the Kodiak data in terms of mean flow, seasonal variability and intense storm forcing. It was extremely useful to examine the small scale and large scale flow features independently owing to the complicated topography of the Kodiak shelf. The solutions

presented here for the cases of boundary current and coastal wind forcing were applied for comparison to the South Atlantic Bight, Mid Atlantic Bight and the Washington/Oregon Shelf. For the S.A.B., the outer shelf flow and along-shelf pressure field are consistent with effects of the Gulf Stream according to the solutions given here. The M.A.B. flow is thought to be driven by an along-shelf pressure field of oceanic origin. However, the geographic and oceanographic similarities to the Kodiak shelf and the presence of a weak boundary current over the slope suggest that the shelf break current forcing mechanism given here may also apply. The Washington/Oregon Coast by comparison is primarily a wind driven regime in the absence of strong ocean boundary currents.

This study of the Kodiak shelf has demonstrated the important steering effects of bottom topography and driving effects of oceanic boundary currents on continental shelf circulation. The insights into shelf dynamics provided by these results make a significant contribution to the goal of understanding and forecasting currents on continental shelves.

#### Acknowledgments

This study was carried out while the senior author was assigned to PMEL as a NOAA Corps Officer. Most of the data were obtained as part of NOAA's Outer Continental Shelf Environmental Assessment Program (OCSEAP). The work was completed following the senior author's reassignment as part of a NOAA fisheries oceanography study. This support is gratefully acknowledged. The results also were used as partial fulfillment of requirements for a Ph.D. degree at the University of Washington. Critiques from L. K. Coachman, B. M. Hickey, H. O. Mofjeld, J. D. Schumacher and R. K. Reed greatly assisted the study.

## Bibliography

- Allen, J.S., 1976: On forced, long continental shelf waves in an f-plane. J. Phys. Oceanogr., 76, 426-431.
- Atkinson, C.P., J.O. Blanton, T.N. Lee, 1981: Observation and cause of southerly flow of inner shelf waters in the Georgia Bight during the Fall. EOS, 62, 927. (Abstract)
- Atkinson, L.P., T.N. Lee, J.O. Blanton, W.S. Chandler, 1983: Climatology of the Southeastern United States continental shelf waters. J. Geophys. Res., 88, C8, 4705-4718.
- Beardsley, R.C. and W.C. Biocourt, 1981: On estuarine and continental shelf circulation in the middle Atlantic Bight, in Evolution of Physical Oceanography, B. Warren and C. Wunsch, eds. M.I.T. Press, Cambridge, MD. pp. 198-233.
- Beardsley, R.C. and B. Butman, 1974: Circulation on the New England continental shelf: Response to strong winter storms. Geophysical Research Letters, 1, 181-184.
- Beardsley, R.C. and C.D. Winant, 1979: On the mean circulation in the Middle Atlantic Bight. J. Phys. Oceanogr., 9, 612-619.
- Blaha, J.P. 1982: Fluctuations in monthly sea level as related to the Gulf Stream from Florida to the South Atlantic Bight. In press, J. Geophys. Res.
- Blanton, J.O., 1982: Circulation over the Continental Shelf off the Southeastern U.S. EOS 63, p.1007. (Abstract)
- Buckwald, V.T. and J.K. Adams, 1968: The propagation of continental shelf waves. Proc. Roy. Soc. London, A305, 235-250.
- Butman, B., 1982: An overview of recent research and the physical oceanography of Georges Bank. EOS, 63, p.1006. (Abstract)
- Butman, B., R.C. Beardsley, B. Magnell, D. Frye, J.A. Vermersch, R. Schlitz, R. Timeburner, W.R. Wright and M.A. Noble, 1982: Recent observations of the mean circulation on Georges Bank. J. Phys. Oceanogr., 12, 569-591.
- Cannon, G.A., 1972: Wind effects on currents observed in the Juan de Fuca submarine canyon. J. Phys. Oceanogr., 2, 281-285.
- Cannon, G.A., N.P. Laird and T.V. Ryan, 1972: Currents observed in the Juan de Fuca submarine canyon and vicinity, 1971. NOAA Tech. Rept. ERL 252-POL 14, 57 pp.

- Cannon, G.A. and G.S.E. Lagerloef, 1983: Topographic influences on coastal circulation (a review). Coastal Oceanography, Physical Aspects. H. Gade, H. Svendsen & A. Edwards (eds.). Plenum Publ. Corp. (In press)
- Carslaw, H.S. and J.C. Jaeger, 1959: Conduction of Heat in Solids 2nd ed. Oxford University Press, 510 pp.
- Csanady, G.T., 1978: The arrested topographic wave. J. Phys. Oceanogr., 8, 47-62.
- Csanady, G.T., 1979: The pressure field along the western margin of the North Atlantic. J. Geophys. Res., 84C, 4905-4915.
- Cutchin, D.L. and R.L. Smith, 1973: Continental shelf waves: low frequency variations in sea level and currents over the Oregon continental shelf. J. Phys. Oceanogr., 3, 73-82.
- Eide, L.I., 1979 Evidence of a topographically trapped vortex on the Norwegian continental shelf. Deep-Sea Res., 26, 601-621.
- Enfield, D.B. and J.S. Allen, 1980: On the structure and dynamics of monthly mean sea level anomalies along the Pacific coast of North America. J. Phys. Oceanogr., 10, 557-578.
- Favorite, F. and W.J. Ingraham, 1977: On the flow in the Northwestern Gulf of Alaska, May 1972. J. Oceanogr. Soc. Japan, 33, 67-81.
- Freeland, H.J. and K.L. Denman, 1983. A topographically controlled upwelling centre off southern Vancouver Island. Coastal Oceanography, Physical Aspects. H. Gade, H. Svendsen & A. Edwards (eds). Plenum Publ. Corp. (In press)
- Galt, J.A., 1980: A finite element solution procedure for the interpolation of current data in complex regions. J. Phys. Oceanogr. 10, 1984-1997.
- Gill, A.E. and E.H. Schumann, 1974: The generation of long shelf waves by the wind. J. Phys. Oceanogr., 4, 83-90.
- Greenspan, G.P., 1969: The Theory of Rotating Fluids. Cambridge University Press, 327 pp.
- Han, G., D.V. Hansen and J.A. Galt, 1980: Steady state diagnostic model of the New York Bight. J. Phys. Oceanogr. 10, 1998-2020.
- Hayes, S.P., 1979: Variability of current and bottom pressure across the shelf in the northeast Gulf of Alaska. J. Phys. Oceanogr., 9, 88-103.
- Hickey, B.M. 1979: The California current system - hypotheses and facts. Progress in Oceanography, 8, 191-280.

- Hickey, B.M. and E.T. Baker, 1981: Time dependant particle distribution in a moderately broad coastal submarine canyon. EOS, 62, 916. (Abstract)
- Hickey, B.M. and D. Hamilton, 1980: A spin-up model as a diagnostic tool for the interpretation of current and density measurements on the continental shelf in the Pacific Northwest. J. Phys. Oceanogr., 10, 12-24.
- Hickey, B.M. and N.E. Pola, 1983: The alongshore pressure gradient on the west coast of the United States. J. Geophys. Res., 88, C12, 7623-7633.
- Hide, R., 1971: On geostrophic motion of a non-homogeneous fluid. J. Fluid Mechanics, 49, 745-751.
- Hogg, N.G., 1973: On the stratified Taylor column. J. Fluid Mech., 58, 517-537.
- Hsueh, Y., 1980: On the theory of deep flow in the Hudson Shelf Valley. J. Geophys. Res. 85C, 4913-4918.
- Hsueh, Y. and C.H. Peng, 1978: A diagnostic model of continental shelf circulation. J. Geophys Res., 83C, 3033-3041.
- Huppert, H.E., 1975: Some remarks on the initiation of inertial Taylor columns. J. Fluid Mech., 67, 397-412.
- Huppert, H.E. and K. Bryan, 1975: Topographically generated eddies. Deep Sea Research, 23, 655-679.
- Hurlburt, H.E., 1974: The influence of coastline geometry and bottom topography on the eastern ocean circulation. Ph.D. thesis, Florida State University, Tallahassee. 103 pp.
- Kundu, P.K., J.S. Allen and R.L. Smith, 1975: Model decomposition of the velocity field near the Oregon coast. J. Phys. Oceanogr., 5, 683-704.
- Lagerloef, G.S.E., R.D. Muench and J.D. Schumacher, 1981: Low frequency variations in currents near the shelf break: Northeast Gulf of Alaska. J. Phys. Oceanogr., 11, 627-638.
- Lee, Thomas N., 1975: Florida Current spin-off eddies. Deep-Sea Research, 22, 753-765.
- Lee, Thomas N. and David A. Brooks, 1979: Initial observations of current, temperature and coastal sea level response to atmospheric and Gulf Stream forcing on the Georgia shelf. Geophys. Res. Letters.

- Lee, Thomas N., Ernest Daddio and Gregory C. Han., 1982: Steady-state diagnostic model of summer mean circulation on the Georgia shelf. J. Phys. Oceanogr., 12, 820-838.
- Loder, John W., 1980: Topographic rectification of tidal currents on the sides of Georges Bank. J. Phys. Oceanogr., 10, 1399-1416.
- Magnell, Bruce A., Stanley L. Spiegel, Richard E. Scarlet and J. Bruce Andrews, 1980: The relationship between tidal and low frequency currents on the north slope of Georges Bank. J. Phys. Oceanogr., 10, 1200-1212.
- Mariners Weather Log, 1978, 22, 292.
- Mayer, Dennis A., D. V. Hansen and D. A. Ortman, 1979: Long-term current and temperature observations on the middle Atlantic shelf. J. Geophys. Res., 84C, 1776-1792
- Mayer, D.A., G.C. Han and D.V. Hansen, 1982: Circulation in the Hudson Shelf Valley. J. Geophys. Res., 87, C12, 9563-9778.
- Muench, R.D., H.O. Mofjeld and R.L. Charnell, 1978: Oceanographic conditions in Lower Cook Inlet: Spring and Summer, 1973. J. Geophys. Res., 83c, 5090-5098.
- Muench, R.D. and J.D. Schumacher, 1980: Physical Oceanographic and meteorological conditions in the Northwest Gulf of Alaska. NOAA Tech. Memo ERL PMEL-22, 147 pp.
- Mysak, L.A., 1982: Barotropic instability of flow along a trench. Geophys. Astrophys. Fluid Dynamics, 19, 1-33.
- Nelson, T.A., P.E. Gadd and T.L. Clarke, 1978: Wind induced current flow in the upper Hudson shelf valley. J. Geophys. Res., 83C, 6073-6082.
- Niebauer, H.J., J. Roberts and T.C. Royer, 1981: Shelf break circulation in the northern Gulf of Alaska. J. Geophys. Res., 4231-4242.
- Pedlosky, J., 1979: Geophysical Fluid Dynamics. Springer-Verlag New York, 624 pp.
- Peffley, M.B. and J.J. O'Brien, 1976: A three-dimensional simulation of coastal upwelling off Oregon. J. Phys. Oceanogr. 6, 164-180.
- Pietrafesa, L.J., J.O. Blanton, T.N. Lee and L.P. Atkinson, 1982: The South Atlantic Bight physical and biological description. Shelf Break Processes on the East Coast of North America. R. Fournier (ed). Springs Verlag (In press).

- Preller, Ruth and J.J. O'Brien, 1980: The influence of bottom topography on upwelling off Peru. J. Phys. Oceanogr., 10, 1377-1398.
- Reed, R.K., 1980: Direct measurement of recirculation in the Alaskan Stream. J. Phys. Oceanogr., 10, 1377-1398.
- Reed, R.K., R.D. Muench and J.D. Schumacher, 1980. On the baroclinic transport of the Alaskan Stream near Kodiak Island. Deep-Sea Res. 27, 509-23.
- Reed, R.K. and J.D. Schumacher, 1981: Sea level variations in relation to coastal flow around the Gulf of Alaska. J. Geophys. Res., 6543-6546.
- Reed, R.K., J.D. Schumacher and J.P. Blaha, 1981: Eulerian measurements in the Alaskan Stream near Kodiak Island. J. Phys. Oceanogr., 11, 1591-1595.
- Reid, J.L. and A.W. Mantyla, 1976: The effect of the geostrophic flow upon coastal sea elevations in the northern North Pacific Ocean. J. Geophys. Res., 81, 3100-3110.
- Rhines, P.B., 1977: The dynamics of unsteady currents. The Sea, Vol. 6. E. D. Goldberg, ed. J. Wiley & Sons, New York, 189-318.
- Robinson, T.S., 1981: Tidal vorticity and residual circulation. Deep-Sea Research, 28A 195-212.
- Royer, R.C., 1975: Seasonal variations of waters in the northern Gulf of Alaska. Deep-Sea Research, 22, 403-416.
- Royer, T.C., 1981: Baroclinic transport in the Gulf of Alaska, Part II. A freshwater driven coastal current. J. Mar. Res., 39(2), 251-266.
- Royer, T.C., D.V. Hansen and D.J. Pashinski, 1979: Coastal flow in the northern Gulf of Alaska as observed by dynamic topography and satellite tracked drogued drift buoys. J. Phys. Oceanogr., 9, 785-801.
- Royer, Thomas C. 1982: Coastal circulation studies in the Gulf of Alaska. EOS, 63, 1007. (Abstract).
- Schumacher, J.D., C.A. Pearson and J.E. Overland, 1982: On exchange of water between the Gulf of Alaska and the Bering Sea through Unimak Pass. J. Geophys. Res., 5785-5795.
- Schumacher, J.D. and R.K. Reed., 1980: Coastal flow in the Northwest Gulf of Alaska: The Kenai Current. J. Geophys. Res., 85C, 6680-6688.

- Schumacher, J.D., R.K. Reed, M. Grigsby and D. Dreves, 1979: Circulation and hydrography near Kodiak Island September to November, 1977. NOAA Tech. Memo. ERL PMEL-13, 49 pp.
- Scott, J.T. and G.T. Csanady, 1976: Nearshore currents off Long Island. J. Geophys. Res., 81, 5401-5409.
- Semtner, A.J. and Y. Mintz, 1977: Numerical simulation of the Gulf Stream and mid-ocean eddies. J. Phys. Oceanogr., 7, 208-230.
- Shaffer, G., 1976: A meso-scale study of coastal upwelling variability off N.W. Africa. "Meteor" Forsch.-Ergebn. A. 17, 21-72.
- Shaw, P.T., 1982: The dynamics of mean circulation on the continental shelf. Doctoral Dissertation, WHOI-82-1, Woods Hole Oceanographic Institution, 226 pp.
- Shay, T.J. and B.M. Hickey, 1983: Low frequency current fluctuations near the shelf break in the northwestern Gulf of Alaska. (In press).
- Stommel, H., 1948: The westward intensification of wind driven ocean currents. Trans. Amer. Geophys. Un., 29, 202-206.
- Stommel, H. and A. Leetmaa, 1972: The circulation on the continental shelf. Proc. Nat. Acad. Sci. U.S., 64, 3380-3384.
- Sturges, W., 1974: Sea level slope along continental boundaries. J. Geophys. Res., 79, 825-830.
- Wang, D.P., 1982: Effects of the continental slope on the mean shelf circulation. J. Phys. Oceanogr., 12, 1524-1526.
- Werner, F. and B.M. Hickey, 1983: The role of a longshore pressure gradient in Pacific Northwest coastal dynamics. J. Phys. Oceanogr., 13, 395-410.
- Winant, Clinton D., 1980: Coastal circulation and wind-induced currents. Ann. Rev. Fluid Mech. 12, 271-301.
- Wright, C. 1981: Observations in the Alaskan Stream during 1980. NOAA Tech. Memo. ERL PMEL-23, 34 pp.

## Appendix

The finite differencing scheme used to solve equation (4.1) incorporated a rectangular grid with the  $i$  and  $j$  subscripts representing the  $x$  and  $y$  axes (Figure 8). The grid spacing,  $\Delta x$ , was 5 km. Finite difference notation for equation (4.1) is

$$\frac{1}{\Delta x^2} (\psi_{i+1,j} + \psi_{i-1,j} + \psi_{i,j+1} + \psi_{i,j-1} - 4\psi_{i,j}) + \eta_{Bi,j} = K(\psi_{i,j}) \quad (\text{A.1})$$

This can be solved for  $\psi_{i,j}$

$$\psi_{i,j} = \frac{1}{4} \{ \psi_{i+1,j} + \psi_{i-1,j} + \psi_{i,j+1} + \psi_{i,j-1} + \Delta x^2 [\eta_{Bi,j} - K(\psi_{i,j})] \} \quad (\text{A.2})$$

Solving for  $\psi_{i,j}$  employed a method of successive approximations. Initially, all values of  $\psi$  were set to zero except at  $i = 1$  and  $j = 1$  ( $x = 0$  and  $y = 0$ ) axes. Along  $j = 1$ ,  $\psi_{i,j}$  were computed according to equation (4.2), and then  $\psi_{1,j}$  was set to  $\psi_{1,1}$  for all  $j$  to initialize the seaward boundary. For each successive iteration a new  $\psi_{i,j}$  was calculated from (A.2) based on the old values. The function  $K(\psi_{i,j})$  was determined by searching along the upstream boundary for the particular value to  $\psi$  and calculating  $K(\psi) = -\zeta_0 \frac{L}{L_x} + \eta_B$  at that point.

Certain constraints were required to keep the iteration stable.  $\psi$  was only allowed to be negative, never to decrease in magnitude from one iteration to the next and never to exceed the magnitude of  $\psi_{1,1}$ . None of these constraints would seem to detract from the relevance of the model.

In general, after 500 or so iterations the change between iterations was less than 0.1% of the numerical value of  $\psi$ . Cases with large  $\varepsilon$  converged more slowly. All of the examples shown in the text were run to more than 500 iterations.

ERRATA SHEET

For: TOPOGRAPHIC EFFECTS OF THE ALASKAN STREAM  
ON SHELF CURRENTS

Lagerloef and Cannon, 1984  
NOAA Technical Memorandum ERL PMEL-53

Page 60	Line 15	Change 0.25 to 0.025
Page 75	Eq. (5.16c)	Should be $y=0$ .
Pages 78-79	Figures 13&14	Curves should be labeled $x/l = 0$ , $x/l = -.5$ etc. rather than $y/l$  The origin for the $\Psi$ -axis should be 0.

---